Nitrogen and Phosphorus Dynamics along the Terrestrial-Ocean Continuum in Changing Environment: Integrating Geospatial Data with Process-based Model

by

Zihao Bian

A dissertation submitted to the Graduate Faculty of
Auburn University
in partial fulfillment of the
requirements for the Degree of
Doctor of Philosophy

Auburn, Alabama
August 6, 2022

Keywords: Nitrogen loading, Phosphorus loading, Land-ocean continuum, Climate variability, Anthropogenic activities, Process-based model

Approved by

Shufen Pan, Chair, Associate Professor of College of Forestry, Wildlife and Environment
Hanqin Tian, Co-Chair, Solon Dixon Professor of College of Forestry, Wildlife and Environment
Latif Kalin, Alumni Professor of College of Forestry, Wildlife and Environment
Christopher J. Anderson, Professor of College of Forestry, Wildlife and Environment

Abstract

Nitrogen (N) and Phosphorus (P) are critical elements required by organisms for cellular processes and are the key limiting nutrients in most terrestrial and aquatic ecosystems. However, massive nutrients have entered the biosphere over the last century, largely through fertilizer use, fossil fuel emissions, and wastewater discharge, substantially perturbing global N and P cycles. Most anthropogenic nutrients are applied on land and can be transported to coastal oceans through the land-river-ocean continuum. Nutrient enrichment in aquatic ecosystems has resulted in a cascading set of environmental problems, such as harmful algal blooms, hypoxia, ocean acidification, and fish-killing. Understanding nutrient dynamics along the land-ocean continuum is essential for reducing eutrophication and protecting the drinking-water supply. In this dissertation, we developed an anthropogenic nutrient input dataset and connected nutrient cycles across terrestrial and aquatic ecosystems in a process-based model framework. The model combined with nutrient input data was applied to quantify N and P dynamics along the land-ocean continuum and comprehensively investigate the impacts of climate and human activities on nutrient loading.

The biogeochemical processes of riverine N and P dynamics and a water transport module were incorporated into a process-based biogeochemical model, Dynamic Land Ecosystem Model (DLEM). The N and P cycles across terrestrial and aquatic ecosystems were coupled within the modeling framework. The model is capable of simulating riverine exports of four N species: ammonium (NH_4^+), nitrate (NO_3^-), dissolved organic nitrogen (DON), and particulate organic nitrogen (PON), as well as four P species: dissolved inorganic phosphorus (DIP), dissolved organic phosphorus (DOP), particulate organic phosphorus (POP), and particulate inorganic phosphorus (PIP).

Livestock manure nutrient is one of the major anthropogenic nutrient sources for agricultural systems. There is still a lack of spatially-explicit estimates of manure nutrient input datasets over a century-long period in the United States (U.S.). We developed datasets of livestock manure N and P production and application in the contiguous U.S. at a 30 arc-second resolution during 1860-2017. The total production of manure N and P increased over the study period driven by increased livestock numbers before the 1980s and enhanced livestock weights after the 1980s. The intense-application region enlarging from the Midwest toward the Southern U.S. may bring high risks to water quality in coastal oceans.

The improved DLEM was applied to assess the long-term dynamics of P loading from a typical agricultural basin, the Mississippi River Basin. Simulations showed that riverine exports of DIP, DOP, POP, and PIP increased by 42%, 33%, 59%, and 54%, respectively, from the 1900s to the 2010s. Riverine DIP and PIP exports were the dominant components of the total P flux. DIP export was mainly enhanced by the growing mineral P fertilizer use in croplands, while increased PIP and POP exports resulted from the intensified soil erosion due to increased precipitation.

The N and P budgets were quantified to evaluate legacy soil nutrients across the Mississippi River Basin based on DLEM and long-term anthropogenic nutrient inputs. Both N and P balances, the difference between nutrient sources and sinks, increased substantially from 1930 to 1980, then P balance decreased dramatically within the 1980s while N balance showed a slight decline. The enhanced crop nutrient use efficiency decreased nutrient surplus and slowed down the accumulation of legacy soil nutrients. The longer resident time of P in soils leads to a much slower release of soil P to rivers than that of N. The increasingly dominant role of legacy

nutrients as loading source combined with enhanced extreme precipitation may contribute to the decreasing N:P loading ratio.

This dissertation filled the knowledge gap of synthetically evaluating dynamics of different nutrient species across the land-ocean interface under the impacts of multiple environmental changes over a century-long time scale and large spatial scale. The results can shed light on nutrient management and water pollution control strategies for the Mississippi River Basin, the Gulf of Mexico, and other similar regions.

Acknowledgments

The four years I spent at Auburn University were some of the most precious times in my life. Studying and living in a very different culture and environment can be a challenge for an international student. But I was so lucky to be surrounded by a group of nice and friendly people. I received a ton of help from these people in both study and life. I am so grateful that I meet them in Auburn; they are just like my family members to support me when I am away from my home. My first appreciation will go to my advisors, Dr. Shufen Pan and Dr. Hanqin Tian. Under their training, my research abilities have been largely improved. I learned how to think critically and creatively, and had a broader vision of my research and career. I would have never completed this dissertation without their support. I deeply appreciate the help and support from my committee members: Dr. Latif Kalin and Dr. Christopher Anderson. I have learned a lot in their classes and enjoyed their wisdom, humor, and kindness. I also thank Dr. Di Tian for reviewing this dissertation and for constructive comments.

The EDGE group is such a great team where everybody collaborates closely and encourages each other. I especially thank previous members: Drs. Shi Hao, Rongting Xu, Yuanzhi Yao, and Zhuonan Wang for providing me with precious advice on my research. I am so glad that I can become friends with Naiqing Pan, Yongfa You, and Xiaoyong Li who really brought me energy and happiness in my everyday life. I also thank Dr. Chengcheng Gang, Dr. Peipei Pan, Dr. Xing Wu, Jing Wang, Lei Zhang, Zhao Jin, Kai Ling, Hua Yan, Bo Cheng, Qiqi Liu, Ya Li, Yu Shi, and other group members.

I am grateful for all the help from Ms. Audrey Grindle and all faculty and staff members in the College of Forestry, Wildlife and Environment. I am very happy for meeting Xiaoxing Zhen, Teng Zhao, Yufei Nan, Wenjing Ren, and Dongjun Lee in Auburn.

I deeply appreciate my parents Guoan Bian and Hong Ji for their unconditional love and support. I have not been home for a long time due to the pandemic. I am looking forward to the day I will reunite with them. I missed them so much!

Last but not least, I appreciate funding supports from NOAA (NA16NOS4780204), NSF (1903722; 1922687), NASA (NNX12AP84G, NNX14AO73G, NNX10AU06G), DOT (MESC-ALCOE-06) and CSC Program.

Table of Contents

List of Tables

List of Figures

Chapter 1. Introduction

Nitrogen (N) and phosphorus (P) are essential elements required by organisms for a variety of biological and chemical processes (Sterner and Elser, 2017). Both N and P are limiting nutrients for biological productivity, and the global N and P cycles are critical to the biogeochemistry of the earth system. Under natural conditions, N flows from the atmosphere into terrestrial and marine ecosystems mainly through biological nitrogen fixation (BNF) and the production of NOx by lightning. The fixed N is subsequently transformed into amino acids and oxidized compounds, and finally returned to the atmosphere as molecular N through microbial denitrification processes (Fowler et al., 2013). Unlike reactive N which can be activated from the abundant atmospheric pool, the bioavailable P in pristine ecosystems is restricted by the release rate of mineral weathering. Therefore, P is generally recycled between biota and terrestrial/aquatic environments (Filippelli, 2002).

Anthropogenic nutrient inputs into agricultural systems have markedly altered the biogeochemical cycles of N and P globally, which remains a concern in recent decades. The N cycle has been accelerated through mineral fertilizer use, the cultivation of leguminous crops, and fossil fuel consumption (Bouwman et al., 2009). Industry development drives the massive production of synthetic fertilizer, which led to cheap fertilizer and increased crop yield (Cao et al., 2018). Since the middle of the 20th century, the global use of N fertilizer has increased nine-fold (Lu and Tian, 2017). In 2010, the industrial fixation of N through Haber-Bosch was 120 Tg N yr^{-1}, which was double the natural terrestrial sources of N (63 Tg N yr^{-1}) (Fowler et al., 2013). Humans have been altering the global P cycle by mining phosphate rock for usage as fertilizer, detergent, and animal feed supplement. Mining of P for fertilizer experienced a 10-fold increase from the 1940s to the 1980s, then declined for several years due to the collapse of the Soviet Union and the decreased P fertilizer demand in Western Europe and North America (Yuan et al., 2018). However, the rapidly growing P fertilizer demand in developing countries resulted in another surge in phosphate rock extraction since 2000. Under human perturbation, the global mobilization of P has roughly tripled compared to its natural flow (Smil, 2000). Considering the magnitude of human impacts on the global N and P cycles, the planetary boundary framework

suggests that the altered biogeochemical flows of N and P could bring high risk to the sustainable Earth system (Steffen et al., 2015).

Although manure and fertilizer application enhance crop production, excessive nutrients might leave the Soil-Plant-Animal system through the biogeochemical flow and potentially contaminate the environment if not properly managed (Mueller and Lassaletta, 2020; Zanon et al., 2019). An increasing amount of N fertilizer that plants do not use is lost to the environment through nitrification, denitrification, volatilization, and leaching (Cassman et al., 2002). N leaks from agricultural land to aquatic systems and the atmosphere, and causes water pollution and acidification, air pollution, loss of biodiversity, and global warming (Liu et al., 2010). The major N gaseous loss from fertilizer use and animal excreta includes the emissions of ammonia (NH_3), nitrous oxide (N_2O), and nitric oxide. NH_3 in the atmosphere can react with other air pollutants and form aerosols to reduce visibility and threaten human health (Bouwman et al., 2002; Xu et al., 2018). Nitrous oxide (N_2O), a long-lived greenhouse gas (GHG), can be produced in nitrification and denitrification processes and be emitted into the atmosphere. The concentration of atmospheric N_2O has increased from 270 ppb in the preindustrial period to 330 ppb in recent years, and the increase rate has become faster recently (Tian et al., 2019). Nitric oxide can catalyze the photochemical formation of ground-level ozone, and cause detrimental effects on human health and crop productivity (Altshuller and Bufalini, 1971; Feng et al., 2015).

The usage of P mineral fertilizers increases P availability in soil, as well as P losses from land to freshwaters and coastal oceans (Yuan et al., 2018). Consequently, the P cycle became a largely one-way flow from rock to soil and finally to streams, lakes, and oceans (Elser and Bennett, 2011). Additionally, different from N, which can be fixed from the atmosphere through microbial symbiosis with plants and the Haber-Bosch process, P is a rock-derived nutrient and there is no biological or atmospheric source for P. The limited and unevenly distributed P-rich rocks can threaten food security and have raised concerns in many resource-limited countries, including the United States (U.S.) (Amundson et al., 2015).

The mobilization of both N and P can have detrimental effects on the aquatic environment (Smith et al., 1998; Van Drecht et al., 2005). Generally, primary productivity in freshwater is limited by P, while that in estuaries and coastal marine ecosystems is limited by N (Conley et al., 2009). Exceptions to these generalities exist, and ecosystems even switch between

N and P limitation seasonally (Howarth et al., 2021). However, massive N and P inputs from land have disrupted the nutrient balance in waters and stimulated harmful algal blooms (HABs), resulting in eutrophication, de-oxygenation, increased toxicity, and the loss of species diversity (Garnier et al., 2015; Smith et al., 2007). Eutrophication symptoms are evident in aquatic systems worldwide, with oxygen-depleted marine coastal "dead zones" expanding and more frequent observations of HABs (Glibert, 2017). Considering these environmental and human health problems caused by the anthropogenic N and P, we must improve our understanding of nutrient dynamics along the land-ocean continuum in order to optimize nutrient usage and minimize negative consequences (Galloway et al., 2008).

Climate and anthropogenic activities mainly influence the long-term N and P dynamics along the land-ocean continuum. Climate changes (e.g., temperature and precipitation) can alter hydrological and biogeochemical processes in both terrestrial and aquatic systems. Increased precipitation can decrease the resident times of N and P within soils, and extreme precipitation events can lead to extreme runoff and nutrient loading (Howarth et al., 2006; Iqbal et al., 2018). Temperature increase, on the contrary, can reduce discharge and loading by enhancing evapotranspiration. Both temperature and precipitation can change soil moisture and a variety of biotic and abiotic mechanisms related to the N and P cycles (Ballard et al., 2019). Interannual variability of nutrient loading is proven to be dominated by climate variability (Sinha and Michalak, 2016). Anthropogenic activities, primarily through synthetic fertilizer and animal manure addition, land-use change, and wastewater discharge have substantially disturbed nutrient cycles and increased reactive nutrients in the terrestrial-aquatic system (Boyer et al., 2002; Dupas et al., 2018). Non-point nutrient sources from agriculture and atmospheric deposition and point source from wastewater discharge play important roles in contributing to the enrichment of N and P in aquatic systems. Deforestation and expanding agricultural land use can enhance soil erosion accompanied by nutrient loss from land to rivers (Bouwman et al., 2013; Seitzinger et al., 2010). An integrative understanding of how climate and anthropogenic activities influence long-term nutrient dynamics along the land-ocean continuum can provide valuable information and nutrient management and pollution mitigation (Yang et al., 2015).

In the U.S., the consumption of N fertilizer has increased nearly 3-fold, while P fertilizer increased 60% from 1960 to 2017. Nutrient usage in the agricultural field often moves beyond

crop demand for the management practices fail to achieve good congruence between nutrient supply and demand (Dobermann, 2007). Lateral nutrient fluxes through riverine systems have become a critical source of N and P from land into the coastal zone and contributed to the occurrence of hypoxia, particularly in the Gulf of Mexico and Chesapeake Bay (Conley et al., 2009). The Mississippi River Basin (MRB) and the Chesapeake Bay Watershed (CBW) are two critical nutrient sources for the northern Gulf of Mexico and the Mid-Atlantic, respectively. Intensive agricultural activities in the MRB, especially corn and soybean production in the Corn Belt, have led to high nutrient loading and water quality degradation in the northern Gulf of Mexico. The northern Gulf of Mexico has become one of the world's largest dead zones, and the hypoxic area often exceeds 15,600 km^2 in midsummer (1968-2016) (Del Giudice et al., 2019). The CBW has experienced a remarkable increase in population and urban area over the last century. Increased occurrence of bottom-water hypoxia, harmful algal blooms, and reduction in water clarity have been observed in the bay since the mid-20th century, coincident with these increased nutrients fluxes (Bever et al., 2013; Hagy et al., 2004; Harding et al., 2019; Kemp et al., 2005).

Watershed-based conservation programs aiming to reduce external nutrient loading to surface waters have not resulted in significant water-quality improvements (Stackpoole et al., 2019). Although the annual N and P fertilizer and manure usage became relatively stable since the 1980s in the U.S., N and P accumulations in the soil due to the historical nutrient application, also called legacy nutrients, may continue to mobilize long after inputs decline. The impairment of water quality caused by legacy N and P has attracted more and more attention (Powers et al., 2016; Sharpley et al., 2013). The losses of nutrients from the agriculture system not only waste resources and increase the costs, but also bring huge pressure on the environment. Hence, increasing nutrient use efficiency continues to be a major challenge for agriculture.

Numerous inventory-based analyses, statistical and mechanistic models have been used to estimate N and P delivery from land to the coastal ocean. The Net Anthropogenic Nitrogen Input (NANI) and Net Anthropogenic Phosphorus Input (NAPI) are widely-used statistical methodologies to assess flows of N and P (Howarth et al., 1996; Hu et al., 2020; Metson et al., 2017). The linear relationship between NANI and N export or NAPI and P export can be interpreted as the proportion of anthropogenic N or P sources flowing to coastal oceans (Swaney

et al., 2012). Watershed models have advantages in simulating interactions between multiple processes in water, N, and P cycles and predicting the transfer of nutrients from land to ocean (Bouwman et al., 2013). Several models have been developed to estimate N and P export to waterways at multiple scales. For example, the SPAtially Referenced Regression On Watershed attributes (SPARROW) model has been applied to evaluate N and P sources and delivery from the Mississippi River Basin (Alexander et al., 2008). The Global Environment—Global Nutrient Model (IMAGE-GNM) is capable of predicting nutrient transport by rivers at the global scale (Harrison et al., 2019), while the Soil and Water Assessment Tool (SWAT) is a smaller scale model and usually used to predict nutrient loading based on fine-scale location-specific data (Douglas-Mankin et al., 2010). However, the N and P cycling processes are still over-simplified in these watershed models. Additionally, the biogeochemical cycles in terrestrial and aquatic ecosystems have not yet been coupled in these models due to the historical separation between approaches of terrestrial and aquatic subdisciplines (Bouwman et al., 2013; Robson, 2014). Human perturbation of biogeochemical cycles calls for an integrative consideration of biogeochemical cycles across terrestrial and aquatic ecosystems. Process-based biogeochemical models simultaneously considering the impact of climate and anthropogenic activities on the nutrient dynamics among the land, aquatic and atmospheric interfaces may help to better elucidate the mechanisms that control riverine N and P export in the study region (Yang et al., 2015). Additionally, most mechanistic watershed models do not satisfactorily consider the potentially long residence times for nutrients within the terrestrial ecosystems and, therefore, cannot account for the effects of nutrient legacies on long-term nutrient loading (Meter et al., 2018). Whereas, process-based biogeochemical models can simulate the long-term changes in nutrient fluxes and pools and estimate the impact of legacy nutrients on N and P loading.

From sustainable nutrient management and water quality control, it is important to incorporate biogeochemical processes across terrestrial and aquatic ecosystems into an integrated modeling framework for accurately predicting and attributing N and P loading and export along the land-ocean continuum. The Dynamic Land Ecosystem Model (DLEM) is a process-based model coupling terrestrial biophysics, plant phenology, soil biogeochemistry, and vegetation dynamics (Pan et al., 2015, 2020; Tian et al., 2015b; Tian et al., 2010). The model is capable of simulating biogeochemical (C and N cycling) and hydrological cycles across the soil–plant–atmosphere continuum, and the model has been applied in the MRB to estimate riverine carbon

(C) and N exports (Ren et al., 2016; Tian et al., 2020). Recently, we have coupled the P processes in terrestrial ecosystems and C–N–P interactions into the DLEM and established the DLEM–CNP modeling scheme (Wang et al., 2020). Building upon our recent progress, we plan to develop a module representation of riverine P dynamics in the DLEM, which further enhances modeling ability for simulating both N and P cycling along the terrestrial–ocean continuum. The model could be used to estimate riverine N and P exports from land to coastal ocean over the past century (Figure 1-1). Based on simulated results, we can quantify the contributions of multiple environmental factors, such as climate, atmospheric CO_2, land conversion, anthropogenic nutrient inputs (i.e., synthetic fertilizer and manure), and wastewater discharge on riverine N and P loading. Long-term input datasets and process-based modeling also provide a reliable pathway to assess sources and sinks of legacy soil nutrients. The impact of legacy soil nutrients on nutrient loading and N:P stoichiometry can be evaluated through scenario simulation experiments. The results will shed light on optimizing nutrient management and evaluating the efficacy of policy on water quality control.

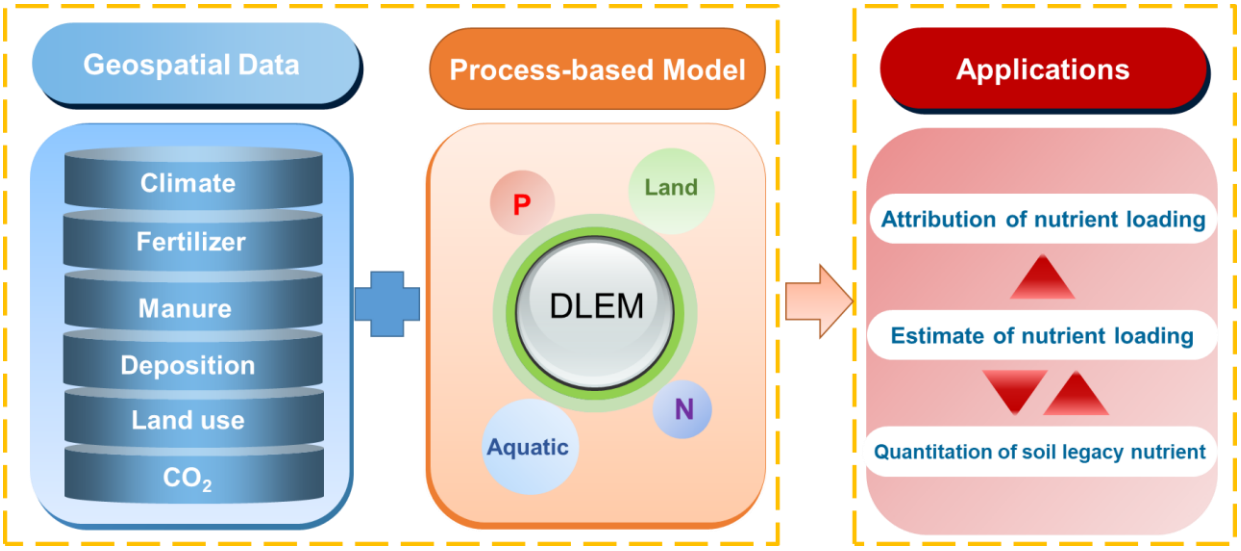

Figure 1-1. The workflow of this study.

1. Objectives

The overarching goal of this study is to estimate the long-term dynamics of N and P loading across the land-ocean interface and understand how human activities and climate have

interactively impacted nutrient loading by using a processes-based biogeochemical model. Specifically:

a. Develop and improve aquatic module coupled with a terrestrial biogeochemical model, DLEM, to connect N and P cycles across terrestrial and aquatic ecosystems.

b. Collect and develop long-time series anthropogenic nutrient input data, and investigate spatial and temporal patterns of anthropogenic nutrient input.

c. Estimate the century-long trajectory of N and P loading from land to coastal ocean based on DLEM model and anthropogenic nutrient input datasets.

d. Explore the impacts of climate, atmospheric CO_2 concentration, land use change, atmospheric deposition, wastewater discharge, and synthetic fertilizer and manure application on the nutrient loading.

e. Quantify the legacy soil nutrients by establishing N and P budgets in terrestrial ecosystems.

f. Investigate the contribution of agricultural legacy nutrients on N and P loading as well as N/P ratio.

2. Modeling and data basis

2.1. The Dynamic Land Ecosystem Model (DLEM)

The DLEM is a process-based land biosphere model which couples vegetation dynamics, soil biogeochemistry, and the associated C, N, P, and water cycles to conduct temporally- and spatially-explicit simulations across site, regional, and global scales (Figure 1-2 a) (Liu et al., 2013; Pan et al., 2015; Tian et al., 2011; Wang et al., 2020). Specifically, in the DLEM, C enters the ecosystems mainly through vegetation CO_2 uptake during photosynthesis, and leaves the ecosystems via ecosystem respiration, harvest, various disturbances, and lateral transport to water bodies. N enters terrestrial ecosystems through biological N fixation, atmospheric N deposition, and fertilizer and manure applications. N leaves ecosystems through different pathways, including NH_3 volatilization, emissions of N_2O, NO, and N_2 during nitrification and denitrification, N leaching from root zones to groundwater, and lateral N transport with surface runoff. The DLEM is capable of simulating daily and spatially-explicit estimates on GHG;

variations in storage pools of C, N, and water in terrestrial ecosystems; river discharge and riverine export of carbon and nitrogen from land to ocean. Recently, we just coupled the land P processes and C-N-P interactions into the DLEM, including weathering, mineralization, adsorption, desorption, leaching, vegetation P uptake and allocation, and P limitation on carbon sequestration (Figure 1-2 b). The land model of DLEM calculates runoff, C, N, and P yields as the inputs to the aquatic module.

The DLEM Terrestrial-Aquatic modeling framework combines the terrestrial ecosystem processes with channel routing and aquatic biogeochemistry processes. The channel routing function is implemented by integrating the physical-based Model Of Scale Adaptive River Transport (MOSART) (Li et al., 2015, 2013) into the DLEM framework. The channel routine processes within a grid cell are separated into three unique parts, namely hillslope flow, subnetwork flow, and main channel flow. Through parameterization (such as flow length, channel slope, and surface roughness) using aggregated high-resolution topography and river network data, the MOSART model can work in a scale-adaptive way.

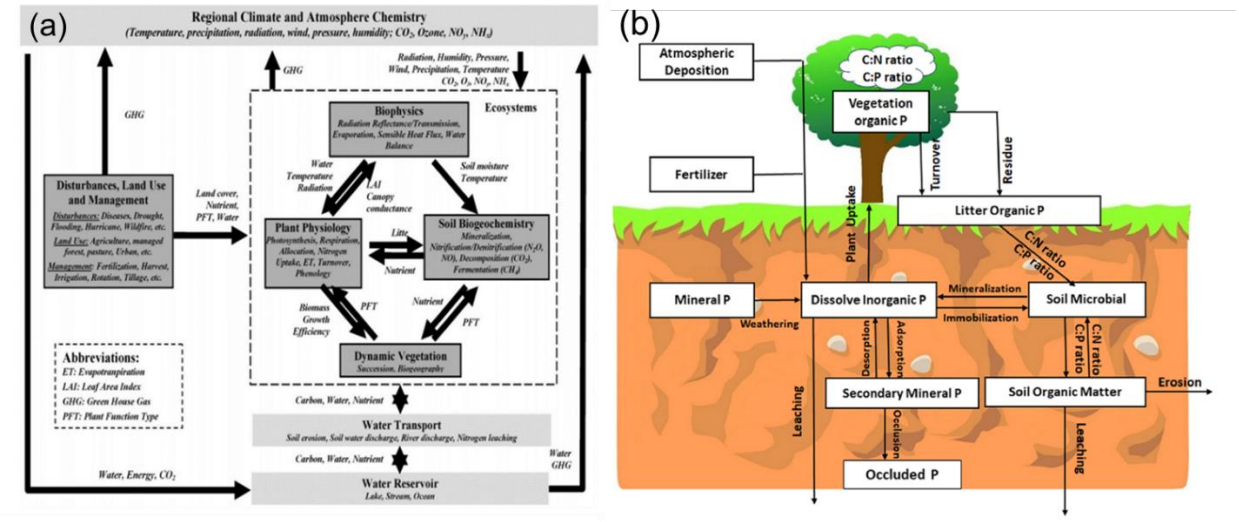

Figure 1-2. (a) The structure of DLEM and (b) P processes in land component.

2.2. Existing databases

Several model input datasets have been developed and/or collected to characterize natural and human disturbances in the conterminous U.S., as summarized in Table 1-1. Based on the datasets, all the required input data in the U.S. at a resolution of 5 arc-min by 5 arc-min were developed. Anthropogenic nutrient input datasets are critical for accurately quantifying nutrient dynamics in terrestrial ecosystems, and synthetic fertilizer and atmospheric deposition data have already been developed in previous studies (Table 1-1). However, a long-term and spatial-explicit livestock manure nutrient input dataset still needed to be developed.

Table 1-1. Model-relevant data developed or collected in previous work.

Data variables	Time period/step	Reference/source
Climate (Tmin, Tmax, Precipitation, Water vapor pressure, Radiation)	1860-2018 daily	Metdata (GRIDMET) CRUNCEP IPSL simulation
Land Cover and Land Use (Crop density /rotation maps)	1850-2016 yearly	(Yu and Lu, 2018)
N fertilizer	1850-2016 yearly	(Cao et al., 2018)
P fertilizer	1961-2013 yearly	USDA National Agricultural Statistics Service (https://quickstats.nass.usda.gov/)
N deposition rate	2000-2014 yearly	(Schwede and Lear, 2014)
P deposition rate	Annual average	(Mahowald et al., 2008)

3. Study area

Figure 1-3. The Mississippi River Basin (MRB).

The Mississippi River Basin (MRB), draining 4.76 million km^2, encompasses 41% of the contiguous U.S. and is the largest contributor of freshwater and nutrients to the Gulf of Mexico. The MRB consists of seven major sub-basins, including Upper Mississippi, Ohio, Missouri, Arkansas, Red, Tennessee, and Lower Mississippi River basins. The MRB now accounts for approximately 70% of U.S. cropland and contains around 90% of all hogs and 60% of all cattle raised within the U.S. (Meter et al., 2017). Widespread agricultural land use in the basin combined with intensive fertilizer application and livestock production has resulted in high levels of nutrient loading to the Gulf of Mexico. Although N is the ultimate limiting nutrient in the Gulf of Mexico, the exchange of deep ocean waters with the waters on the continental shelf is more limited in the Gulf compared with other shelves, which makes the Gulf hypoxic zone more prone to a switch to P limitation (Howarth et al., 2011).

In this study, we chose MRB as a typical region to evaluate the impacts of climate and human activities on nutrient dynamics along the land-ocean continuum. Since the DLEM-simulated N loading from the MRB has been reported in Tian et al. (2020), here, we mainly reported P loading results. The legacy soil nutrient is a more important issue for agriculture-dominated regions, therefore, we assessed the impact of legacy soil nutrients on riverine N and P loading in the MRB.

4. Approaches

Dataset development:

a. Develop grid-level manure N and P datasets from 1860 to 2017 in the U.S.

Model improvement:

a. Improve aquatic N module in the DLEM based on the new scale adaptive water transport scheme.

b. Develop a model representation of riverine P dynamics in the DLEM and link it to P processes in the land component.

Model validation and application:

a. Model validation and application in the Mississippi River Basin to simulate the P loading.

Attribution analysis:

a. Analyze the impacts of climate, atmospheric CO_2 concentration, land use change, and synthetic fertilizer and manure application on P exports.

b. Estimate the contribution of agricultural legacy N and P on nutrient loading as well as N/P ratio in riverine export.

5. Dissertation structure

This dissertation is organized according to the structure as Figure 1-4:

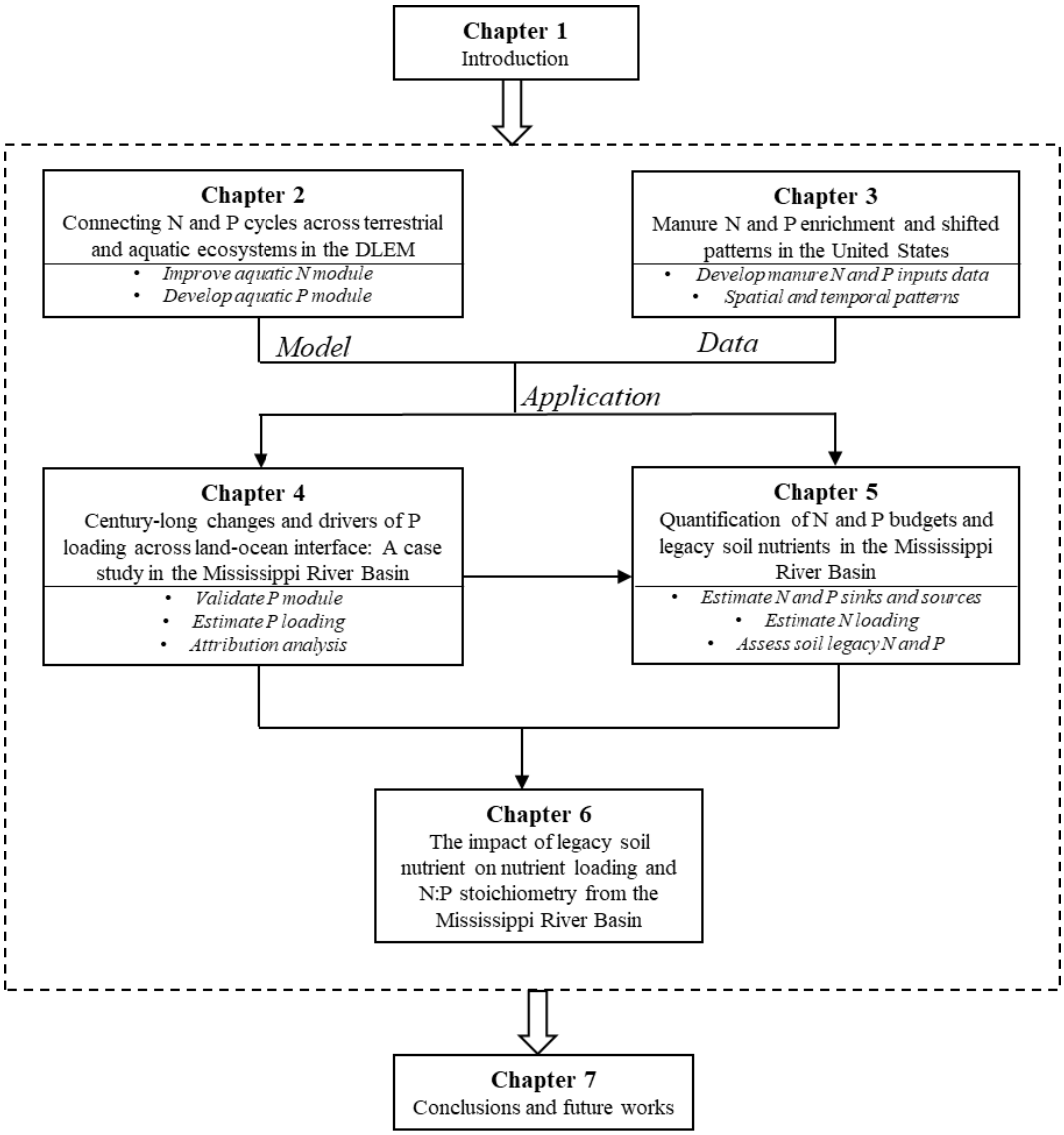

Figure 1-4. The structure of this dissertation

Chapter 1. Introduction.

We describe the background and significance of this study, research objectives, existing model and data basis, study areas, and approaches to study these research questions.

Chapter 2. Connecting N and P cycles across terrestrial and aquatic ecosystems in the DLEM.

We provide a detailed description of hydrological and biogeochemical processes in the DLEM Terrestrial-Aquatic modeling framework. The development of aquatic P module is introduced. The N and P cycling in terrestrial and aquatic ecosystems are connected in the model framework.

Chapter 3. Manure N and P enrichment and shifted patterns in the United States.

We describe the methods to develop grid-level production and application of manure N and P datasets. The temporal and spatial patterns of manure N and P input across the continental U.S. during 1860-2017 are evaluated. The impact of manure nutrient enrichment on nutrient loading is assessed based on the dataset. This chapter has been published in Bian et al. (2021).

Chapter 4. Century-long changes and drivers of P loading across land-ocean interface: A case study in the Mississippi River Basin.

We calibrate and validate the coupled terrestrial-aquatic P module in DLEM in the MRB. The riverine P exports from the basin over 1901-2018 are estimated based on the model. We assess the spatial and temporal variations in dissolved inorganic phosphorus, dissolved organic phosphorus, particulate inorganic phosphorus, and particulate organic phosphorus. We further investigate the contributions of climate, synthetic fertilizer, livestock manure, land-use change on the export changes in four P species.

Chapter 5. Quantification of N and P budgets and legacy soil nutrients in the Mississippi River Basin.

We quantify the major sources and sinks of soil legacy N and P in the MRB. The long-term dynamics of soil legacy N is calculated based on major N inputs (N fixation, N fertilizer, manure N, atmospheric N deposition) and major N outputs (harvest crop N, N loading, NH_3 emission, N_2O emission, NO emission, and N_2 emission). Similarly, the soil legacy P is

quantified based P inputs (weathering P, P fertilizer, manure P, and atmospheric P deposition) and P outputs (harvest crop P and P loading).

Chapter 6. The impact of legacy soil nutrient on nutrient loading and N:P stoichiometry from the Mississippi River Basin.

We investigate the impact of legacy soil nutrients on N and P loading by setting two scenarios: the NORMAL scenario and the LEGACY scenario where the N and P inputs in cropland are assumed to be fully used by crops. The impact of legacy soil nutrients on the N/P ratio of riverine export is also evaluated. We further discuss the potential impact of other factors on N/P ratio change.

Chapter 7. Conclusions and future works

We summarize the significant findings in this study. The uncertainties in this study and future study plans are discussed.

References

Alexander, R.B., Smith, R.A., Schwarz, G.E., Boyer, E.W., Nolan, J.V., Brakebill, J.W., 2008. Differences in Phosphorus and Nitrogen Delivery to The Gulf of Mexico from the Mississippi River Basin. Environ. Sci. Technol. 42, 822–830. https://doi.org/10.1021/es0716103

Altshuller, A.P., Bufalini, J.J., 1971. Photochemical aspects of air pollution. Review. Environ. Sci. Technol. 5, 39–64.

Amundson, R., Berhe, A.A., Hopmans, J.W., Olson, C., Sztein, A.E., Sparks, D.L., 2015. Soil and human security in the 21st century. Science 348, 1261071–1261071. https://doi.org/10.1126/science.1261071

Ballard, T.C., Sinha, E., Michalak, A.M., 2019. Long-Term Changes in Precipitation and Temperature Have Already Impacted Nitrogen Loading. Environ. Sci. Technol. 53, 5080–5090. https://doi.org/10.1021/acs.est.8b06898

Bever, A.J., Friedrichs, M.A.M., Friedrichs, C.T., Scully, M.E., Lanerolle, L.W.J., 2013. Combining observations and numerical model results to improve estimates of hypoxic volume within the Chesapeake Bay, USA. J. Geophys. Res. Oceans 118, 4924–4944. https://doi.org/10.1002/jgrc.20331

Bian, Z., Tian, H., Yang, Q., Xu, R., Pan, S., Zhang, B., 2021. Production and application of manure nitrogen and phosphorus in the United States since 1860. Earth Syst. Sci. Data 13, 515–527. https://doi.org/10.5194/essd-13-515-2021

Bouwman, A.F., Beusen, A.H., Billen, G., 2009. Human alteration of the global nitrogen and phosphorus soil balances for the period 1970–2050. Glob. Biogeochem. Cycles 23.

Bouwman, A.F., Bierkens, M.F.P., Griffioen, J., Hefting, M.M., Middelburg, J.J., Middelkoop, H., Slomp, C.P., 2013. Nutrient dynamics, transfer and retention along the aquatic continuum from land to ocean: towards integration of ecological and biogeochemical models. Biogeosciences 10, 1–22. https://doi.org/10.5194/bg-10-1-2013

Bouwman, A.F., Boumans, L.J.M., Batjes, N.H., 2002. Estimation of global NH3 volatilization loss from synthetic fertilizers and animal manure applied to arable lands and grasslands. Glob. Biogeochem. Cycles 16, 8-1-8–14.

Boyer, E.W., Goodale, C.L., Jaworski, N.A., Howarth, R.W., 2002. Anthropogenic nitrogen sources and relationships to riverine nitrogen export in the northeastern USA. Biogeochemistry 57, 137–169.

Cao, P., Lu, C., Yu, Z., 2018. Historical nitrogen fertilizer use in agricultural ecosystems of the contiguous United States during 1850–2015: application rate, timing, and fertilizer types. Earth Syst. Sci. Data 10, 969–984. https://doi.org/10.5194/essd-10-969-2018

Cassman, K.G., Dobermann, A., Walters, D.T., 2002. Agroecosystems, nitrogen-use efficiency, and nitrogen management. AMBIO J. Hum. Environ. 31, 132–141.

Conley, D.J., Paerl, H.W., Howarth, R.W., Boesch, D.F., Seitzinger, S.P., Havens, K.E., Lancelot, C., Likens, G.E., 2009. Controlling Eutrophication: Nitrogen and Phosphorus. Science 323, 1014–1015. https://doi.org/10.1126/science.1167755

Del Giudice, D., Matli, V.R.R., Obenour, D.R., 2019. Bayesian mechanistic modeling characterizes Gulf of Mexico hypoxia: 1968–2016 and future scenarios. Ecol. Appl. https://doi.org/10.1002/eap.2032

Dobermann, A., 2007. Fertilizer best management practices: General principles, strategy for their adoption and voluntary initiatives vs. regulations, in: Proceedings of the IFA International Workshop on Fertilizer Best Management Practices. pp. 1–28.

Douglas-Mankin, K.R., Srinivasan, R., Arnold, J.G., 2010. Soil and Water Assessment Tool (SWAT) Model: Current Developments and Applications. Trans. ASABE 53, 1423–1431. https://doi.org/10.13031/2013.34915

Dupas, R., Minaudo, C., Gruau, G., Ruiz, L., Gascuel-Odoux, C., 2018. Multidecadal trajectory of riverine nitrogen and phosphorus dynamics in rural catchments. Water Resour. Res. 54, 5327–5340.

Elser, J., Bennett, E., 2011. A broken biogeochemical cycle. Nature 478, 29–31. https://doi.org/10.1038/478029a

Feng, Z., Hu, E., Wang, X., Jiang, L., Liu, X., 2015. Ground-level O3 pollution and its impacts on food crops in China: a review. Environ. Pollut. 199, 42–48.

Filippelli, G.M., 2002. The Global Phosphorus Cycle. Rev. Mineral. Geochem. 48, 391–425. https://doi.org/10.2138/rmg.2002.48.10

Fowler, D., Coyle, M., Skiba, U., Sutton, M.A., Cape, J.N., Reis, S., Sheppard, L.J., Jenkins, A., Grizzetti, B., Galloway, J.N., Vitousek, P., Leach, A., Bouwman, A.F., Butterbach-Bahl, K., Dentener, F., Stevenson, D., Amann, M., Voss, M., 2013. The global nitrogen cycle in the twenty-first century. Philos. Trans. R. Soc. B Biol. Sci. 368, 20130164. https://doi.org/10.1098/rstb.2013.0164

Galloway, J.N., Townsend, A.R., Erisman, J.W., Bekunda, M., Cai, Z., Freney, J.R., Martinelli, L.A., Seitzinger, S.P., Sutton, M.A., 2008. Transformation of the Nitrogen Cycle: Recent Trends, Questions, and Potential Solutions. Science. https://doi.org/10.1126/science.1136674

Garnier, J., Lassaletta, L., Billen, G., Romero, E., Grizzetti, B., Némery, J., Le, T.P.Q., Pistocchi, C., Aissa-Grouz, N., Luu, T.N.M., 2015. Phosphorus budget in the water-agro-food system at nested scales in two contrasted regions of the world (ASEAN-8 and EU-27). Glob. Biogeochem. Cycles 29, 1348–1368.

Glibert, P.M., 2017. Eutrophication, harmful algae and biodiversity — Challenging paradigms in a world of complex nutrient changes. Mar. Pollut. Bull., Special Issue: Hong Kong Conference 2016 124, 591–606. https://doi.org/10.1016/j.marpolbul.2017.04.027

Hagy, J.D., Boynton, W.R., Keefe, C.W., Wood, K.V., 2004. Hypoxia in Chesapeake Bay, 1950–2001: Long-term change in relation to nutrient loading and river flow. Estuaries 27, 634–658. https://doi.org/10.1007/BF02907650

Harding, L.W., Mallonee, M.E., Perry, E.S., Miller, W.D., Adolf, J.E., Gallegos, C.L., Paerl, H.W., 2019. Long-term trends, current status, and transitions of water quality in Chesapeake Bay. Sci. Rep. 9, 6709. https://doi.org/10.1038/s41598-019-43036-6

Harrison, J.A., Beusen, A.H., Fink, G., Tang, T., Strokal, M., Bouwman, A.F., Metson, G.S., Vilmin, L., 2019. Modeling phosphorus in rivers at the global scale: recent successes, remaining challenges, and near-term opportunities. Curr. Opin. Environ. Sustain., Environmental Change Assessment 36, 68–77. https://doi.org/10.1016/j.cosust.2018.10.010

Howarth, R.W., Billen, G., Swaney, D., Townsend, A., Jaworski, N., Lajtha, K., Downing, J.A., Elmgren, R., Caraco, N., Jordan, T., 1996. Riverine inputs of nitrogen to the North Atlantic Ocean: fluxes and human influences. Biogeochemistry 35, 75–139.

Howarth, R.W., Chan, F., Conley, D.J., Garnier, J., Doney, S.C., Marino, R., Billen, G., 2011. Coupled biogeochemical cycles: eutrophication and hypoxia in temperate estuaries and coastal marine ecosystems. Front. Ecol. Environ. 9, 18–26. https://doi.org/10.1890/100008

Howarth, R.W., Chan, F., Swaney, D.P., Marino, R.M., Hayn, M., 2021. Role of external inputs of nutrients to aquatic ecosystems in determining prevalence of nitrogen vs. phosphorus limitation of net primary productivity. Biogeochemistry. https://doi.org/10.1007/s10533-021-00765-z

Howarth, R.W., Swaney, D.P., Boyer, E.W., Marino, R., Jaworski, N., Goodale, C., 2006. The influence of climate on average nitrogen export from large watersheds in the Northeastern United States, in: Nitrogen Cycling in the Americas: Natural and Anthropogenic Influences and Controls. Springer, pp. 163–186.

Hu, M., Liu, Y., Zhang, Y., Shen, H., Yao, M., Dahlgren, R.A., Chen, D., 2020. Long-term (1980–2015) changes in net anthropogenic phosphorus inputs and riverine phosphorus export in the Yangtze River basin. Water Res. 177, 115779. https://doi.org/10.1016/j.watres.2020.115779

Iqbal, J., Necpalova, M., Archontoulis, S.V., Anex, R.P., Bourguignon, M., Herzmann, D., Mitchell, D.C., Sawyer, J.E., Zhu, Q., Castellano, M.J., 2018. Extreme weather-year sequences have nonadditive effects on environmental nitrogen losses. Glob. Change Biol. 24, e303–e317.

Kemp, W.M., Boynton, W.R., Adolf, J.E., Boesch, D.F., Boicourt, W.C., Brush, G., Cornwell, J.C., Fisher, T.R., Glibert, P.M., Hagy, J.D., Harding, L.W., Houde, E.D., Kimmel, D.G., Miller, W.D., Newell, R.I.E., Roman, M.R., Smith, E.M., Stevenson, J.C., 2005. Eutrophication of Chesapeake Bay: historical trends and ecological interactions. Mar. Ecol. Prog. Ser. 303, 1–29. https://doi.org/10.3354/meps303001

Li, H., Leung, L.R., Getirana, A., Huang, M., Wu, H., Xu, Y., Guo, J., Voisin, N., 2015. Evaluating global streamflow simulations by a physically based routing model coupled with the community land model. J. Hydrometeorol. 16, 948–971.

Li, H., Wigmosta, M.S., Wu, H., Huang, M., Ke, Y., Coleman, A.M., Leung, L.R., 2013. A physically based runoff routing model for land surface and earth system models. J. Hydrometeorol. 14, 808–828.

Liu, J., You, L., Amini, M., Obersteiner, M., Herrero, M., Zehnder, A.J.B., Yang, H., 2010. A high-resolution assessment on global nitrogen flows in cropland. Proc. Natl. Acad. Sci. 107, 8035–8040. https://doi.org/10.1073/pnas.0913658107

Liu, M., Tian, H., Yang, Q., Yang, J., Song, X., Lohrenz, S.E., Cai, W.-J., 2013. Long-term trends in evapotranspiration and runoff over the drainage basins of the Gulf of Mexico during 1901–2008. Water Resour. Res. 49, 1988–2012.

Lu, C.C., Tian, H., 2017. Global nitrogen and phosphorus fertilizer use for agriculture production in the past half century: shifted hot spots and nutrient imbalance. Earth Syst. Sci. Data 9, 181.

Mahowald, N., Jickells, T.D., Baker, A.R., Artaxo, P., Benitez-Nelson, C.R., Bergametti, G., Bond, T.C., Chen, Y., Cohen, D.D., Herut, B., Kubilay, N., Losno, R., Luo, C., Maenhaut, W., McGee, K.A., Okin, G.S., Siefert, R.L., Tsukuda, S., 2008. Global distribution of atmospheric phosphorus sources, concentrations and deposition rates, and anthropogenic impacts: GLOBAL ATMOSPHERIC PHOSPHORUS. Glob. Biogeochem. Cycles 22, n/a-n/a. https://doi.org/10.1029/2008GB003240

Meter, K.J.V., Basu, N.B., Cappellen, P.V., 2017. Two centuries of nitrogen dynamics: Legacy sources and sinks in the Mississippi and Susquehanna River Basins. Glob. Biogeochem. Cycles 31, 2–23. https://doi.org/10.1002/2016GB005498

Meter, K.J.V., Cappellen, P.V., Basu, N.B., 2018. Legacy nitrogen may prevent achievement of water quality goals in the Gulf of Mexico. Science 360, 427–430. https://doi.org/10.1126/science.aar4462

Metson, G.S., Lin, J., Harrison, J.A., Compton, J.E., 2017. Linking terrestrial phosphorus inputs to riverine export across the United States. Water Res. 124, 177–191. https://doi.org/10.1016/j.watres.2017.07.037

Mueller, N.D., Lassaletta, L., 2020. Nitrogen challenges in global livestock systems. Nat. Food 1, 400–401. https://doi.org/10.1038/s43016-020-0117-7

Pan, S., Tian, H., Dangal, S.R., Ouyang, Z., Lu, C., Yang, J., Tao, B., Ren, W., Banger, K., Yang, Q., 2015. Impacts of climate variability and extremes on global net primary production in the first decade of the 21st century. J. Geogr. Sci. 25, 1027–1044.

Pan, S., Yang, J., Tian, H., Shi, H., Chang, J., Ciais, P., Francois, L., Frieler, K., Fu, B., Hickler, T., Ito, A., Nishina, K., Ostberg, S., Reyer, C.P.O., Schaphoff, S., Steinkamp, J., Zhao, F., 2020. Climate Extreme Versus Carbon Extreme: Responses of Terrestrial Carbon Fluxes to Temperature and Precipitation. J. Geophys. Res. Biogeosciences 125, e2019JG005252. https://doi.org/10.1029/2019JG005252

Powers, S.M., Bruulsema, T.W., Burt, T.P., Chan, N.I., Elser, J.J., Haygarth, P.M., Howden, N.J.K., Jarvie, H.P., Lyu, Y., Peterson, H.M., Sharpley, A.N., Shen, J., Worrall, F., Zhang, F., 2016. Long-term accumulation and transport of anthropogenic phosphorus in three river basins. Nat. Geosci. 9, 353–356. https://doi.org/10.1038/ngeo2693

Ren, W., Tian, H., Cai, W.-J., Lohrenz, S.E., Hopkinson, C.S., Huang, W.-J., Yang, J., Tao, B., Pan, S., He, R., 2016. Century-long increasing trend and variability of dissolved organic carbon export from the Mississippi River basin driven by natural and anthropogenic forcing: Export of DOC from the Mississippi River. Glob. Biogeochem. Cycles 30, 1288–1299. https://doi.org/10.1002/2016GB005395

Robson, B.J., 2014. State of the art in modelling of phosphorus in aquatic systems: Review, criticisms and commentary. Environ. Model. Softw. 61, 339–359. https://doi.org/10.1016/j.envsoft.2014.01.012

Schwede, D.B., Lear, G.G., 2014. A novel hybrid approach for estimating total deposition in the United States. Atmos. Environ. 92, 207–220.

Seitzinger, S.P., Mayorga, E., Bouwman, A.F., Kroeze, C., Beusen, A.H., Billen, G., Van Drecht, G., Dumont, E., Fekete, B.M., Garnier, J., 2010. Global river nutrient export: A scenario analysis of past and future trends. Glob. Biogeochem. Cycles 24.

Sharpley, A., Jarvie, H.P., Buda, A., May, L., Spears, B., Kleinman, P., 2013. Phosphorus Legacy: Overcoming the Effects of Past Management Practices to Mitigate Future Water Quality Impairment. J. Environ. Qual. 42, 1308. https://doi.org/10.2134/jeq2013.03.0098

Sinha, E., Michalak, A.M., 2016. Precipitation dominates interannual variability of riverine nitrogen loading across the continental United States. Environ. Sci. Technol. 50, 12874–12884.

Smil, V., 2000. Phosphorus in the environment: natural flows and human interferences. Annu. Rev. Energy Environ. 25, 53–88.

Smith, D.R., Owens, P.R., Leytem, A.B., Warnemuende, E.A., 2007. Nutrient losses from manure and fertilizer applications as impacted by time to first runoff event. Environ. Pollut. 147, 131–137.

Smith, K.A., Chalmers, A.G., Chambers, B.J., Christie, P., 1998. Organic manure phosphorus accumulation, mobility and management. Soil Use Manag. 14, 154–159. https://doi.org/10.1111/j.1475-2743.1998.tb00634.x

Stackpoole, S.M., Stets, E.G., Sprague, L.A., 2019. Variable impacts of contemporary versus legacy agricultural phosphorus on US river water quality. Proc. Natl. Acad. Sci. 116, 20562–20567. https://doi.org/10.1073/pnas.1903226116

Steffen, W., Richardson, K., Rockstrom, J., Cornell, S.E., Fetzer, I., Bennett, E.M., Biggs, R., Carpenter, S.R., de Vries, W., de Wit, C.A., Folke, C., Gerten, D., Heinke, J., Mace, G.M., Persson, L.M., Ramanathan, V., Reyers, B., Sorlin, S., 2015. Planetary boundaries: Guiding human development on a changing planet. Science 347, 1259855–1259855. https://doi.org/10.1126/science.1259855

Sterner, R.W., Elser, J.J., 2017. Ecological stoichiometry. Princeton university press.

Swaney, D.P., Hong, B., Ti, C., Howarth, R.W., Humborg, C., 2012. Net anthropogenic nitrogen inputs to watersheds and riverine N export to coastal waters: a brief overview. Curr. Opin. Environ. Sustain., Carbon and nitrogen cycles 4, 203–211. https://doi.org/10.1016/j.cosust.2012.03.004

Tian, H., Chen, G., Liu, M., Zhang, C., Sun, G., Lu, C., Xu, X., Ren, W., Pan, S., Chappelka, A., 2010. Model estimates of net primary productivity, evapotranspiration, and water use efficiency in the terrestrial ecosystems of the southern United States during 1895–2007. For. Ecol. Manag. 259, 1311–1327.

Tian, H., Chen, G., Lu, C., Xu, X., Hayes, D.J., Ren, W., Pan, S., Huntzinger, D.N., Wofsy, S.C., 2015. North American terrestrial CO2 uptake largely offset by CH4 and N2O emissions: toward a full accounting of the greenhouse gas budget. Clim. Change 129, 413–426. https://doi.org/10.1007/s10584-014-1072-9

Tian, H., Melillo, J., Lu, C., Kicklighter, D., Liu, M., Ren, W., Xu, X., Chen, G., Zhang, C., Pan, S., 2011. China's terrestrial carbon balance: contributions from multiple global change factors. Glob. Biogeochem. Cycles 25.

Tian, H., Xu, R., Pan, S., Yao, Y., Bian, Z., Cai, W.-J., Hopkinson, C.S., Justic, D., Lohrenz, S., Lu, C., Ren, W., Yang, J., 2020. Long-Term Trajectory of Nitrogen Loading and Delivery From Mississippi River Basin to the Gulf of Mexico. Glob. Biogeochem. Cycles 34, e2019GB006475. https://doi.org/10.1029/2019GB006475

Tian, H., Yang, J., Xu, R., Lu, C., Canadell, J.G., Davidson, E.A., Jackson, R.B., Arneth, A., Chang, J., Ciais, P., Gerber, S., Ito, A., Joos, F., Lienert, S., Messina, P., Olin, S., Pan, S., Peng, C., Saikawa, E., Thompson, R.L., Vuichard, N., Winiwarter, W., Zaehle, S., Zhang, B., 2019. Global soil nitrous oxide emissions since the preindustrial era estimated by an ensemble of terrestrial biosphere models: Magnitude, attribution, and uncertainty. Glob. Change Biol. 25, 640–659. https://doi.org/10.1111/gcb.14514

Van Drecht, G., Bouwman, A.F., Boyer, E.W., Green, P., Siebert, S., 2005. A comparison of global spatial distributions of nitrogen inputs for nonpoint sources and effects on river nitrogen export: GLOBAL NEWS-COMPARISON OF GLOBAL NITROGEN INPUTS. Glob. Biogeochem. Cycles 19, n/a-n/a. https://doi.org/10.1029/2005GB002454

Wang, Z., Tian, H., Yang, J., Shi, H., Pan, S., Yao, Y., Banger, K., Yang, Q., 2020. Coupling of Phosphorus Processes With Carbon and Nitrogen Cycles in the Dynamic Land

Ecosystem Model: Model Structure, Parameterization, and Evaluation in Tropical Forests. J. Adv. Model. Earth Syst. 12, e2020MS002123. https://doi.org/10.1029/2020MS002123

Xu, R., Pan, S.F., Chen, J., Chen, G.S., Yang, J., Dangal, S.R.S., Shepard, J.P., Tian, H.Q., 2018. Half-century ammonia emissions from agricultural systems in Southern Asia: Magnitude, spatiotemporal patterns, and implications for human health. GeoHealth 2, 40–53.

Yang, Q., Tian, H., Friedrichs, M.A., Hopkinson, C.S., Lu, C., Najjar, R.G., 2015. Increased nitrogen export from eastern North America to the Atlantic Ocean due to climatic and anthropogenic changes during 1901–2008. J. Geophys. Res. Biogeosciences 120, 1046–1068.

Yu, Z., Lu, C., 2018. Historical cropland expansion and abandonment in the continental U.S. during 1850 to 2016. Glob. Ecol. Biogeogr. 27, 322–333. https://doi.org/10.1111/geb.12697

Yuan, Z., Jiang, S., Sheng, H., Liu, Xin, Hua, H., Liu, Xuewei, Zhang, Y., 2018. Human Perturbation of the Global Phosphorus Cycle: Changes and Consequences. Environ. Sci. Technol. 52, 2438–2450. https://doi.org/10.1021/acs.est.7b03910

Zanon, J.A., Favaretto, N., Goularte, G.D., Dieckow, J., Barth, G., 2019. Manure application at long-term in no-till: Effects on runoff, sediment and nutrients losses in high rainfall events. Agric. Water Manag. 105908.

Chapter 2. Connecting N and P cycles across terrestrial and aquatic ecosystems in the DLEM

Abstract

Terrestrial ecosystems have received large amounts of anthropogenic nitrogen (N) and phosphorus (P) inputs and are a source of N and P enrichment in water bodies. Characterizing linkages between N and P cycles in land and aquatic systems is critical for understanding the N and P dynamics along the land-ocean aquatic continuum. However, modeling tools that effectively couple terrestrial and aquatic biogeochemical N and P processes are still in their infancy. In this study, we incorporated the biogeochemical processes of riverine N and P dynamics and a water transport module into a process-based biogeochemical model, Dynamic Land Ecosystem Model (DLEM). The biogeochemical processes in aquatic systems were linked to those in terrestrial ecosystems through leaching and erosion processes. The full consideration of terrestrial and aquatic processes in the DLEM can provide both prognostic and predictive assessments of interactions of N and P dynamics among soil, water, and vegetation.

1. Introduction

Evaluating N and P loading and export from land to ocean is critical for sustainable nutrient management and water security. Numerous statistical and mechanistic models have been used to estimate N and P losses from terrestrial ecosystems to waterways. The net anthropogenic nitrogen/phosphorus inputs (NANI/NAPI) method is a classic statistical approach to link terrestrial water and nutrient budgets to water quality (Hu et al., 2020; Metson et al., 2017). Watershed models have been developed to simulate distributed landscape N and P generation by combining statistical and mechanistic approaches. However, terrestrial N and P cycling processes are still over-simplified in these watershed models compared with terrestrial biogeochemical models (Harrison et al., 2019). As a result, these models can only simulate the loading of a limited number of N and P species. Total N and Total P loads are the only variable that can be simulated in many watershed models, e.g., the SPARROW and the IMAGE–GNM models (Alexander et al., 2008; Beusen et al., 2015). In contrast, terrestrial biogeochemical models are capable of simulating a relatively complete N and P cycle in terrestrial ecosystems, as

well as investigating the effects of multiple environmental factors on N and P fluxes and pools over long time scales (Goll et al., 2017; Wang et al., 2020; Yang et al., 2013).

In-stream N and P processes within many watershed models have generally only considered N and P retention, while the interactions between various N and P components have often been neglected (Robson, 2014). Nutrient fluxes to aquatic ecosystems are strongly influenced by climate, land-use conditions, and soil N and P concentration in terrestrial ecosystems (Bennett et al., 2001). Riverine biogeochemical and physical processes during riverine transport also matter, especially for large basins where the residence time of nutrients inside rivers is longer than the time-scale of in-channel nutrient transformation (Ruttenberg, 2003). Different from watershed models, aquatic N and P models often incorporate more N and P components and complex biogeochemical processes (Robson, 2014). For example, the RIVE and CE–QUAL–W2 models are capable of simulating N and P transfers and stocks of various forms between abiotic environment, organic matter, and inorganic matter (Aissa-Grouz et al., 2018; Cole and Wells, 2006). Nevertheless, aquatic N and P models usually rely on accurate boundary conditions determined from water samples or land inputs. The gap between a single N or P variable (e.g., TN, TP) output from watershed models and multiple N and P variables in the boundary condition required by aquatic models can create difficulties when trying to link two different types of models (Debele et al., 2008). In contrast, terrestrial biogeochemical models usually incorporate several N and P variables and can provide detailed boundary information for aquatic models. Therefore, coupling the terrestrial nutrient cycle, including soil, plant, and microbial processes, with the nutrient cycle in aquatic ecosystems in a modeling framework can provide more detailed information regarding the variations of multiple nutrient variables.

Connecting N and P cycling across terrestrial and aquatic ecosystems can improve our understanding of how human activities and climate alter N and P dynamics along the land-ocean continuum at a long-term scale. DLEM (the C and N coupled version) has been applied to investigate riverine exports of C and N from the MRB (Ren et al., 2016a; Tian et al., 2020). This study improved the N processes in the DLEM terrestrial-aquatic scheme based on a newly developed water transport module (Yao et al., 2021, 2020). Moreover, we developed and incorporate the biogeochemical processes of riverine P dynamics module into DLEM terrestrial-

aquatic scheme based on the recently developed land P component (Wang et al., 2020) and the water transport module.

2. The Land component

DLEM is an integrated process-based model that couples terrestrial biophysics, plant phenology, soil biogeochemistry, vegetation dynamics, and disturbance to simulate the responses of water, carbon, N, and P cycling to anthropogenic activities and climate variability (Figure 2-1a). The overview of the land component of DLEM has been reported in previous publications (Liu et al., 2013; Pan et al., 2015; Pan et al. 2020; Tian et al., 2010, 2016). DLEM is capable of simulating key N-related processes, including mineralization, nitrification, denitrification, immobilization, volatilization, N uptake, N fixation, and N leaching (Tian et al., 2012; Xu et al., 2018; Tian 2019). The P processes and C-N-P interactions have been coupled into the DLEM, where the C, N, and P cycles are fully coupled through photosynthesis, allocation, turnover, nutrient uptake, and decomposition (Wang et al., 2020). Other land P processes in the DLEM include weathering from the mineral P pool, adsorption and desorption between the labile P pool and the secondary mineral P pool, and occlusion of the secondary mineral P to the occluded P pool. The biogeochemical and hydrological cycles were coupled in the model to simulate daily, spatially explicit patterns of water runoff, and nutrient and carbon leaching, which can serve as water and nutrient sources to the aquatic module (Ren et al., 2016b; Tian et al., 2020, 2015; Yang et al., 2015).

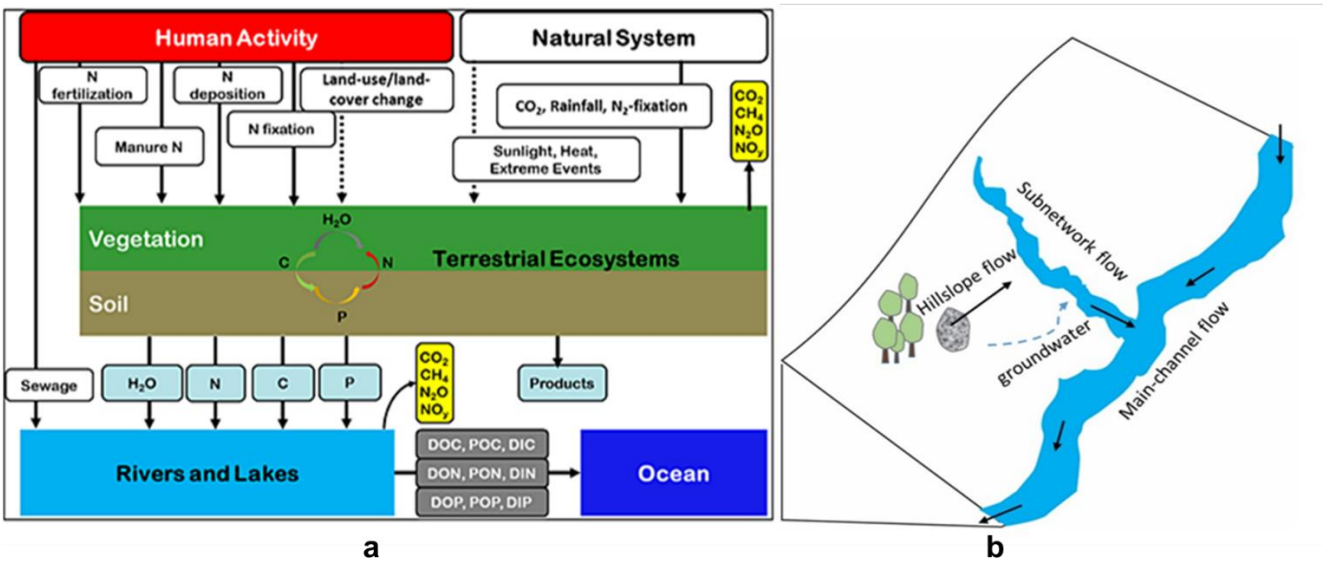

Figure 2-1. (a) The general framework of DLEM terrestrial–aquatic interface, which is coupled with (b) conceptual model of the scale-adaptive water transport scheme.

3. Water and nutrient processes within each grid cell

The water and nutrient transport module in the previous version of DLEM only considered the transport process between grid cells. Recently, a scale-adaptive water transport scheme (Model of Scale Adaptive River Transport, MOSART) (Li et al., 2013) was coupled into DLEM to quantify the daily river discharge of each grid cell in the landform (Figure 2-1b). The newly developed module separates the water transport within the grid cells into three sub-grid processes: hillslope flow, subnetwork flow, and main channel flow. The hillslope flow merges water from surface runoff and flows into subnetworks. The subnetwork flow receives water from hillslope flow and subsurface runoff, and drains into the main river channel of the unit. The main river channel receives water from local subnetworks and upstream grid cells, and ultimately flows into the downstream grid cell. The river-routing processes are fully physically based and simulated with the kinematic wave method (Te Chow, 2010), which requires physical variables (channel length, bankfull depth, channel slope, and channel roughness) derived from fine-resolution hydrography data (Li et al., 2015). This feature of MOSART allows our aquatic module to operate at a relatively coarse spatial resolution but without a decrease in the simulation accuracy. Vertical soil moisture movement from the earth surface to the root zone

was lumped together, and the lateral groundwater transport from a groundwater pool to the local subnetworks was simulated with parameterized outflow rates. Additional biogeochemical processes have been included in the scale-adaptive water transport scheme, which specifically addresses the small-river processes aligned with the advanced features of the water transport scheme (Yao et al., 2021, 2020).

The advective transport of P components through the subnetwork and main channel (Figure 2-1b) can be expressed as:

$$\frac{dM_{x,sub}}{dt} = F_{x,hill} + F_{x,subsurface} - F_{x,sub-main} \quad (1)$$

$$\frac{dM_{x,main}}{dt} = \sum_{i=1}^{n} F_{x,up,i} + F_{x,sub-main} - F_{x,down} \quad (2)$$

where $M_{x,sub}$ is advective water transport in subnetwork flow (m^3); $F_{x,hill}$ and $F_{x,subsurface}$ are flow rates in hillslope flow and subsurface flow, respectively, calculated in DLEM land module; $F_{x,sub-main}$ is flow rate from subnetwork to main-channel; $M_{x,main}$ is advective water transport in main-channel flow; $F_{x,up,i}$ and $F_{x,down}$ are the flow rates of upstream grid cell *i* and the main-channel flow rate to downstream grid cell, respectively. The advective transport of nutrients through hillslope flow, subnetwork flow, and main-channel is consistent with water transport.

The transport rates of water and nutrients in the subnetwork flow and the main channel flow were calculated based on the Kinematic Wave Method, a simplified version of Saint-Venant equations that ignores backwater effects (Chow et al., 1988), which is given as:

$$\begin{cases} \frac{\partial Q}{\partial x} + B\frac{\partial h}{\partial t} = q \\ S_f - S_0 = 0 \end{cases} \quad (3)$$

where Q is outflow rate ($m^3\ s^{-1}$); x is the direction of flow; h is the depth of river channel (m) and B is the width of the river channel (m) (we assumed the channel is rectangular); q is lateral inflow from subnetwork or main channel ($m^3\ s^{-1}$); S_f is friction gradient and S_0 is channel slope. The equations were solved using the Newton–Raphson method (Stępień, 1984). The river-network parameters (e.g., flow direction, channel length, and channel slope) derived from a global river network database (Wu et al., 2012), and geomorphological parameters (e.g., channel width and channel depth) were obtained according to empirical hydraulic geometry relationships

(Li et al., 2013, 2015) or remote sensing-based water surface extent data (Homer et al., 2015; Yamazaki et al., 2014).

4. Nitrogen processes in the terrestrial-aquatic scheme

4.1 N yields from terrestrial ecosystems

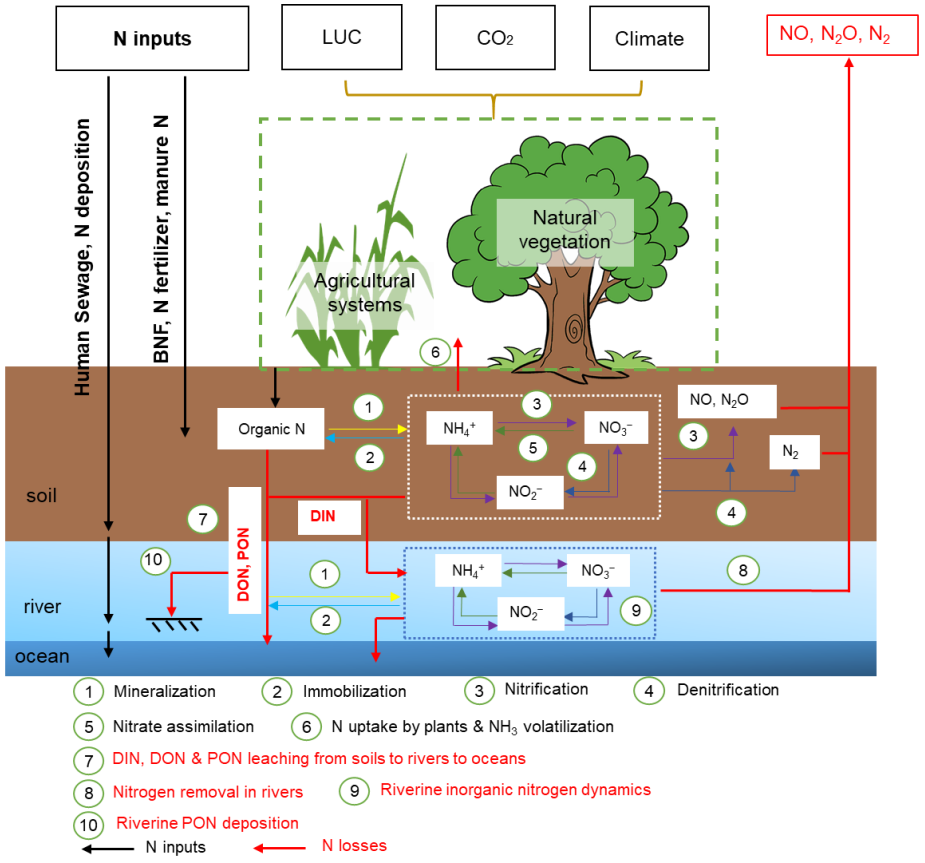

Figure 2-2. The conceptual framework of key N processes in the DLEM (Tian et al., 2020).

In DLEM, N yields from terrestrial ecosystems include ammonium (NH_4^+), nitrate (NO_3^-), dissolved organic N (DON), and particulate organic N (PON) (Figure 2-2). DIN (NH_4^+ and NO_3^-) and DON enter aquatic systems through leaching while PON enters aquatic systems through erosion during runoff generation processes. Yields of NH_4^+, NO_3^-, and DON (g N m^{-2}) in each grid at daily scale are calculated as:

$$Y_{NH4} = SNH \cdot \frac{Q}{Q+W} / b_{NH4} \quad (4)$$

$$Y_{NO3} = SNO \cdot \frac{Q}{Q+W} / b_{NO3} \quad (5)$$

$$Y_{DON} = DON \cdot \frac{Q}{Q+W} \quad (6)$$

where SNH and SNO represent soil available NH_4^+ and soil available NO_3^- pools (g N m^{-2}), respectively. DON represents dissolved organic N pools (g N m^{-2}). Q is water yield (surface runoff and subsurface runoff) (mm) of the terrestrial ecosystem and W is the soil water content (mm) in the surface layer (0.5 m); b_{NH4} and b_{NO3} are the parameter controlling the adsorption capacity of soil for NH_4^+ and NO_3^- (unitless).

Yield of PON is calculated as follows:

$$Y_{PON} = E \cdot C_{PON} \quad (7)$$

where C_{PON} represents the concentration of total organic N in the surface soil column (g N g^{-1} soil); E is the sediment yield due to soil erosion (g soil m^{-2}) and was calculated according to the modified universal soil loss equation (MUSLE) (Neitsch et al., 2011; Williams, 1995).

$$E = a \cdot \left(Q \cdot q_{peak} \cdot \ area\right)^b \cdot K_{USLE} \cdot C_{USLE} \cdot P_{USLE} \cdot LS_{USLE} \cdot CFRG \quad (8)$$

where q_{peak} is daily peak runoff rate (m^3 s^{-1}) and $area$ is the land area (ha) within the grid (we assumed each grid represents a hydrological unit; Tesfa et al., 2014); K_{USLE}, C_{USLE}, P_{USLE}, LS_{USLE} represent factors for soil erodibility, cover and management, support practice, and topography , respectively; $CFRG$ is the course fragment factor; a and b are the fit coefficients in the equation.

4.2 In-stream N processes

The major within-stream N dynamics include lateral N transport, mineralization of organic matter, particle organic matter deposition, nitrification, and denitrification. The calculations of these biochemical processes were improved based on the original version of DLEM (Yang et al., 2015). Riverine N dynamics were calculated during both subnetwork flow and main channel flow. The conservation equations for the riverine N constituents are:

$$\frac{\Delta M_{PON}}{\Delta t} = F_{PON} + v_s A_s c_{PON} - R_{PON} M_{PON} \quad (9)$$

$$\frac{\Delta M_{DON}}{\Delta t} = F_{DON} - R_{DON} M_{DON} \quad (10)$$

$$\frac{\Delta M_{NO3}}{\Delta t} = F_{NO3} + k_n V c_{NH4} - k_d V c_{NO3} \quad (11)$$

$$\frac{\Delta M_{NH4}}{\Delta t} = F_{a,NH4} + R_{DON} M_{DON} + R_{PON} M_{PON} - k_n V c_{NH4} + k_d V c_{NO3} \quad (12)$$

where M_x is the total mass of constituent x (PON, DON, NO_3^-, NH_4^+) in the main channel or subnetwork (g N), c_x is the concentration of x in water body, Δt is the time step, F is advective N transport (g N d^{-1}), R_{DOM} and R_{PON} are the mineralization rate coefficients of organic N (d^{-1}), k_n and k_d are the rates of nitrification and denitrification (g N d^{-1}), respectively, V is the total volume of the water body (m^3), and v_s is the deposition rate (m d^{-1}).

The net deposition velocity of particulate organic N is estimated by Stokes' law (Thomann and Mueller, 1987):

$$v_s = 0.033634 (\rho_s - \rho_w) d^2 \quad (13)$$

where ρ_s and ρ_w are the density of water and particulate matter (g cm^{-3}), respectively; d is the average diameter of the particulate matter (μm) (Chapra, 2008).

The mineralization rate of the organic N is linearly correlated to the respiration rate of organic matter, which can be simulated by a first-order kinetics equation with temperature dependence:

$$R_{DON,PON} = k_m (Q_{10})^{\frac{T-T_s}{10}} \quad (14)$$

where k_m is the reduction rate (m d^{-1}), Q_{10} is the change fraction of N reaction rates at a temperature change of 10 °C, T is the water temperature (° C), and T_s is the reference temperature (20 °C).

The inorganic N removal rate is estimated as:

$$k_{d,n} = 1 - exp \frac{-V_f}{H_l} \quad (15)$$

where V_f is the settling velocity for N species (m s^{-1}), and H_l is the hydraulic load (m s^{-1}) for rivers and lakes, which can be expressed as:

$$H_l = \frac{Q}{A_s} \quad (16)$$

where Q is discharge (m^3 s^{-1}), A_s is the surface area of the water body (m^2), in which the surface area of the main channel was derived from remote sensing, and surface area of small streams was estimated as the product of the known stream length and the following empirical estimate of the width (Allen et al., 2018):

$$width = Q^{\frac{3}{5r+3}} \ (0.5\,A^{0.42})_i^{\frac{r-1}{r+0.6}} \left(8.1(gS)^{0.5}k^{-\frac{1}{6}}14^{-\frac{5}{3}}(1-\frac{1}{r+1})\right)^{-\frac{3}{5r+3}} \quad (17)$$

$$k = (8.1g^{0.5}n)^6 \quad (18)$$

where A is upstream area (ha), k is a bed roughness length scale, r is a shape parameter, g is gravitational acceleration, n is the Gauckler-Manning friction coefficient ($ms^{-1/3}$), and S is the channel slope (which can be obtained from topographic data).

5. Development of aquatic P module

5.1. P yields from terrestrial ecosystems

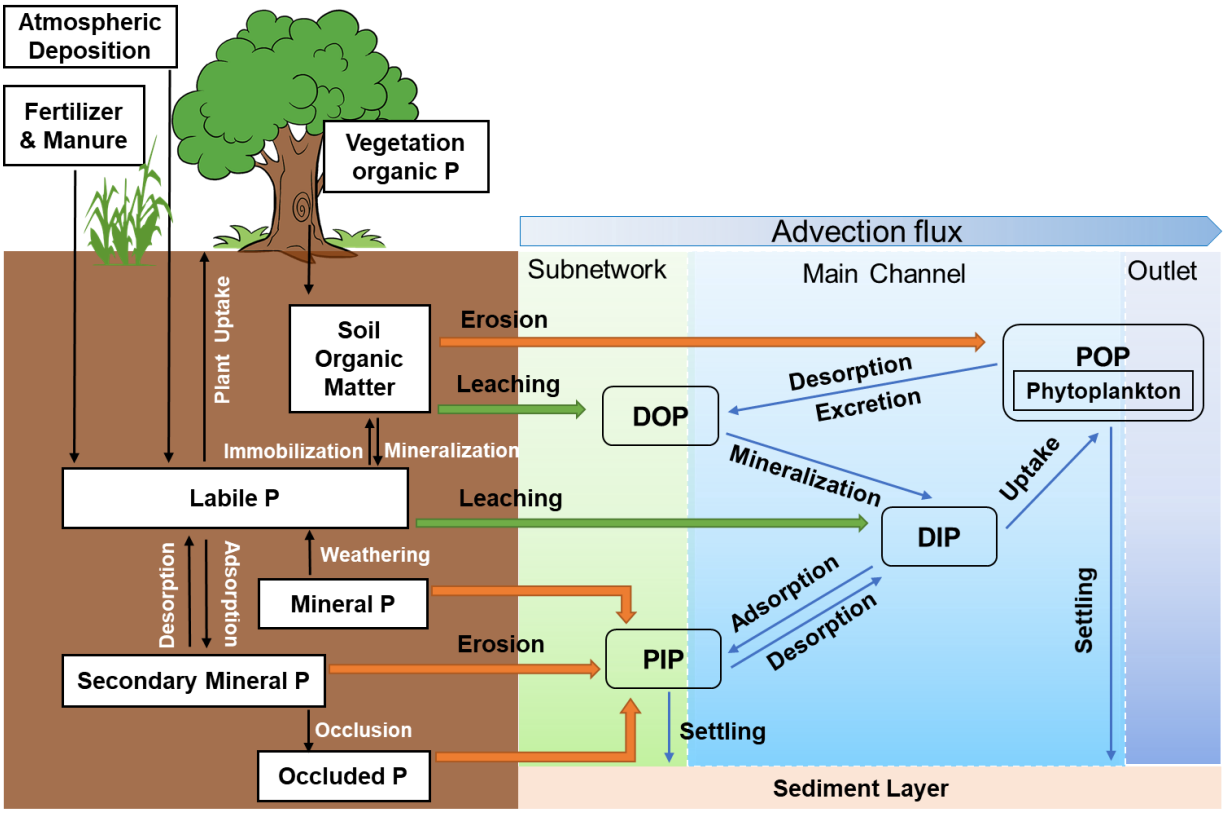

Figure 2-3. The coupled terrestrial and aquatic P cycling processes in the Dynamic Land Ecosystem Model–Terrestrial/Aquatic scheme.

Phosphorus yields from terrestrial ecosystems include dissolved inorganic phosphorus (DIP), dissolved organic phosphorus (DOP), particulate organic phosphorus (POP), and particulate inorganic phosphorus (PIP) (Figure 2-3). DIP is derived from the labile P pool and

enters aquatic systems through leaching and runoff. Similarly, DOP is the dissolved organic form of P, and can be leached out of soil through surface or subsurface runoff. Both POP and PIP enter aquatic systems through soil erosion during runoff generation processes. POP is derived from the organic matter pool while PIP is derived from the mineral P pool, the secondary mineral P pool, and the occluded P pool. Daily Y_x (g P m^{-2} day^{-1}), the yield of constituent *x* (DIP and DOP) in each grid, is calculated as:

$$Y_{DIP} = SLP \cdot \frac{Q}{Q+W} / \, b_{DIP} \tag{19}$$

$$Y_{DOP} = DOP \cdot \frac{Q}{Q+W} \tag{20}$$

where *SLP* and *DOP* represent soil labile P and dissolved organic P pools (g P m^{-2}), respectively; Q is water yield (surface runoff and subsurface runoff) (mm) of the terrestrial ecosystem and W is the soil water content (mm) in the surface layer (0.5 m); b_{DIP} is the parameter controlling the adsorption capacity of soil for labile P (unitless). Yields of POP and PIP are as follows:

$$Y_{POP} = E \cdot C_{POP} \tag{21}$$

$$Y_{PIP} = E \cdot (C_{MP} + C_{SMP} + C_{OP}) \tag{22}$$

where $C_{POP,MP,SMP,OP}$ represents the concentration of total organic P, mineral P, secondary mineral P, and occluded P in the surface soil column (g P g^{-1} soil); E is the sediment yield due to soil erosion (g soil m^{-2}) (equation 8) (Neitsch et al., 2011; Williams, 1995).

5.2. In-stream P processes

The major in-stream P dynamics include decomposition and mineralization of organic matter, particle organic and inorganic matter deposition, P uptake and release by autotrophs, and adsorption and desorption between particle matter and dissolved P (Figure 2-3). Autotrophs assimilate DIP into cellular material, and form POP. DOP is eventually released or excreted by phytoplankton and is then further broken down to DIP through mineralization. DIP tends to attach to sediment particles and, thus, transforms to PIP. The net deposition of POP and PIP from water as sediment is a major P retention process in rivers. Riverine P dynamics were calculated within each grid-cell throughout both subnetwork flow and main channel flow. The dynamics of riverine P constituents are given by:

$$\frac{\Delta M_{POP}}{\Delta t} = F_{POP} + U_{DIP} - v_s A_s c_{POP} - R_{POP} M_{POP} \quad (23)$$

$$\frac{\Delta M_{DOP}}{\Delta t} = F_{DOP} + R_{POP} M_{POP} - R_{DOP} M_{DOP} \quad (24)$$

$$\frac{\Delta M_{DIP}}{\Delta t} = F_{DIP} + R_{DOP} M_{DOP} - U_{DIP} - A_{DIP} \quad (25)$$

$$\frac{\Delta M_{PIP}}{\Delta t} = F_{PIP} + A_{DIP} - v_s A_s c_{PIP} \quad (26)$$

where M_x is the total mass of constituent x (DIP, DOP, POP, PIP) in the main channel or subnetwork (g P); c_x is the concentration of x in water bodies (mg L^{-1}); Δt is the time step (hour); F_x is advective P transport from upstream or land (g P $hour^{-1}$) and the land P inputs are assumed to enter into streams at a constant rate within a day; U_{DIP} represents the uptake of phosphate by phytoplankton (g P $hour^{-1}$); v_s is the net deposition rate (m $hour^{-1}$); A_s is the surface area of the water body (m^2) obtained from the remote sensing products (Allen and Pavelsky, 2018; Homer et al., 2015); R_{POP} represents the desorption and excretion rate of particulate organic P ($hour^{-1}$); R_{DOP} is the mineralization rate coefficient of dissolved organic P ($hour^{-1}$); and A_{DIP} is the net adsorption of DIP (g P $hour^{-1}$) (negative value represents the desorption of PIP).

The excretion and mineralization rates of the organic P are consistent with the decomposition rate of organic matter, which can be estimated by a first-order kinetics equation with temperature dependence:

$$R_{DOP,POP} = k_{mDOP,mPOP} (Q_{10})^{\frac{T-T_s}{10}} \quad (27)$$

where $k_{mDOP,mPOP}$ is the base of excretion and mineralization rates of the organic P ($hour^{-1}$); Q_{10} is the change fraction of the P reaction rate for a temperature change of 10 °C; T is the water temperature (°C) and T_s is the reference temperature (20 °C).

The uptake of DIP by phytoplankton is linearly related to primary production in aquatic ecosystems, with C, N, and P coupling in this process. The uptake of DIP is estimated according to the method proposed in Maavara et al. (2015, 2017), which assumes the primary production is limited by P.

$$U_{DIP} = Pro \cdot RPC_{phyto} \quad (28)$$

$$Pro = Pro_{max} \cdot \frac{c_{DIP}}{K_s + c_{DIP}} \quad (29)$$

where Pro is primary production in aquatic ecosystems (g C hour^{-1}) and RPC_{phyto} is the P:C ratio of phytoplankton (set as 0.025 according to the Redfield ratio); K_s is the half-saturation DIP concentration (0.62–21.7 mg L^{-1}); Pro_{max} is the maximum value of primary production under nutrient saturated condition (g C hour^{-1}), which is calculated as:

$$Pro_{max} = B \cdot P_{chl} \cdot V \cdot M \quad (30)$$

where B is average depth-integrated chlorophyll concentration (mg Chl-a km^{-3}) which is calculated based the method provided by Reynolds (2006); P_{chl} is the maximum chlorophyll-specific carbon fixation rate (2.5 g C (mg Chl-a)$^{-1}$ hour^{-1}), V is water volume (km^3), and M is the metabolic correction factor for water temperature, which is equal to 1 when water temperature is higher than 28 ℃, and decreases with temperatures with a Q_{10} of 2 (Lewis Jr, 2011).

The adsorption-desorption process is estimated by using the kinetic form of the Langmuir sorption isotherm equation (McGechan and Lewis, 2002; van der Zee et al., 1989):

$$A_{DIP} = k_a \cdot c_{DIP} \cdot (A_{max} - M_{PIP}) - k_d \cdot M_{PIP} \quad (31)$$

where k_a is adsorption rate constant (m^3 g^{-1} hour^{-1}) and k_d is and desorption rate constant (hour^{-1}), respectively; A_{max} is maximum P sorption capacity of particulate matter (g P). The major parameters introduced in this study were given in Table 2-1.

Table 2-1. Phosphorus Export-Related Parameters in the Dynamic Land Ecosystem Model-Terrestrial/Aquatic scheme.

Parameters	Unit	Values in DLEM	Description	References
b_{DIP}	dimensionless	200–800	Adsorption capacity of soil for labile P	Calibrated
a	dimensionless	11.8–20.2	Coefficient in the MUSLE	(Neitsch et al., 2011)
b	dimensionless	0.56	Coefficient in the MUSLE	(Neitsch et al., 2011)
d	μm	1–10	Average diameter of the particulate matter	(Chapra, 2008)

Parameters	Unit	Values in DLEM	Description	References
Q_{10}	dimensionless	2	Change fraction of the P reaction rate for a temperature change of 10 ºC;	(Kätterer et al., 1998)
k_{mDOP}	$hour^{-1}$	0.00008–0.0004	Base of mineralization rate of DOP	(Koehler et al., 2012)
k_{mPOP}	$hour^{-1}$	0.00002–0.0004	Base of excretion and desorption rates of POP	(Enríquez et al., 1993)
k_a	$m^3\ g^{-1}\ hour^{-1}$	0.416	Adsorption rate in water	(van der Zee et al., 1989)
k_d	$hour^{-1}$	0.15	Desorption rate in water	(van der Zee et al., 1989)

5.3. Parameter sensitivity analysis

Six key parameters controlling P fluxes were selected to conduct local sensitivity analyses based on our model calibration experience (Table 2-2). The riverine DIP export is most sensitive to the b_{DIP} and k_d, reflecting the important role of land leaching and adsorption-desorption processes within streams. The riverine DOP export shows similar responses (varied around 2-3%) to a, k_{mDOP}, and k_{mPOP}. Changes in POP and PIP are predominantly controlled by the land erosion process (a). The TP export is generally more sensitive to land P inputs-related parameters (b_{DIP} and a) compared with in-steam retention-related parameters (d).

Table 2-2. Sensitivity of riverine P fluxes to major parameters in DLEM

Parameters	Changes in Parameters	Changes in DIP	Changes in DOP	Changes in POP	Changes in PIP	Changes in TP
b_{DIP}	10%	-7.33%	0.00%	0.00%	-0.01%	-1.99%
	-10%	8.96%	0.00%	0.00%	0.01%	2.43%
a	10%	0.09%	3.16%	10.72%	10.40%	7.16%
	-10%	-0.07%	-2.59%	-8.78%	-8.52%	-5.87%
d	10%	-0.02%	-0.23%	-0.98%	-1.23%	-0.82%
	-10%	0.02%	0.22%	0.90%	1.17%	0.78%
k_{mDOP}	10%	0.64%	-2.67%	0.00%	0.00%	0.00%

	-10%	-0.67%	2.79%	0.00%	0.00%	0.00%
k_{mPOP}	10%	0.14%	2.38%	-2.74%	0.00%	0.00%
	-10%	-0.14%	-2.47%	2.84%	0.00%	0.00%
k_d	10%	6.25%	0.00%	0.00%	-2.71%	0.07%
	-10%	-6.66%	0.00%	0.00%	2.89%	-0.08%

Note: the simulations were conducted in the MRB

6. Discussion

The delivery of N and P from land to ocean through river systems is the major pathway for N and P leaving terrestrial and entering coastal ecosystems. Studies on N and P loading across the land-ocean interface call for a connection of nutrient fluxes between terrestrial and aquatic ecosystems. However, due to the physical and biological differences between aquatic and terrestrial ecosystems, the modeling approaches for terrestrial and aquatic biogeochemistry have developed somewhat independently (Bouwman et al., 2013). Our study fills in a critical gap by integrating a terrestrial biogeochemical model with an aquatic biogeochemical module and connecting the cycle of different N and P species between terrestrial and aquatic ecosystems. The DLEM-Terrestrial/Aquatic scheme is capable of simulating N and P fluxes across soil and vegetation to headwaters, main-channel rivers, and eventually coastal oceans. The full consideration of terrestrial and aquatic processes in the DLEM-Terrestrial/Aquatic scheme can provide both prognostic and predictive assessments of interactions of N and P dynamics among soil, water, and vegetation. Furthermore, impacts of human disturbances on N and P loading can be tracked under multiple environmental conditions. Independent aquatic models usually rely on detailed boundary conditions and are applied at relatively short-time scales (hour, day, month, year), while terrestrial biosphere models can be applied over long-time scales (decade, century). With terrestrial modules providing long-time scale nutrient input for aquatic modules, the DLEM-Terrestrial/Aquatic scheme can be used to investigate N and P loading at time scales from days to centuries. Simultaneously, the scale-adaptive water and nutrient transport scheme can simulate the delivery process at the sub-grid level by incorporating hillslope flow, subnetwork flow, and main-channel flow. Thus, our model is capable of simulating N and P transport at multiple spatial scales from basin to continental to global (Yao et al., 2020).

7. Conclusion

In this study, a riverine N and P module were coupled with a terrestrial biogeochemical model, the DLEM, to simulate N and P dynamics across the land-aquatic interface. The model linked N and P cycles in terrestrial and aquatic ecosystems by leaching and erosion processes. Nutrients are transported from land, through hillslope flow, subnetwork flow, and main-channel flow, and finally to river outlet. The model is capable of simulating the long-term dynamics of the loading and exports of four N species (NO_3^-, NH_4^+, DON, and PON) as well as four P species (DIP, DOP, PIP, and POP). The model can be applied to evaluate the impacts of climate and anthropogenic activities on N and P dynamics along the land-ocean continuum.

References

Aissa-Grouz, N., Garnier, J., Billen, G., 2018. Long trend reduction of phosphorus wastewater loading in the Seine: determination of phosphorus speciation and sorption for modeling algal growth. Environ. Sci. Pollut. Res. 25, 23515–23528. https://doi.org/10.1007/s11356-016-7555-7

Alexander, R.B., Smith, R.A., Schwarz, G.E., Boyer, E.W., Nolan, J.V., Brakebill, J.W., 2008. Differences in Phosphorus and Nitrogen Delivery to The Gulf of Mexico from the Mississippi River Basin. Environ. Sci. Technol. 42, 822–830. https://doi.org/10.1021/es0716103

Allen, G.H., Pavelsky, T.M., 2018. Global extent of rivers and streams. Science 361, 585–588. https://doi.org/10.1126/science.aat0636

Allen, G.H., Pavelsky, T.M., Barefoot, E.A., Lamb, M.P., Butman, D., Tashie, A., Gleason, C.J., 2018. Similarity of stream width distributions across headwater systems. Nat. Commun. 9, 1–7.

Bennett, E.M., Carpenter, S.R., Caraco, N.F., 2001. Human Impact on Erodable Phosphorus and Eutrophication: A Global Perspective. BioScience 51, 227. https://doi.org/10.1641/0006-3568(2001)051[0227:HIOEPA]2.0.CO;2

Beusen, A.H.W., Van Beek, L.P.H., Bouwman, A.F., Mogollón, J.M., Middelburg, J.J., 2015. Coupling global models for hydrology and nutrient loading to simulate nitrogen and phosphorus retention in surface water – description of IMAGE–GNM and analysis of performance. Geosci. Model Dev. 8, 4045–4067. https://doi.org/10.5194/gmd-8-4045-2015

Bouwman, A.F., Bierkens, M.F.P., Griffioen, J., Hefting, M.M., Middelburg, J.J., Middelkoop, H., Slomp, C.P., 2013. Nutrient dynamics, transfer and retention along the aquatic continuum from land to ocean: towards integration of ecological and biogeochemical models. Biogeosciences 10, 1–22. https://doi.org/10.5194/bg-10-1-2013

Chapra, S.C., 2008. Surface water-quality modeling. Waveland press.

Chow, V.T., Maidment, D.R., Mays, L.W., 1988. Applied hydrology.

Cole, T.M., Wells, S.A., 2006. CE-QUAL-W2: A two-dimensional, laterally averaged, hydrodynamic and water quality model, version 3.5.

Debele, B., Srinivasan, R., Parlange, J.-Y., 2008. Coupling upland watershed and downstream waterbody hydrodynamic and water quality models (SWAT and CE-QUAL-W2) for better water resources management in complex river basins. Environ. Model. Assess. 13, 135–153. https://doi.org/10.1007/s10666-006-9075-1

Enríquez, S., Duarte, C.M., Sand-Jensen, K.A.J., 1993. Patterns in decomposition rates among photosynthetic organisms: the importance of detritus C: N: P content. Oecologia 94, 457–471.

Goll, D.S., Vuichard, N., Maignan, F., Jornet-Puig, A., Sardans, J., Violette, A., Peng, S., Sun, Y., Kvakic, M., Guimberteau, M., Guenet, B., Zaehle, S., Penuelas, J., Janssens, I., Ciais, P., 2017. A representation of the phosphorus cycle for ORCHIDEE (revision 4520). Geosci. Model Dev. 10, 3745–3770. https://doi.org/10.5194/gmd-10-3745-2017

Harrison, J.A., Beusen, A.H., Fink, G., Tang, T., Strokal, M., Bouwman, A.F., Metson, G.S., Vilmin, L., 2019. Modeling phosphorus in rivers at the global scale: recent successes, remaining challenges, and near-term opportunities. Curr. Opin. Environ. Sustain.,

Environmental Change Assessment 36, 68–77. https://doi.org/10.1016/j.cosust.2018.10.010
Homer, C., Dewitz, J., Yang, L., Jin, S., Danielson, P., Xian, G., Coulston, J., Herold, N., Wickham, J., Megown, K., 2015. Completion of the 2011 National Land Cover Database for the conterminous United States–representing a decade of land cover change information. Photogramm. Eng. Remote Sens. 81, 345–354.
Hu, M., Liu, Y., Zhang, Y., Shen, H., Yao, M., Dahlgren, R.A., Chen, D., 2020. Long-term (1980–2015) changes in net anthropogenic phosphorus inputs and riverine phosphorus export in the Yangtze River basin. Water Res. 177, 115779. https://doi.org/10.1016/j.watres.2020.115779
Kätterer, T., Reichstein, M., Andrén, O., Lomander, A., 1998. Temperature dependence of organic matter decomposition: a critical review using literature data analyzed with different models. Biol. Fertil. Soils 27, 258–262.
Koehler, B., von Wachenfeldt, E., Kothawala, D., Tranvik, L.J., 2012. Reactivity continuum of dissolved organic carbon decomposition in lake water. J. Geophys. Res. Biogeosciences 117.
Lewis Jr, W.M., 2011. Global primary production of lakes: 19th Baldi Memorial Lecture. Inland Waters 1, 1–28.
Li, H., Leung, L.R., Getirana, A., Huang, M., Wu, H., Xu, Y., Guo, J., Voisin, N., 2015. Evaluating global streamflow simulations by a physically based routing model coupled with the community land model. J. Hydrometeorol. 16, 948–971.
Li, H., Wigmosta, M.S., Wu, H., Huang, M., Ke, Y., Coleman, A.M., Leung, L.R., 2013. A physically based runoff routing model for land surface and earth system models. J. Hydrometeorol. 14, 808–828.
Liu, M., Tian, H., Yang, Q., Yang, J., Song, X., Lohrenz, S.E., Cai, W.-J., 2013. Long-term trends in evapotranspiration and runoff over the drainage basins of the Gulf of Mexico during 1901–2008. Water Resour. Res. 49, 1988–2012.
Maavara, T., Lauerwald, R., Regnier, P., Van Cappellen, P., 2017. Global perturbation of organic carbon cycling by river damming. Nat. Commun. 8, 15347. https://doi.org/10.1038/ncomms15347
Maavara, T., Parsons, C.T., Ridenour, C., Stojanovic, S., Dürr, H.H., Powley, H.R., Van Cappellen, P., 2015. Global phosphorus retention by river damming. Proc. Natl. Acad. Sci. 112, 15603–15608. https://doi.org/10.1073/pnas.1511797112
McGechan, M.B., Lewis, D.R., 2002. SW—Soil and Water. Biosyst. Eng. 82, 1–24. https://doi.org/10.1006/bioe.2002.0054
Metson, G.S., Lin, J., Harrison, J.A., Compton, J.E., 2017. Linking terrestrial phosphorus inputs to riverine export across the United States. Water Res. 124, 177–191. https://doi.org/10.1016/j.watres.2017.07.037
Neitsch, S.L., Arnold, J.G., Kiniry, J.R., Williams, J.R., 2011. Soil and water assessment tool theoretical documentation version 2009. Texas Water Resources Institute.
Pan, S., Tian, H., Dangal, S.R., Ouyang, Z., Lu, C., Yang, J., Tao, B., Ren, W., Banger, K., Yang, Q., 2015. Impacts of climate variability and extremes on global net primary production in the first decade of the 21st century. J. Geogr. Sci. 25, 1027–1044.
Petersen, B.M., Berntsen, J., Hansen, S., Jensen, L.S., 2005. CN-SIM—a model for the turnover of soil organic matter. I. Long-term carbon and radiocarbon development. Soil Biol. Biochem. 37, 359–374.

Ren, W., Tian, H., Cai, W.-J., Lohrenz, S.E., Hopkinson, C.S., Huang, W.-J., Yang, J., Tao, B., Pan, S., He, R., 2016a. Century-long increasing trend and variability of dissolved organic carbon export from the Mississippi River basin driven by natural and anthropogenic forcing: Export of DOC from the Mississippi River. Glob. Biogeochem. Cycles 30, 1288–1299. https://doi.org/10.1002/2016GB005395

Ren, W., Tian, H., Cai, W.-J., Lohrenz, S.E., Hopkinson, C.S., Huang, W.-J., Yang, J., Tao, B., Pan, S., He, R., 2016b. Century-long increasing trend and variability of dissolved organic carbon export from the Mississippi River basin driven by natural and anthropogenic forcing. Glob. Biogeochem. Cycles 30, 1288–1299.

Reynolds, C.S., 2006. The ecology of phytoplankton. Cambridge University Press.

Robson, B.J., 2014. State of the art in modelling of phosphorus in aquatic systems: Review, criticisms and commentary. Environ. Model. Softw. 61, 339–359. https://doi.org/10.1016/j.envsoft.2014.01.012

Ruttenberg, K.C., 2003. The global phosphorus cycle. TrGeo 8, 682.

Stępień, I., 1984. On the numerical solution of the Saint-Vénant equations. J. Hydrol. 67, 1–11. https://doi.org/10.1016/0022-1694(84)90228-2

Te Chow, V., 2010. Applied hydrology. Tata McGraw-Hill Education.

Tesfa, T.K., Leung, L.R., Huang, M., Li, H.-Y., Voisin, N., Wigmosta, M.S., 2014. Scalability of grid- and subbasin-based land surface modeling approaches for hydrologic simulations. J. Geophys. Res. Atmospheres 119, 3166–3184. https://doi.org/10.1002/2013JD020493

Thomann, R.V., Mueller, J.A., 1987. Principles of surface water quality modeling and control. Harper & Row Publishers.

Tian, H., Chen, G., Liu, M., Zhang, C., Sun, G., Lu, C., Xu, X., Ren, W., Pan, S., Chappelka, A., 2010. Model estimates of net primary productivity, evapotranspiration, and water use efficiency in the terrestrial ecosystems of the southern United States during 1895–2007. For. Ecol. Manag. 259, 1311–1327.

Tian, H., Lu, C., Ciais, P., Michalak, A.M., Canadell, J.G., Saikawa, E., Huntzinger, D.N., Gurney, K.R., Sitch, S., Zhang, B., 2016. The terrestrial biosphere as a net source of greenhouse gases to the atmosphere. Nature 531, 225.

Tian, H., Lu, C., Melillo, J., Ren, W., Huang, Y., Xu, X., Liu, M., Zhang, C., Chen, G., Pan, S., 2012. Food benefit and climate warming potential of nitrogen fertilizer uses in China. Environ. Res. Lett. 7, 044020.

Tian, H., Xu, R., Pan, S., Yao, Y., Bian, Z., Cai, W.-J., Hopkinson, C.S., Justic, D., Lohrenz, S., Lu, C., Ren, W., Yang, J., 2020. Long-Term Trajectory of Nitrogen Loading and Delivery From Mississippi River Basin to the Gulf of Mexico. Glob. Biogeochem. Cycles 34, e2019GB006475. https://doi.org/10.1029/2019GB006475

Tian, H., Yang, Q., Najjar, R.G., Ren, W., Friedrichs, M.A., Hopkinson, C.S., Pan, S., 2015. Anthropogenic and climatic influences on carbon fluxes from eastern North America to the Atlantic Ocean: A process-based modeling study. J. Geophys. Res. Biogeosciences 120, 757–772.

van der Zee, S., Leus, F., Louer, M., 1989. Prediction of phosphate transport in small columns with an approximate sorption kinetics model. Water Resour. Res. 25, 1353–1365. https://doi.org/10.1029/WR025i006p01353

Wang, Z., Tian, H., Yang, J., Shi, H., Pan, S., Yao, Y., Banger, K., Yang, Q., 2020. Coupling of Phosphorus Processes With Carbon and Nitrogen Cycles in the Dynamic Land Ecosystem Model: Model Structure, Parameterization, and Evaluation in Tropical

Forests. J. Adv. Model. Earth Syst. 12, e2020MS002123. https://doi.org/10.1029/2020MS002123
Williams, J.R., 1995. The EPIC model. Comput. Models Watershed Hydrol. 909–1000.
Wu, H., Kimball, J.S., Li, H., Huang, M., Leung, L.R., Adler, R.F., 2012. A new global river network database for macroscale hydrologic modeling. Water Resour. Res. 48. https://doi.org/10.1029/2012WR012313
Xu, R., Pan, S.F., Chen, J., Chen, G.S., Yang, J., Dangal, S.R.S., Shepard, J.P., Tian, H.Q., 2018. Half-century ammonia emissions from agricultural systems in Southern Asia: Magnitude, spatiotemporal patterns, and implications for human health. GeoHealth 2, 40–53.
Yamazaki, D., O'Loughlin, F., Trigg, M.A., Miller, Z.F., Pavelsky, T.M., Bates, P.D., 2014. Development of the Global Width Database for Large Rivers. Water Resour. Res. 50, 3467–3480. https://doi.org/10.1002/2013WR014664
Yang, Q., Tian, H., Friedrichs, M.A., Hopkinson, C.S., Lu, C., Najjar, R.G., 2015. Increased nitrogen export from eastern North America to the Atlantic Ocean due to climatic and anthropogenic changes during 1901–2008. J. Geophys. Res. Biogeosciences 120, 1046–1068.
Yang, X., Post, W.M., Thornton, P.E., Jain, A., 2013. The distribution of soil phosphorus for global biogeochemical modeling. Biogeosciences 10, 2525–2537. https://doi.org/10.5194/bg-10-2525-2013
Yao, Y., Tian, H., Pan, S., Najjar, R.G., Friedrichs, M.A.M., Bian, Z., Li, H.-Y., Hofmann, E.E., 2021. Riverine Carbon Cycling Over the Past Century in the Mid-Atlantic Region of the United States. J. Geophys. Res. Biogeosciences 126, e2020JG005968. https://doi.org/10.1029/2020JG005968
Yao, Y., Tian, H., Shi, H., Pan, S., Xu, R., Pan, N., Canadell, J.G., 2020. Increased global nitrous oxide emissions from streams and rivers in the Anthropocene. Nat. Clim. Change 10, 138–142.

Chapter 3. Manure N and P enrichment and shifted patterns in the United States

Abstract

Livestock manure nitrogen (N) and phosphorus (P) play an important role in biogeochemical cycling. Accurate estimation of manure nutrient is important for assessing regional nutrient balance, greenhouse gas emission, and water environmental risk. Currently, spatially explicit manure nutrient datasets over a century-long period are scarce in the United States (U.S.). Here, we developed four datasets of annual animal manure N and P production and application in the contiguous U.S. at a 30 arc-second resolution over the period of 1860-2017. The dataset combined multiple data sources including county-level inventory data, as well as high-resolution livestock and crop maps. The total production of manure N and P increased during 1860-2017, which was associated with increased livestock numbers before the 1980s and enhanced livestock weights after the 1980s. The manure application amount was primarily dominated by production and its spatial pattern was impacted by the nutrient demand of crops. The intense-application region mainly enlarged from the Midwest toward the Southern U.S., and became more concentrated in numerous hot spots after the 1980s. The South Atlantic-Gulf and Mid-Atlantic basins were exposed to high environmental risks due to the enrichment of manure nutrient production and application from the 1970s to the period of 2000-2017. Our long-term manure N and P datasets provide detailed information for national and regional assessments of nutrient budgets. Additionally, the datasets can serve as the input data for ecosystem and hydrological models to examine biogeochemical cycles in terrestrial and aquatic ecosystems.

1. Introduction

As a fertility package, animal manure is a traditional source of nutrients and can provide abundant nitrogen (N), phosphorus (P), and potassium for cropland and pasture. Animal manure nutrients circulate widely in the Soil-Plant-Animal system and are highly involved in global nutrient cycling (Bouwman et al., 2013; Sheldrick et al., 2003). Although synthetic fertilizer has been widely used since the mid-20th century, livestock excreta is still the major nutrient source in agricultural soils, accounting for approximately 18% and 28% of the total N and P applied to global cropland, respectively (Sheldrick et al., 2003; Zhang et al., 2020). Moreover, the total

global animal manure N and P production has exceeded global fertilizer use (Bouwman et al., 2009). Therefore, the efficient recycling of manure can potentially meet the growing nutrient demand of crops. The circular nutrient source provided by manure enables nations to sustain their agricultural production with less reliance on imported fertilizer, especially mineral P fertilizer (Koppelaar and Weikard, 2013; Powers et al., 2019). Different from N which can be fixed from the atmosphere through microbial symbiosis with plants and the Haber-Bosch process, P is a rock-derived nutrient and there is no biological or atmospheric source for P. The limited and unevenly distributed P-rich rocks can threaten food security and have raised concerns in many resource-limited countries, including the United States (U.S.) (Amundson et al., 2015). Enhanced recovery of nutrients from manure can not only increase agricultural dependence, but may also reduce nutrient losses out of the Soil-Plant-Animal system. Additionally, the improvement of livestock operations in recent decades also facilitated the recoverability and utilization of animal manure (Kellogg et al., 2000).

Although manure and fertilizer application enhanced crop production, excessive nutrients might leave the Soil-Plant-Animal system through biogeochemical flow and potentially contaminate the environment if not properly managed (Mueller and Lassaletta, 2020; Zanon et al., 2019). Specifically, agricultural land is a sink for anthropogenic N and P inputs (e.g. synthetic fertilizer, manure, atmospheric deposition), and simultaneously acts as N and P sources for aquatic systems as well as a N source for the atmosphere (Bouwman et al., 2013; Elser and Bennett, 2011; Schlesinger and Bernhardt, 2013). The major N gaseous loss from fertilizer use and animal excreta includes the emissions of ammonia (NH_3), nitrous oxide (N_2O), and nitric oxide. NH_3 and nitric oxide can react with other air pollutants and form aerosols to reduce visibility and threaten human health (Bouwman et al., 2002; Xu et al., 2018), and N_2O is a potent greenhouse gas (Davidson, 2009). N_2O emission from animal manure is one of the major contributors to global anthropogenic N_2O emissions (Tian et al., 2020). Additionally, large fractions of the N and P applied to cropland lost through leaching, erosion, and surface runoff and are transported into rivers toward lakes and coastal oceans (Smith et al., 1998; Van Drecht et al., 2005). Excess N and P could dramatically impair freshwater and coastal ecosystems, causing eutrophication, hypoxia, and fish-kills (Garnier et al., 2015; Smith et al., 2007). Oxygen-depleted marine coastal “dead zones” associated with nutrient-stimulated algal blooms continue to expand globally. For example, the northern Gulf of Mexico is one of the largest dead zones in the world

and the hypoxic area often exceeds 15,600 km^2 in midsummer (1968-2016) (Del Giudice et al., 2019).

Considering the importance of manure nutrients on crop production, greenhouse gas emission, and water pollution, it is vital to have a better understanding of livestock manure nutrient production and application at national or even global scales (Potter et al., 2010; Sheldrick et al., 2002; Tian et al., 2016). Quantified and spatialized manure nutrient data can help stakeholders find a local recyclable nutrient source or make strategies to minimize N and P losses. Currently, most studies only provided county-level manure nutrient production data in the U.S., with short periods (from 1980 to 2014) (Kellogg et al., 2000; Ruddy et al., 2006). Nevertheless, terrestrial biosphere models usually require spatially explicit manure nutrient input data to simulate the anthropogenic effect on biogeochemical cycles since the preindustrial period (Tian et al., 2019). Studies focusing on soil nutrient storage change and legacy soil nutrients need long-term series manure nutrient data (MacDonald et al., 2012; Rowe et al., 2016). Moreover, previous studies usually assumed that nutrient excretion per animal is constant over time when quantifying nutrient production based on livestock number, which may lead to uncertainties (Zhang et al., 2020). Geographically explicit manure nutrient application in cropland (excluding pasture), as the direct nutrient input for the soil-crop system, hasn't been specifically estimated across the U.S. In this study, our objectives are to (1) develop grid-level manure N and P production datasets in the U.S. based on county-level livestock populations, dynamic livestock weight over time, and high-resolution livestock distribution maps; (2) develop grid-level manure N and P application in cropland datasets by integrating manure nutrient production and nutrient demand of crops; (3) investigate the spatiotemporal patterns of manure nutrient production and application based on these datasets, and (4) further identify regions with a high risk of excessive nutrient loading related to manure applications. The four datasets display the masses of manure N and P per area in each 30×30 arc-second grid-cell during 1860-2017. The datasets can be used to drive ecosystem, land surface, and hydrological models to simulate manure-induced greenhouse gas emissions and nutrient loadings.

2. Methods

Datasets of manure N and P production and application were developed by incorporating multiple existing datasets (Table 3-1). The geographically explicit manure N and P production

data were first calculated based on county-level livestock populations, dynamic livestock weights, and livestock distribution maps. Then the crop nutrient demand maps were developed by merging cropland distribution maps with crop-specific harvest area and nutrient assimilative capacities (uptake and nutrients removed by harvesting). Finally, the spatially explicit manure N and P application data were estimated by incorporating county-level manure production, recoverability factors, cropland fraction, and cropland nutrient demand maps. To facilitate studying the impact of manure nutrients on water quality, we further analyzed the average annual manure production and application in four decades (the 1860s, 1930s, 1970s, and 2010-2017) across the major 18 basins (Figure 3-1).

Table 3-1. Summary of data sources.

Data variables	Time period	Resolution	Reference/source
Livestock numbers	1930-2017	County	USDA National Agricultural Statistics Service https://www.nass.usda.gov/index.php
Livestock weights	1921-2017	Country	USDA Economic Research Service database http://www.ers.usda.gov/
Livestock distribution	2007	30 arc-second	Global Livestock Impact Mapping System (GLIMS) (Robinson et al., 2014)
Manure recoverability rates	1987-2014	County	Nutrient Use Geographic Information System (NuGIS) http://nugis.ipni.net/
Crop harvested area and yield	2000	5 arc-min	(Monfreda et al., 2008)

Crop and pasture distributions	1860-2016	5 arc-min	History Database of the Global Environment (HYDE 3.2) (Klein Goldewijk et al., 2017)
Crop density	1850-2016	1×1 km	(Yu and Lu, 2018)

Figure 3-1. Eighteen Hydrologic Units (level-1 HUC) in the contiguous U.S. (Recreated from the U.S. hydrologic unit map: https://water.usgs.gov/GIS/regions.html)

2.1. Manure nutrient production

Manure nutrient production refers to the animal excretion in this study. The county-level manure N and P production during 1930-2017 were calculated based on the livestock population, animal body weight, and nutrient excretion rates according to the method (Equation 1) proposed by Puckett et al. (1998).

County-level manure nutrient production was calculated as follows:

$$Pro_{x,c} = \sum_{i=1}^{n} Pop_{i,c} \cdot W_i \cdot Er_{x,i} \cdot Days \quad (1)$$

where $Pro_{x,c}$ is the annual manure nutrient *x* (N or P) production in county *c* (kg N/P yr^{-1}); *i* is animal type; $Pop_{i,c}$ is the county-level animal population (head); W_i is the annual average live body weight of animal (kg); $Er_{x,i}$ represents the excreted manure nutrients rate per unit weight of animal (kg N/P kg^{-1} day^{-1}) (Table 3-2); *Days* is the number of days in the life cycle of animal within a year.

Table 3-2. Excreted manure nutrients rates per unit weight of livestock.

Livestock	N excretion rate (kg N / 1000 kg animal weight /day)	P excretion rate (kg P / 1000 kg animal weight / day)
Beef cows	0.315	0.105
Milk cows	0.400	0.060
Heifers	0.310	0.040
Steers	0.315	0.105
Hogs	0.280	0.150
Sheep	0.450	0.070
Horses	0.280	0.050
Chickens	0.830	0.310
Pullets	0.620	0.240
Broilers	1.100	0.340
Turkey	0.740	0.280

Note: The excreted rate parameters derived from Puckett et al. (1998)

Data of livestock and poultry population were derived from the U.S. Department of Agriculture (USDA) census reports from 1930 to 2017 at 4- or 5-year intervals. Eleven livestock

and poultry categories were considered in this study, including beef cows, milk cows, heifers, steers, hogs, sheep, horses, chickens, pullets, broilers, and turkeys. Livestock population data for the recent five census reports (1997–2017) can be directly collected from the USDA Census Data Query Tool. Livestock population data before 1997 were collected from Cornell Institute for Social and Economic Research Data Archive (1949–1992), or manually digitalized from the USDA reports (1930–1945). More details of data collection, methods of dealing with missing data can be found in Yang et al. (2016). Annual average live weights of livestock and poultry, including cattle, hogs, sheep, broilers, chickens, and turkeys, were derived from the USDA Economic Research Service. We developed annual manure nutrient production by assuming a linear change between every two census years.

Global Livestock Impact Mapping System (GLIMS) provided gridded livestock population maps at a resolution of 30 arc-second (https://livestock.geo-wiki.org/home-2/). These maps were developed according to statistical relationships between livestock inventory data and multiple environmental variables, including climate, land cover, and human activities (Robinson et al., 2014). Combining with the GLIMS data, we spatially allocated manure nutrient production within each county based on the distribution of livestock. The grid-level manure nutrient production was first calculated based on the GLIMS data, and the total quantity of manure nutrient production in each county was obtained by calculating the sum of productions in all grid-cells within each county. Then, we calculated ratios of USDA-based county-level manure nutrient production to GIMS-based county-level data, and these ratios were used to adjust grid-cell values within each county. After this step, the developed grid-level products were in line with USDA-based annual county-level data in total quantities, with the spatial pattern inside each county inherited from the GLIMS-based manure nutrient production data (Equation 2).

$$Pro_{x,j} = GPro_{x,j} \cdot \frac{Pro_{x,c}}{GPro_{x,c}} \quad (2)$$

where $Pro_{x,j}$ is manure nutrient production in grid-cell j (kg N/P km^{-2} yr^{-1}); $GPro_{x,j}$ is manure nutrient production in grid-cell j calculated based on the GLIMS livestock data (kg N/P km^{-2} yr^{-1}); $GPro_{x,c}$ is the GLIMS-based manure nutrient production at county c where grid cell j is located (kg N/P yr^{-1}).

To generate grid-level manure production from 1860 to 1930, we obtained manure production change rates (1860-1930) from the dataset developed by Holland et al. (2005) and applied them to the grid-level manure nutrient production in 1930. Holland et al. (2005) provided global annual manure N production data from 1860 to 1960. In order to combine this dataset with the U.S. manure nutrient production data, we assumed manure production changes in the U.S. were consistent with the global trend and the manure N:P ratio was constant during 1860-1930 (Zhang et al., 2017).

2.2. Manure nutrient application

Manure nutrient application data were developed by allocating the county-level recoverable manure nutrient according to the grid-level manure nutrient demand of crops. The recoverable manure nutrient represents the proportion of manure nutrients that could reasonably be expected to be collected from the confinement facility and later be applied to the land (Kellogg et al., 2000). The recoverable manure nutrient was applied to cropland and pastureland according to their demands. We calculated recoverable manure nutrient amounts by adjusting the county-level manure production with recoverability factors provided by the Nutrient Use Geographic Information System (NuGIS, http://nugis.ipni.net/). The nutrient demand was estimated according to the assimilative capacity, the maximum amount of manure nutrient application without building up nutrient level in the soil over time (Kellogg et al., 2000). For cropland, assimilative capacity is estimated to be the amount of nutrients taken up by the crop and removed at harvest. We obtained the proportion of recoverable manure nutrient that can be applied to cropland by combining the assimilative capacities and areas of cropland and pastureland. The areas of cropland and pastureland during 1860-2016 were derived from the HYDE 3.2 (Klein Goldewijk et al., 2017).

The above-mentioned processes are represented by the following equations:

$$APP_{x,c} = Pro_{x,c} \cdot Rf_{x,c} \cdot f_{x,crop,c} \tag{3}$$

$$f_{x,crop,c} = \frac{A_{crop,c} \cdot S_{x,crop}}{A_{crop,c} \cdot S_{x,crop} + A_{past,c} \cdot S_{x,past}} \tag{4}$$

where, $APP_{x,c}$ is the recoverable animal manure nutrient available for application on cropland in county c (kg N/P yr^{-1}); $Rf_{x,c}$ is the manure nutrient recoverability rate (the recoverability rates

are unitless and county-specific with average values 0.19 for N and 0.35 for P), and $f_{x,crop,c}$ refers to the fraction of manure nutrient that is available for cropland (unitless); $A_{crop,c}$ and $A_{past,c}$ represent the annual area of cropland and pasture in each county (km^2), respectively, while $S_{x,crop}$ and $S_{x,past}$ represent the average assimilative capacities of cropland and pastureland (kg N/P km^{-2}), respectively (Table 3-3).

Table 3-3. Nutrient assimilative capacity of cropland and pastureland.

Land-use type	N	P
	kg N / km^2	kg P / km^2
Cropland	13792	1626
Pastureland	6937	2768

Note: Assimilative capacities of cropland and pastureland were calculated based on the data in Kellogg et al., (2000)

To spatialize county-level recoverable animal manure nutrient to gridded maps, we first developed annual grid-level crop nutrient demands data as the base maps (Equation 5). Nutrient demands of crops were estimated by combining the assimilative capacities, harvested areas and yields of 13 crops (maize, soybeans, sorghum, cotton, barley, wheat, oats, rye, rice, peanuts, sugar beets, tobacco, and potatoes). The grid-level average assimilative capacity of cropland was calculated based on crop-specific yield and harvested area maps in 2000 provided by Monfreda et al. (2008). Next, this map of cropland assimilative capacity was integrated with dynamic cropland fraction data (Yu and Lu, 2018) to obtain annual nutrient demand maps from 1860 to 2016. Original cropland fraction data was at a resolution of 1 km in the projected coordinate system which approximates 30 arc-second resolution in the geographic coordinate. We resampled the cropland fraction maps into the resolution of 30 arc-second to match the manure nutrient production data.

$$Dem_{x,j} = \sum_{k=1}^{m} Y_{j,k} S_{x,k} \cdot Den_j \quad (5)$$

where, $Dem_{x,j}$ is the crop demand for manure nutrient in grid j (kg N/P km^{-2} yr^{-1}); $Y_{j,k}$ is the yield of crop k (ton per area of cropland) and $S_{x,k}$ is the manure nutrient assimilative of crop k (kg N/P per ton product) (Table 3-4); Den_j represents the cropland density in each grid (unitless).

The downscaling of county-level recoverable manure nutrient data into grid maps was similar to the method used in developing manure nutrient production data (Equation 2). The grid values on manure nutrient demand maps were adjusted to match annual county-level recoverable manure nutrient data (Equation 6). The manure nutrient application data from 1860 to 2017 were developed through the above-mentioned processes, however, several variables and parameters in these processes were not available through the whole study period (e.g., manure recoverability rate, crop yield). Therefore, we assumed these variables or parameters did not change before or after the data-available period (Kellogg et al., 2000; Puckett et al., 1998).

$$APP_{x,j} = Dem_{x,j} \cdot \frac{APP_{x,c}}{Dem_{x,c}} \quad (6)$$

where, $APP_{x,j}$ is the manure nutrient application in grid j (kg N/P km^{-2} yr^{-1}) and $Dem_{x,c}$ refers to the demand for manure nutrients in county c where grid j is located (kg N/P yr^{-1}).

Table 3-4. Nutrient assimilative capacity of 13 types of crop.

Crop type	N	P
	kg N / ton product	kg P / ton product
Maize	12.96	2.43
Soybeans	53.67	5.44
Sorghum	15.88	2.92
Cotton	27.56	3.43
Barley	17.01	3.40
wheat	18.65	3.27
Oats	16.73	3.12
Rye	17.33	2.92
Rice	11.34	2.63
Peanuts	36.29	2.72
Sugar beets	2.16	0.43
Tobacco	28.43	2.00
Potatoes	3.27	0.54

Note: Assimilative capacities of crops were derived from Kellogg et al., (2000)

3. Results

3.1. Temporal and spatial patterns of manure nutrient production

We estimate that the total manure N and P production increased from 1.4 Tg N yr^{-1} and 0.3 Tg P yr^{-1} in 1860 to 7.4 Tg N yr^{-1} and 2.3 Tg P yr^{-1} in 2017, respectively (Figure 3-2). The estimated manure N and P production reached the first peak in 1975 (6.1 Tg N yr^{-1} and 1.8 Tg P yr^{-1}), and slightly declined thereafter, then regrew after 1987 with the second peaks occurring in 2007 (N) and 2017 (P), respectively. The slight decrease in manure nutrient production between 2008 and 2012 may be associated with the financial crisis and the low demand for livestock products. The total manure N and P production increased 5-fold and 7-fold during 1860-2017, with the increasing rates of 0.03 Tg N yr^{-2} and 0.006 Tg P yr^{-2} during 1860-1930, 0.05 Tg N yr^{-2} and 0.02 Tg P yr^{-2} during 1930-2017 ($p<0.01$), respectively. The N:P ratio in total manure production changed from 4.33 in 1930 to 3.25 in 2017. The decrease in the N:P ratio in total manure production was related to the change in the structure of animal population. For example, the proportion of beef cows and broilers (N:P ratio in excretion: 3.0-3.2) increased while that of milk cows and horses (N:P ratio in excretion: 5.5-6.7) decreased over the study period.

The dominant livestock contributing to total manure nutrient production changed over the study period (Figure 3-3). Manure production from milk cows was the dominant contributor to both total manure N and P before 1940, but it decreased during 1945-1992. Manure nutrients from beef cows had the largest share in both total manure N and P production from 1964 to1992, accounting for 22-24% of N and 25-32% of P. Poultry manure nutrient production substantially increased since the 1960s and became the dominant contributor (21-31% of N and 23-33% of P) to total manure nutrient production after 1997. Steer, heifer and hog were also important for manure nutrient production, with heifer being a major contributor for N, hog for P, and steer for both N and P.

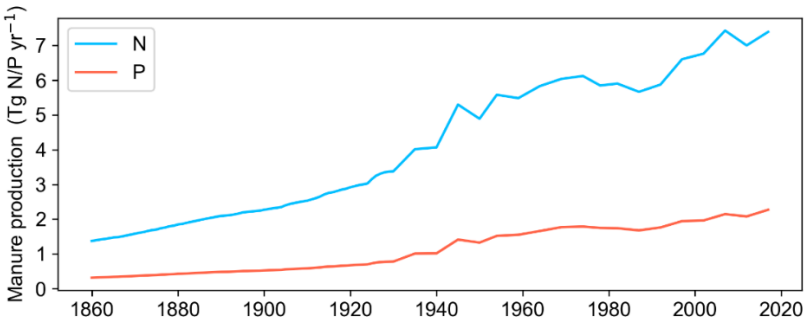

Figure 3-2. Trend and variation of total manure N and P production in the contiguous U.S from 1860 to 2017.

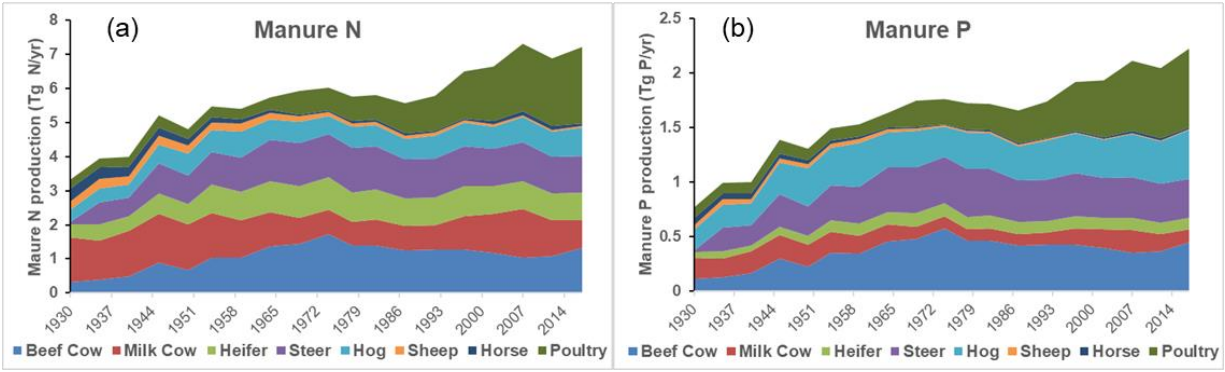

Figure 3-3. Changes in manure (a) N and (b) P production of different livestock during 1930-2017. The "Poultry" category includes chicken, broiler, pullet, and turkey.

The spatial pattern of animal manure N and P production showed a similar change over the study period (Figure 3-4). The distribution maps showed that the Midwestern U.S. (e.g., Iowa, Missouri, and Illinois) was the core region (> 300 kg N km^{-2} yr^{-1} or 100 kg P km^{-2} yr^{-1}) of manure N (P) production in 1860. From 1860 to 1930, the high manure nutrient production region (> 600 kg N km^{-2} yr^{-1} or 200 kg P km^{-2} yr^{-1}) mainly enlarged outwards from the Midwest. Between 1930 and 1980, manure N (P) production not only intensified in the Midwest but also in the Southern U.S. (e.g., Texas, Georgia, and North Carolina). After 1980, manure N (P) production became more concentrated in many hot spots (> 6000 kg N km^{-2} yr^{-1} or 3000 kg P km^{-2} yr^{-1}), especially in the southeastern U.S. Meanwhile, part of regions around these hot pots experienced a decline in manure production.

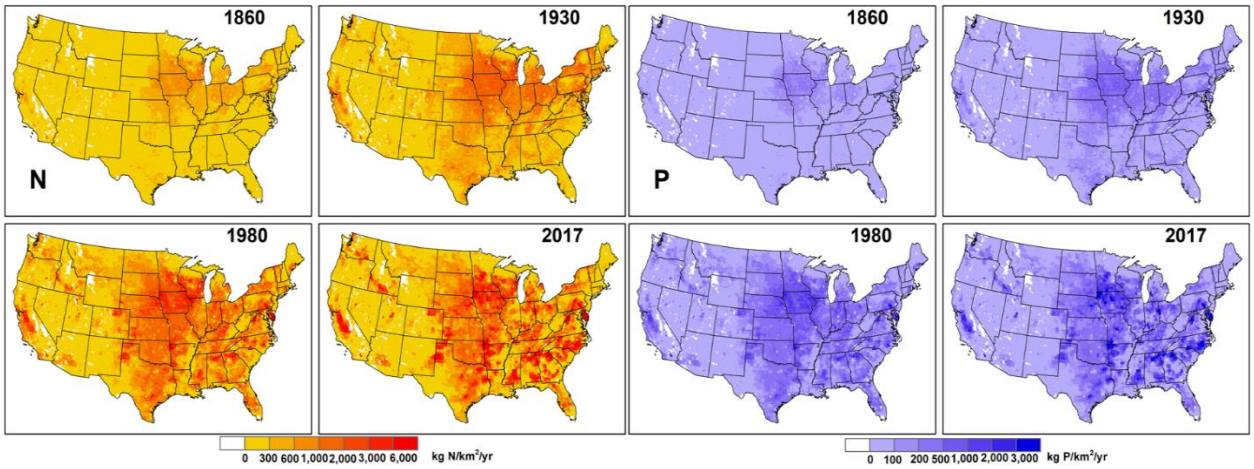

Figure 3-4. Spatial distribution of manure N and P production across the contiguous U.S. in 1860, 1930, 1980, and 2017. (Note: 1930 and 2017 were the earliest and latest years of available USDA census data, respectively, and 1980 was chosen as the year at the middle of these two years)

According to the change rates of manure nutrient production from 1860 through 2017 (Figure 3-5), several growth poles (change rates > 20 kg N km^{-2} yr^{-2} or 5 kg P km^{-2} yr^{-2}, p<0.01) located in Iowa, Arkansas, California, Alabama, Pennsylvania were identified. The belt (change rates > 5 kg N km^{-2} yr^{-2} or 1 kg P km^{-2} yr^{-2}, p<0.01) from Minnesota to Texas, as well as scattered areas along the east and west coasts, were the primary contributors to the increase in manure N (P) production. Aside from the huge increase in the Midwest and Southeast, decreasing trends were exhibited in some regions, particularly the northeastern border of the U.S.

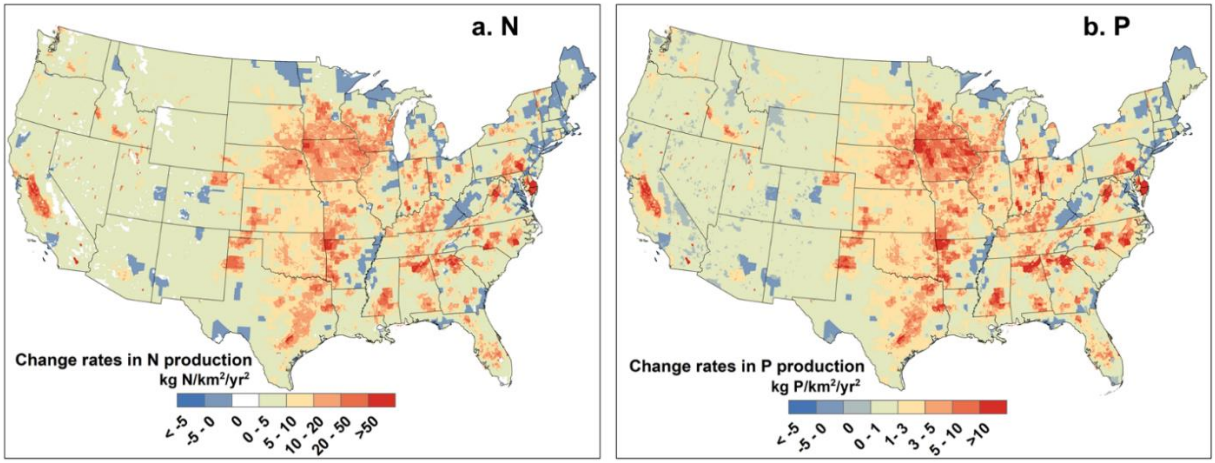

Figure 3-5. Change rates of manure (a) N and (b) P production across the contiguous U.S. during 1860-2017.

3.2. Comparison of manure nutrient demand and production

We assumed that the capacity of crops to assimilate nutrients was manure nutrient demand of crops. From 1860 to 1930, the manure N (P) demand of cropland intensified and enlarged inside the Corn Belt region (e.g. Iowa, Illinois, Minnesota, Nebraska, North Dakota, and South Dakota), as well as the Southern U.S. (e.g., Texas, Oklahoma, Arkansas, Mississippi, Alabama, Georgia, and Tennessee) (Figure 3-6). After 1930, change in the spatial pattern of manure nutrient demand was dominated by the abandonment of cropland, and the magnitude of demand slightly decreased, especially after 1980. Compared to the spatial patterns of manure production and demand (Figures 3-4 and 3-6), it is worth noting that the high manure production and demand regions overlapped in the Midwest and Southeastern U.S., but a large deficit (demand higher than production) existed along the Lower Mississippi River Valley.

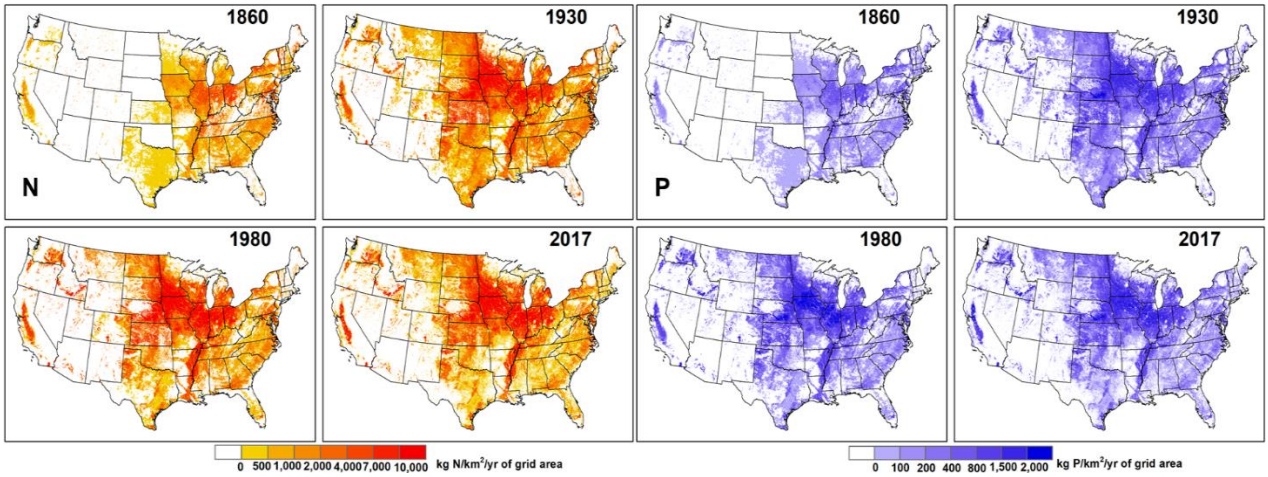

Figure 3-6. Spatial distribution of N and P demand of crops in 1860, 1930, 1980, and 2017.

For the contiguous U.S., the total demand for manure N was higher than the production over the study period while the total production of manure P started to exceed demand after the 1980s (Figure 3-7). The gap between production and demand has considerably narrowed since the 1920s due to the cease of the increase in nutrient demand. In 2017, total manure N and P productions reached 7.4 Tg N yr^{-1} and 2.3 Tg P yr^{-1}, while total demands were 11.7 Tg N yr^{-1} and 1.8 Tg P yr^{-1}. However, the total numbers here only displayed limited information on the relationship between production and demand due to the difficulty of collecting and transporting manure for widespread application in cropland.

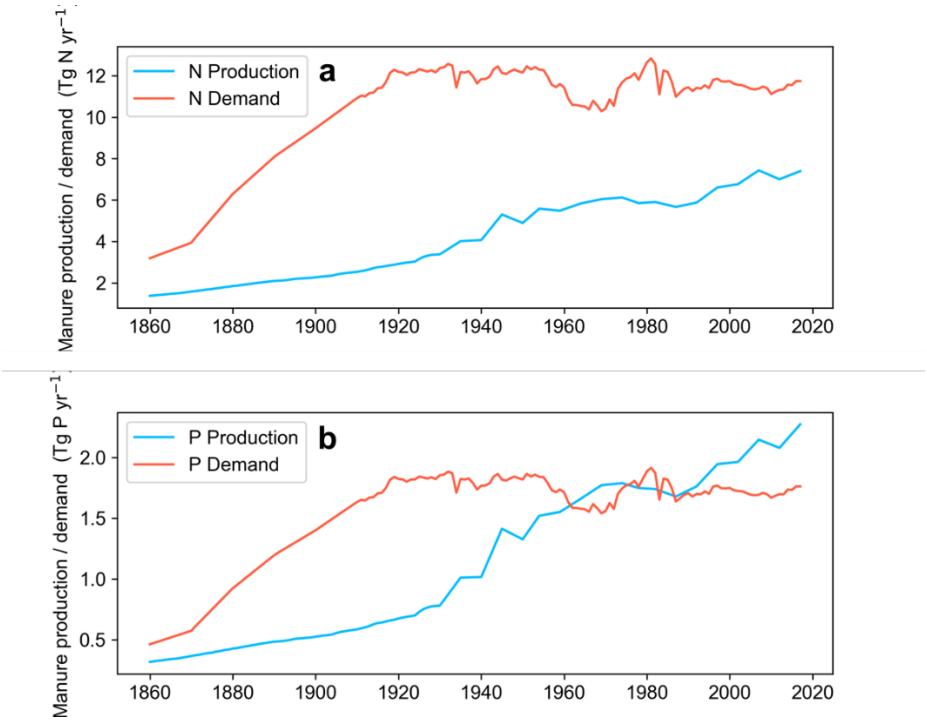

Figure 3-7. Comparing total productions and demands of manure (a) N and (b) P in the contiguous U.S. from 1860 to 2017.

3.3. Temporal and spatial patterns of manure nutrient application in cropland

Animal manure N (P) application amount is primarily dominated by production and its spatial pattern is impacted by demand. The overall manure application to production ratios were 0.15 and 0.23 for N and P, respectively. Driven by cropland expansion and enhanced manure production, total manure N and P application in croplands increased 9-fold and 10-fold since 1860, reaching 1.3 Tg N yr^{-1} and 0.6 Tg P yr^{-1} in 2017 (Figure 3-8). The N:P ratio in manure application decreased from 2.62 to 2.32 during 1930-2017. The substantial increase of manure N and P application mainly happened in two periods: 1924-1970 (increase rates: 0.009 Tg N yr^{-2} and 0.005 Tg P yr^{-2}, p<0.01) and 1987-2017 (increase rates: 0.01 Tg N yr^{-2} and 0.005 Tg P yr^{-2}, p<0.01). The variations of total application and production quantities didn't follow the same trajectory. For example, from 1975 to 1987, when manure N production decreased, the total manure application still remained stable. The application to production ratios reached the first peak in 1891 (N: 0.14, P: 0.25) followed by a decrease until 1945 (N: 0.13, P: 0.20) when World War II ended, and then resumed the increasing trend through 2017 (N: 0.18, P: 0.25).

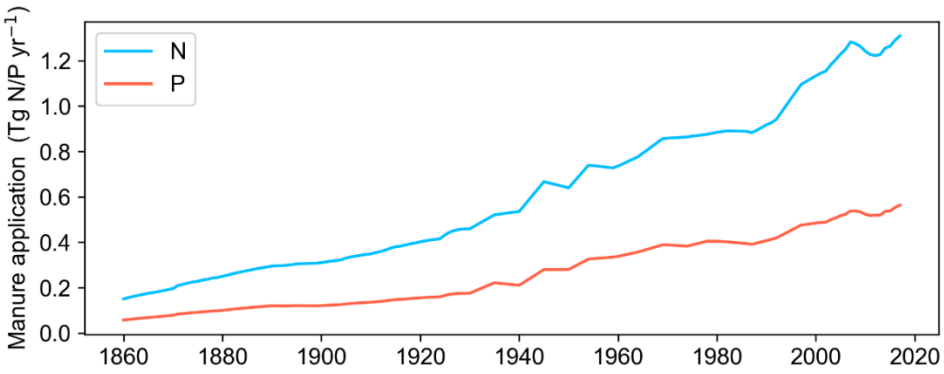

Figure 3-8. Trend and variations of total manure N and P application in the contiguous U.S. from 1860 to 2017.

The spatial shift of manure application, similar to manure nutrient demand, gradually expanded inside the Corn Belt and toward the Southern U.S. (Figure 3-9). The expansion of manure application region primarily occurred during 1860-1930, induced by cropland expansion. After 1930, the changed spatial patterns of manure N (P) application were characterized by intensified application in the Midwest and multiple hot spots (> 2000 kg N km^{-2} yr^{-1} or 1000 kg P km^{-2} yr^{-1}). The spatial distribution of hot spots on application maps was similar to that on manure nutrient production maps. In 2017, high manure nutrient application regions (> 500 kg N km^{-2} yr^{-1} or 200 kg P km^{-2} yr^{-1}) mainly distributed in the Midwestern U.S., Southern U.S., Mid-Atlantic (e.g., Pennsylvania, Maryland, and Virginia), and California, where abundant recoverable manure nutrients were applied in the local cropland to meet the high nutrient demand of crops. A quite low manure nutrient application rate (< 100 kg N km^{-2} yr^{-1} or 50 kg P km^{-2} yr^{-1}) was observed in regions with less cropland demand (e.g., Southwestern U.S.) and low manure production (e.g., Lower Mississippi River Valley).

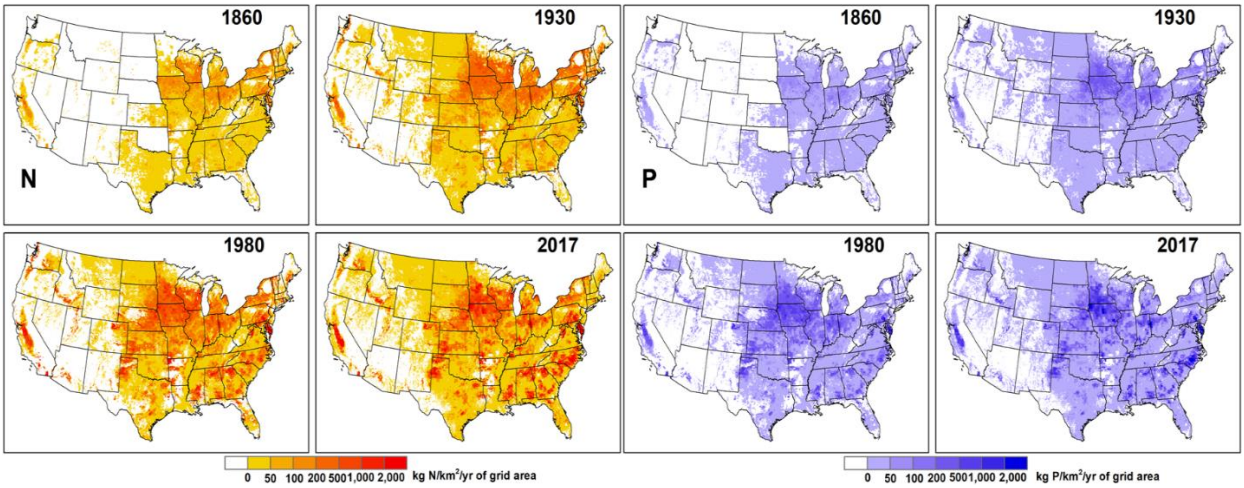

Figure 3-9. Spatial distributions of manure N and P application in the U.S. cropland in 1860, 1930, 1980, and 2017.

3.4. Manure production and application across the major river basins

From the 1860s to the 1970s, all basins exhibit increased manure nutrient production (Figures 3-10a and 3-10b). However, from the 1970s to the 2010s, the manure N and P production decreased in the New England and Missouri basins, while a dramatic increase was shown in the South Atlantic-Gulf, Mid-Atlantic, and Arkansas-White-Red basins (Figure 3-1). Manure application demonstrated a similar pattern across different basins (Figures 3-10c and 3-10d), but it increased from the 1970s to the 2010s in most basins except the two basins (the New England and Souris-Red-Rainy) in the northern regions. In the 1970s, the Missouri basin was the largest source contributing ~20% N (P) of the total manure production, while the Upper Mississippi basin had the highest manure N (P) application in cropland accounting for 19% N and 24% P of the total manure N (P) application. During 2011-2017, however, the dominant regions of manure nutrient production and application were shifted to the South Atlantic-Gulf basin which accounted for the largest single share (18% N and 19% P of the total N (P) production, 24% N and 21% P of the total N (P) application). The uneven distribution of manure application intensified during 1860-2017, demonstrated by the standard deviation of manure N and P application across all basins consistently increasing from 0.013 Tg N yr^{-1} and 0.005 Tg P yr^{-1} in the 1860s to 0.081 Tg N yr^{-1} and 0.038 Tg P yr^{-1} during 2010-2017.

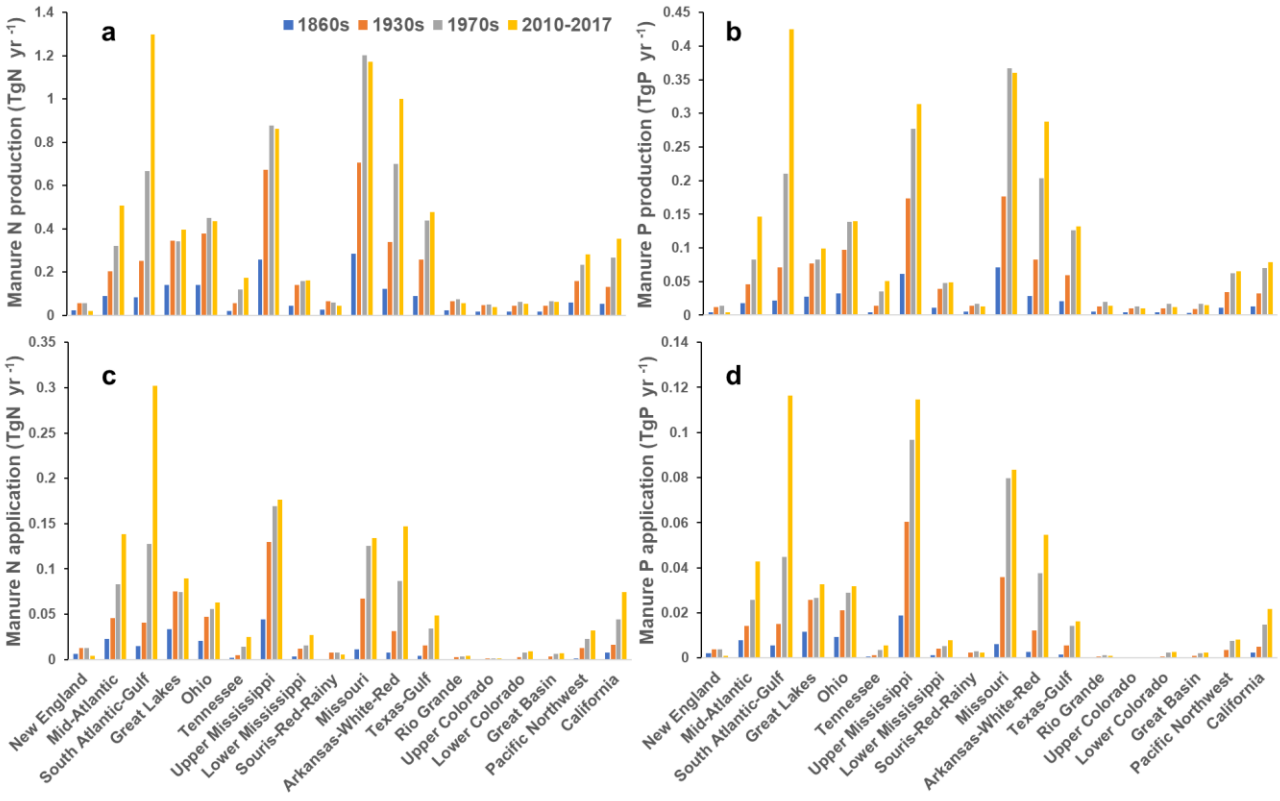

Figure 3-10. Average annual manure production (a. N, b. P) and application (c. N, d. P) across 18 major basins in the 1860s, 1930s, 1970s, and 2010-2017.

4. Discussion

4.1. Comparison with previous investigations

Within this study, we compared manure nutrients production data with other four datasets from Food and Agriculture Organization Corporate Statistical Database (FAOSTAT, 2019), NuGIS, Kellogg et al. (2000), and Yang et al. (2016). FAOSTAT provides total manure N production at the national level from 1961 to 2017, while the other three datasets provide county-level manure N and P production data. The estimated manure N (P) production from this study was lower than the other two datasets (FAOSTAT and Yang et al.) before 1982 and became the highest one after 2003 (Figure 3-11). During 1982-2007, the estimation from this study is very close to other estimations developed at the county-level. The average total manure N (P) production over 1987-1997 was 6.02 Tg N yr^{-1} (1.79 Tg P yr^{-1}), 6.75 Tg N yr^{-1}, 5.96 Tg N yr^{-1} (1.75 Tg P yr^{-1}), 5.64 Tg N yr^{-1} (1.67 Tg P yr^{-1}), and 6.01 Tg N yr^{-1} (1.86 Tg P yr^{-1}),

respectively, for this study, FAOSTAT, NuGIS, Kellogg et al., and Yang et al. The differences among the datasets were derived from calculation methods, chosen livestock types and numbers, as well as parameters, such as animal-specific excreted manure nutrient rates and the number of days in the life cycle. In terms of changing trends, manure N and P production were relatively stable after the 1960s in FAOSTAT, Kellogg et al., and Yang et al., while the NuGIS data increased slightly between 1987 and 2007 and then decreased sharply after 2010. In contrast, our results showed an increasing trend after the 1980s due to the consideration of the increased animal body sizes.

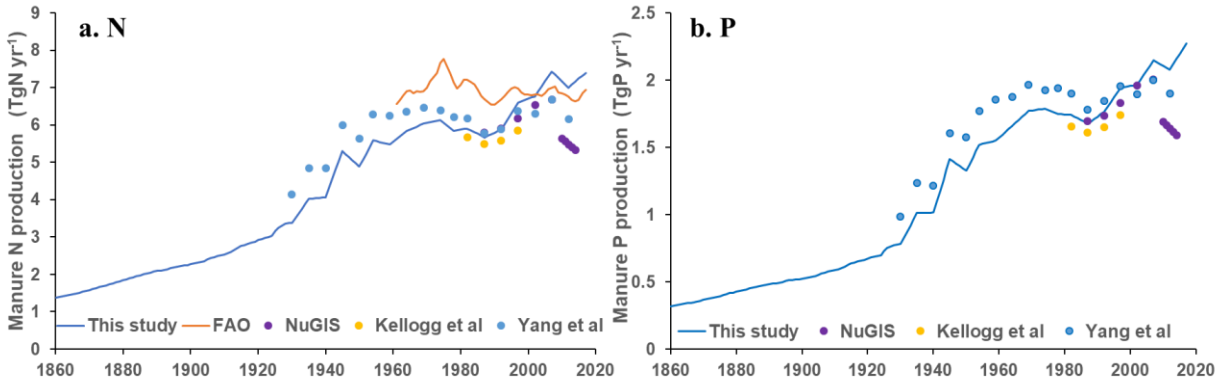

Figure 3-11. Comparison of manure nutrient production in this study with the four previous datasets.

In the previous four datasets, temporal changes in manure N (P) production are driven by animal numbers. It is worth noting that manure N (P) production can still increase despite the stabilization of livestock numbers in recent years. Driven by the advanced technology, livestock live weight and size consistently increased, which may enhance the manure nutrient excretion rate of each animal (Lassaletta et al., 2014; Sheldrick et al., 2003; Thornton, 2010). We compared manure nutrient production calculated with constant average weights and with dynamic weights of livestock. The results showed that manure production with dynamic weights increased dramatically after the 1990s (Figure 3-12). Enhanced livestock weights contributed 59% and 54% of the increase in manure N and P production, respectively, from 1987 to 2017

when the differences between the two total production data reached 0.98 Tg N yr^{-1} and 0.31 Tg P yr^{-1}.

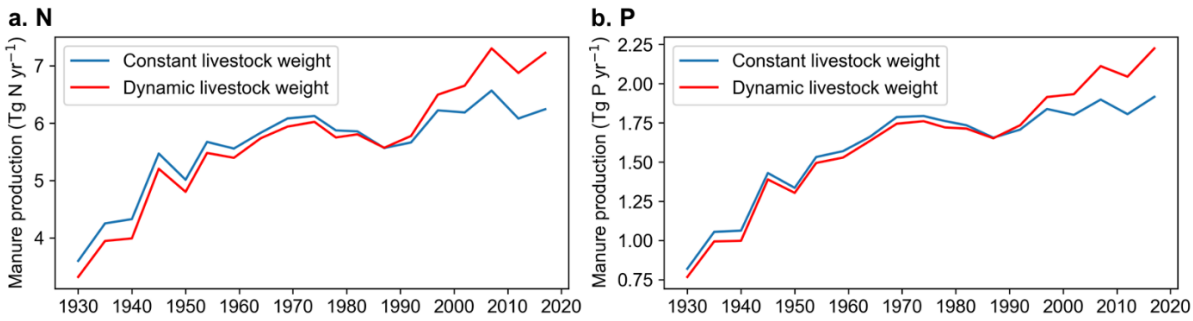

Figure 3-12. Comparison of manure N (P) production calculated based on dynamic weight of livestock and constant weight.

It is difficult to compare our dataset of manure N (P) application in soils with previous studies since these datasets provided reference values with various definitions and were generated based on different statistical methods. For example, FAOSTAT provided annual data of "Manure applied to soils" in the U.S., whereas this dataset was developed based on the assumption that all treated manure, net of losses (e.g., NH_3 volatilization, N leaching, and runoff), is applied to soils following the method in the 2006 IPCC guidelines (Eggleston et al., 2006). Kellogg et al. (2000) and NuGIS both estimated recoverable manure nutrients by multiplying confined livestock units, recoverability factors, and nutrients per ton of manure after losses. All three datasets do not separate manure application to cropland and pastureland. This study developed manure nutrient application data in cropland by applying the method of recoverability factor in combination with the cropland nutrient assimilative capacity. Compared to the other three datasets, our data subtracted the proportion of manure application on pastureland and considered the impact of the change in cropland area, which can lead to relatively low data values.

4.2. The impact of manure nutrient enrichment on coastal oceans

Animal manure N (P) that is lost through surface runoff or leaching exacerbated eutrophication and hypoxia in the aquatic system in the U.S. (Feyereisen et al., 2010; Williams et

al., 2011). During the expansion of manure production from the Midwest to the Southeastern coastline, massive amounts of nutrients get more of a chance to be transported to the estuary. When rivers transport nutrients from land to coastal oceans, nutrients could be removed or retained through denitrification, plant and microbial uptake, organic matter burial in sediment, and sediment sorption (Billen et al., 1991; Seitzinger et al., 2002). However, proportionate nutrient retention from rivers in the coastal plain may be lower because of the shorter distance to the coast. Additionally, the risk of massive manure loss in hurricane events increases under the background of enhanced Atlantic hurricane activities since 1995 (Saunders and Lea, 2008; Trenberth, 2005). Flooding rains and high winds may destroy manure storage structures (e.g., pad, pond, lagoon, tank, and building), resulting in the direct release of untreated manure into rivers (Tabachow et al., 2001).

The South Atlantic-Gulf and Mid-Atlantic basins are two critical coastal regions with the enrichment of manure nutrient production and application from the 1970s to the 2010s due to intensive livestock farming. The low recovery and reuse rate of animal manure N (P) can potentially cause a significant amount of manure N and P exports from the basins into the Gulf of Mexico and the Atlantic Ocean (Sheldrick et al., 2003). The Upper Mississippi, Missouri, and Arkansas-White-Red sub-basins within the Mississippi River basin were the three largest sources of manure production and were the dominant contributors to N and P loads into the Gulf of Mexico (David et al., 2010; Jones et al., 2019). The Upper Mississippi and Missouri basins had the highest manure nutrient production and application in the 1970s and maintained the high quantities until 2010, while manure N (P) production and application largely increased in the Arkansas-White-Red basin during 2011-2017. The enhanced total manure production may continually be responsible for the enriched loads of N and P that can lead to coastal water pollution (Rabalais and Turner, 2019).

4.3. Implication for manure nutrient management

The structure of animal agriculture has shifted toward concentrated animal feeding operations (CAFOs), which led to increased animal density, particularly in poultry and swine production (Kellogg et al., 2000). Thus, manure production became increasingly concentrated in several regions with large operations, such as the southeastern U.S where land is flat, relatively inexpensive, and CAFOs are easily constructed. Meanwhile, the decreased manure production in

partial areas of the Midwestern and Southern U.S was due to the disappearance of small family farms. On the other hand, the enhanced animal weight caused an additional increase in manure production in operations with plenty of confined animals. The unevenly intensified distribution of manure production may have further exacerbated the imbalance of regional nutrient allocation. Currently, opportunities for widespread manure application are limited because the transport of manure can be costly. Furthermore, the long distance between livestock farms and cropland can bring difficulties to practical operations (MacDonald, 2009). There remain gaps between manure production and demand in some regions of the U.S. (e.g., the Lower Mississippi River Valley). In contrast, manure collected from many farms cannot be properly used to fertilize crops. The unusable manure is not only a waste of manure resources, but may also cause serious environmental problems through nutrient losses into the atmosphere and aquatic systems.

The efficient recovery and processing of manure nutrients, the transportation of manure from the CAFOs to the specific crop area, and the utilization of manure as bioenergy can be important pathways to control pollution caused by the uneven distribution of manure production (He et al., 2016). The CAFOs facilitate the recovery of animal manure, which has created conditions for large-scale utilization and management of manure. Because of the economies of scale, the cost of transportation and management for per unit animal manure can be reduced, making the utilization of manure more feasible. Establishing a direct link between CAFOs and specific crop area ensures that animal manure production can be consumed in large quantities and thereby improving economic efficiency. For the centralized management of animal manure, nutrient losses during collection, storage, and application should be constrained or avoided, because a small proportion of nutrient losses can even contaminate regional environment if manure nutrient amounts are huge. Manure management systems with the integrated package of measures are necessary for controlling nutrient losses from the feed–animal–manure–crop chain (Oenema et al., 2007).

4.4. Assumptions and Uncertainties

Uncertainties in this study are primarily associated with data sources and methods that were used. First, multiple data sources were used to develop the datasets of manure production and application data; however, biases exist in these source data. For instance, the non-disclosure of livestock numbers in some counties in the USDA Census of Agriculture can cause an

underestimate of manure production in numerous counties (Yang et al., 2016). Moreover, high uncertainties exist in this census data itself. Second, the parameters in the calculation model, e.g., excreted manure nutrient rates, could bring uncertainties in the estimation of animal manure nutrient production and application. Third, various assumptions were made in this study to extend the time series of data and spatialize data from the county-level to the grid-level. These assumptions were established based on available data and experience, but uncertainties still existed and influenced the accuracy of the dataset. The limitations and uncertainties of these assumptions were further discussed and explained in the following part.

The livestock distribution maps from the GLIMS dataset were the reference of the spatial pattern of manure nutrient production data within each county. The GLIMS data were developed by establishing statistical relationships between livestock inventory data and multiple environmental variables (e.g., climate, land cover, human activities), and using these relationships to predict livestock distributions across the globe. We assumed livestock distribution within each county was stable over the study period because the dynamic livestock maps were unavailable. However, the environmental variables can change and induce the variation in livestock distribution inside each county. The accuracy of this manure nutrient production dataset can be improved once dynamic livestock maps are developed in the future. Although manure nutrient production within counties has not been well validated due to the lack of survey-based data at site level, this dataset still can provide a reference of how manure production may be distributed at a high-resolution level.

The manure nutrient production before 1930 was generated based on change rates in global manure N datasets from Holland et al. (2005). There is a period of overlap (1930-2004) between this global dataset and the USDA census data. During 1930-2004, the average annual change rates of manure N production were 1.08% in the global dataset and 1.01% in this study. Therefore, the changes in estimated manure N production in the U.S. before 1930 might be reasonable at a long-time scale. The ratio of N to P in animal manure varies among different animal species and changes along with proportions of different animal populations over time. From 1930 to 2017, the N:P ratio in the total manure production slightly decreased from 4.33 to 3.25. Due to the lack of manure P production data before 1930, we calculated manure P production in this period according to manure N production and the constant N:P ratio in 1930. If

the N:P ratio kept decreasing before 1930, the total manure P production may be overestimated during 1860-1929.

Changes in recoverability factors, assimilative capacity and crop yields over the study period were ignored due to lack of data support and that may cause a bias in quantifying manure nutrient application. With the development of livestock confinement facilities, the confinement and recoverability factors of animal manure may increase in recent decades (Kellogg et al., 2000). Hence, manure application can be overestimated before the 1980s and underestimated after the 2000s. The yields of different crops may change at different speeds over the study period, and that can affect the spatial patterns of manure nutrient demand of cropland as well as manure nutrient application. Similarly, assimilative capacity can vary from farm to farm and year to year. The average crop-specific assimilative capacity values used in this study, however, ignored these variations and could cause errors in the spatial and temporal patterns of manure nutrient demands. Additionally, the crop nutrient demand could also be satisfied by synthetic fertilizer, thereby, manure application may be complementary to fertilizer application on cropland. However, the impacts of synthetic fertilizer application on manure application were not considered when generating manure application data.

In addition, the development of manure application data was based on two assumptions: (1) The allocation of manure nutrient application within the county was proportional to crop nutrient demands; (2) Manure is assumed to be applied in the county where it was produced. Manure application is controlled by distance, cost, and operating practice of humans. Currently, the specific locations of animal farms across the country are not available, thus it is difficult to evaluate the influence of distances between farms and croplands. Due to the practical limits of manure transportation (Buckwell and Nadeu, 2016; MacDonald, 2009), it is reasonable to assume manure production and application happen within the same county on a large scale. However, ignoring the impact of multiple factors on manure application within the county can still result in biases in the spatial distribution of manure application.

5. Conclusion

Manure nutrient production and application in the livestock-crop system substantially altered the regional and global N and P cycle. In this study, we developed geographically explicit datasets of animal manure N and P production and their application in cropland across the

contiguous U.S. from 1860 to 2017. The dataset indicated that both manure N and P production and application significantly increased over the study period. Although livestock numbers became stable in recent decades, manure nutrient production still increased due to the enhanced livestock body weight after the 1980s. Enhanced livestock weights contributed 59% and 54% of the increase in manure N and P production, respectively, from 1987 to 2017. Meanwhile, manure nutrient production intensified and enlarged inside the Midwest and toward the Southern U.S. from 1980 to 2017, and became more concentrated in numerous hot spots. As manure nutrient application also expanded toward the Southeastern coastline, massive amounts of nutrients get more of a chance to be transported to the estuary. The enrichment of manure nutrients in the South Atlantic-Gulf, Mid-Atlantic, and Mississippi River basins increased the risk of excessive nutrient loading into the Gulf of Mexico and the Atlantic Ocean under extreme weather conditions. Therefore, it is important to effectively store, utilize, and transport animal manure to reduce nutrient pollution and restore the environment.

References

Amundson, R., Berhe, A.A., Hopmans, J.W., Olson, C., Sztein, A.E., Sparks, D.L., 2015. Soil and human security in the 21st century. Science 348, 1261071–1261071. https://doi.org/10.1126/science.1261071

Bian, Z., Tian, H., Yang, Q., Xu, R., Pan, S., Zhang, B., 2020. Gridded datasets of animal manure nitrogen and phosphorus production and application in the continental U.S. from 1860 to 2017.

Billen, G., Lancelot, C., Meybeck, M., 1991. N, P, and Si retention along the aquatic continuum from land and ocean, in: Dahlem Workshop on Ocean Margin Processes in Global Change. pp. 19–44.

Bouwman, A.F., Beusen, A.H., Billen, G., 2009. Human alteration of the global nitrogen and phosphorus soil balances for the period 1970–2050. Glob. Biogeochem. Cycles 23.

Bouwman, A.F., Boumans, L.J.M., Batjes, N.H., 2002. Estimation of global NH3 volatilization loss from synthetic fertilizers and animal manure applied to arable lands and grasslands. Glob. Biogeochem. Cycles 16, 8-1-8–14.

Bouwman, L., Goldewijk, K.K., Van Der Hoek, K.W., Beusen, A.H.W., Van Vuuren, D.P., Willems, J., Rufino, M.C., Stehfest, E., 2013. Exploring global changes in nitrogen and phosphorus cycles in agriculture induced by livestock production over the 1900-2050 period. Proc. Natl. Acad. Sci. 110, 20882–20887. https://doi.org/10.1073/pnas.1012878108

Buckwell, A., Nadeu, E., 2016. Nutrient Recovery and Reuse (NRR) in European agriculture. A review of the issues, opportunities, and actions. Bruss. RISE Found.

David, M.B., Drinkwater, L.E., McIsaac, G.F., 2010. Sources of nitrate yields in the Mississippi River Basin. J. Environ. Qual. 39, 1657–1667.

Davidson, E.A., 2009. The contribution of manure and fertilizer nitrogen to atmospheric nitrous oxide since 1860. Nat. Geosci. 2, 659.

Del Giudice, D., Matli, V.R.R., Obenour, D.R., 2019. Bayesian mechanistic modeling characterizes Gulf of Mexico hypoxia: 1968–2016 and future scenarios. Ecol. Appl. https://doi.org/10.1002/eap.2032

Eggleston, S., Buendia, L., Miwa, K., Ngara, T., Tanabe, K., 2006. 2006 IPCC guidelines for national greenhouse gas inventories. Institute for Global Environmental Strategies Hayama, Japan.

Elser, J., Bennett, E., 2011. A broken biogeochemical cycle. Nature 478, 29–31. https://doi.org/10.1038/478029a

Feyereisen, G.W., Kleinman, P.J., Folmar, G.J., Saporito, L.S., Way, T.R., Church, C.D., Allen, A.L., 2010. Effect of direct incorporation of poultry litter on phosphorus leaching from coastal plain soils. J. Soil Water Conserv. 65, 243–251.

Garnier, J., Lassaletta, L., Billen, G., Romero, E., Grizzetti, B., Némery, J., Le, T.P.Q., Pistocchi, C., Aissa-Grouz, N., Luu, T.N.M., 2015. Phosphorus budget in the water-agro-food system at nested scales in two contrasted regions of the world (ASEAN-8 and EU-27). Glob. Biogeochem. Cycles 29, 1348–1368.

He, Z., Pagliari, P.H., Waldrip, H.M., 2016. Applied and environmental chemistry of animal manure: A review. Pedosphere 26, 779–816.

Holland, E.A., Lee-Taylor, J., Nevison, C., Sulzman, J.M., 2005. Global N Cycle: fluxes and N2O mixing ratios originating from human activity. ORNL DAAC.

Jones, C.S., Drake, C.W., Hruby, C.E., Schilling, K.E., Wolter, C.F., 2019. Livestock manure driving stream nitrate. Ambio 48, 1143–1153.
Kellogg, R.L., Lander, C.H., Moffitt, D.C., Gollehon, N., 2000. Manure nutrients relative to the capacity of cropland and pastureland to assimilate nutrients. US Dep. Agric. Nat. Resour. Conserv. Serv. Agric. Res. Serv.
Klein Goldewijk, K., Beusen, A., Doelman, J., Stehfest, E., 2017. Anthropogenic land use estimates for the Holocene – HYDE 3.2. Earth Syst. Sci. Data 9, 927–953. https://doi.org/10.5194/essd-9-927-2017
Koppelaar, R.H.E.M., Weikard, H.P., 2013. Assessing phosphate rock depletion and phosphorus recycling options. Glob. Environ. Change 23, 1454–1466. https://doi.org/10.1016/j.gloenvcha.2013.09.002
Lassaletta, L., Billen, G., Grizzetti, B., Anglade, J., Garnier, J., 2014. 50 year trends in nitrogen use efficiency of world cropping systems: the relationship between yield and nitrogen input to cropland. Environ. Res. Lett. 9, 105011. https://doi.org/10.1088/1748-9326/9/10/105011
MacDonald, G.K., Bennett, E.M., Taranu, Z.E., 2012. The influence of time, soil characteristics, and land-use history on soil phosphorus legacies: a global meta-analysis. Glob. Change Biol. 18, 1904–1917. https://doi.org/10.1111/j.1365-2486.2012.02653.x
MacDonald, J.M., 2009. Manure use for fertilizer and for energy: report to congress. DIANE Publishing.
Monfreda, C., Ramankutty, N., Foley, J.A., 2008. Farming the planet: 2. Geographic distribution of crop areas, yields, physiological types, and net primary production in the year 2000. Glob. Biogeochem. Cycles 22.
Mueller, N.D., Lassaletta, L., 2020. Nitrogen challenges in global livestock systems. Nat. Food 1, 400–401. https://doi.org/10.1038/s43016-020-0117-7
Oenema, O., Oudendag, D., Velthof, G.L., 2007. Nutrient losses from manure management in the European Union. Livest. Sci., Recycling of Livestock Manure in a Whole-Farm Perspective 112, 261–272. https://doi.org/10.1016/j.livsci.2007.09.007
Potter, P., Ramankutty, N., Bennett, E.M., Donner, S.D., 2010. Characterizing the Spatial Patterns of Global Fertilizer Application and Manure Production. Earth Interact. 14, 1–22. https://doi.org/10.1175/2009EI288.1
Powers, S.M., Chowdhury, R.B., MacDonald, G.K., Metson, G.S., Beusen, A.H.W., Bouwman, A.F., Hampton, S.E., Mayer, B.K., McCrackin, M.L., Vaccari, D.A., 2019. Global Opportunities to Increase Agricultural Independence Through Phosphorus Recycling. Earths Future 7, 370–383. https://doi.org/10.1029/2018EF001097
Puckett, L., Hitt, K., Alexander, R., 1998. County-based estimates of nitrogen and phosphorus content of animal manure in the United States for 1982, 1987, and 1992. US Geological Survey.
Rabalais, N.N., Turner, R.E., 2019. Gulf of Mexico Hypoxia: Past, Present, and Future. Limnol. Oceanogr. Bull. 28, 117–124. https://doi.org/10.1002/lob.10351
Robinson, T.P., Wint, G.R.W., Conchedda, G., Van Boeckel, T.P., Ercoli, V., Palamara, E., Cinardi, G., D'Aietti, L., Hay, S.I., Gilbert, M., 2014. Mapping the Global Distribution of Livestock. PLoS ONE 9, e96084. https://doi.org/10.1371/journal.pone.0096084
Rowe, H., Withers, P.J.A., Baas, P., Chan, N.I., Doody, D., Holiman, J., Jacobs, B., Li, H., MacDonald, G.K., McDowell, R., Sharpley, A.N., Shen, J., Taheri, W., Wallenstein, M., Weintraub, M.N., 2016. Integrating legacy soil phosphorus into sustainable nutrient

management strategies for future food, bioenergy and water security. Nutr. Cycl. Agroecosystems 104, 393–412. https://doi.org/10.1007/s10705-015-9726-1
Ruddy, B.C., Lorenz, D.L., Mueller, D.K., 2006. County-level estimates of nutrient inputs to the land surface of the conterminous United States, 1982-2001.
Saunders, M.A., Lea, A.S., 2008. Large contribution of sea surface warming to recent increase in Atlantic hurricane activity. Nature 451, 557–560. https://doi.org/10.1038/nature06422
Schlesinger, W.H., Bernhardt, E.S., 2013. Biogeochemistry: An Analysis of Global Change. Academic Press.
Seitzinger, S.P., Styles, R.V., Boyer, E.W., Alexander, R.B., Billen, G., Howarth, R.W., Mayer, B., Van Breemen, N., 2002. Nitrogen retention in rivers: model development and application to watersheds in the northeastern USA, in: The Nitrogen Cycle at Regional to Global Scales. Springer, pp. 199–237.
Sheldrick, W., Syers, J.K., Lingard, J., 2003. Contribution of livestock excreta to nutrient balances. Nutr. Cycl. Agroecosystems 66, 119–131.
Sheldrick, W.F., Syers, J.K., Lingard, J., 2002. A conceptual model for conducting nutrient audits at national, regional, and global scales. Nutr. Cycl. Agroecosystems 62, 61–72.
Smith, D.R., Owens, P.R., Leytem, A.B., Warnemuende, E.A., 2007. Nutrient losses from manure and fertilizer applications as impacted by time to first runoff event. Environ. Pollut. 147, 131–137.
Smith, K.A., Chalmers, A.G., Chambers, B.J., Christie, P., 1998. Organic manure phosphorus accumulation, mobility and management. Soil Use Manag. 14, 154–159. https://doi.org/10.1111/j.1475-2743.1998.tb00634.x
Tabachow, R.M., Peirce, J.J., Essiger, C., 2001. Hurricane-Loaded Soil. J. Environ. Qual. 30, 1904–1910. https://doi.org/10.2134/jeq2001.1904
Thornton, P.K., 2010. Livestock production: recent trends, future prospects. Philos. Trans. R. Soc. B Biol. Sci. 365, 2853–2867. https://doi.org/10.1098/rstb.2010.0134
Tian, H., Lu, C., Ciais, P., Michalak, A.M., Canadell, J.G., Saikawa, E., Huntzinger, D.N., Gurney, K.R., Sitch, S., Zhang, B., 2016. The terrestrial biosphere as a net source of greenhouse gases to the atmosphere. Nature 531, 225.
Tian, H., Xu, R., Canadell, J.G., Thompson, R.L., Winiwarter, W., Suntharalingam, P., Davidson, E.A., Ciais, P., Jackson, R.B., Janssens-Maenhout, G., Prather, M.J., Regnier, P., Pan, N., Pan, S., Peters, G.P., Shi, H., Tubiello, F.N., Zaehle, S., Zhou, F., Arneth, A., Battaglia, G., Berthet, S., Bopp, L., Bouwman, A.F., Buitenhuis, E.T., Chang, J., Chipperfield, M.P., Dangal, S.R.S., Dlugokencky, E., Elkins, J.W., Eyre, B.D., Fu, B., Hall, B., Ito, A., Joos, F., Krummel, P.B., Landolfi, A., Laruelle, G.G., Lauerwald, R., Li, W., Lienert, S., Maavara, T., MacLeod, M., Millet, D.B., Olin, S., Patra, P.K., Prinn, R.G., Raymond, P.A., Ruiz, D.J., van der Werf, G.R., Vuichard, N., Wang, J., Weiss, R.F., Wells, K.C., Wilson, C., Yang, J., Yao, Y., 2020. A comprehensive quantification of global nitrous oxide sources and sinks. Nature 586, 248–256. https://doi.org/10.1038/s41586-020-2780-0
Tian, H., Yang, J., Xu, R., Lu, C., Canadell, J.G., Davidson, E.A., Jackson, R.B., Arneth, A., Chang, J., Ciais, P., Gerber, S., Ito, A., Joos, F., Lienert, S., Messina, P., Olin, S., Pan, S., Peng, C., Saikawa, E., Thompson, R.L., Vuichard, N., Winiwarter, W., Zaehle, S., Zhang, B., 2019. Global soil nitrous oxide emissions since the preindustrial era estimated by an ensemble of terrestrial biosphere models: Magnitude, attribution, and uncertainty. Glob. Change Biol. 25, 640–659. https://doi.org/10.1111/gcb.14514

Trenberth, K., 2005. Uncertainty in Hurricanes and Global Warming. Science 308, 1753–1754. https://doi.org/10.1126/science.1112551

Van Drecht, G., Bouwman, A.F., Boyer, E.W., Green, P., Siebert, S., 2005. A comparison of global spatial distributions of nitrogen inputs for nonpoint sources and effects on river nitrogen export: GLOBAL NEWS-COMPARISON OF GLOBAL NITROGEN INPUTS. Glob. Biogeochem. Cycles 19, n/a-n/a. https://doi.org/10.1029/2005GB002454

Williams, M.R., Feyereisen, G.W., Beegle, D.B., Shannon, R.D., Folmar, G.J., Bryant, R.B., 2011. Manure application under winter conditions: Nutrient runoff and leaching losses. Trans. ASABE 54, 891–899.

Xu, R., Pan, S.F., Chen, J., Chen, G.S., Yang, J., Dangal, S.R.S., Shepard, J.P., Tian, H.Q., 2018. Half-century ammonia emissions from agricultural systems in Southern Asia: Magnitude, spatiotemporal patterns, and implications for human health. GeoHealth 2, 40–53.

Yang, Q., Tian, H., Li, X., Ren, W., Zhang, B., Zhang, X., Wolf, J., 2016. Spatiotemporal patterns of livestock manure nutrient production in the conterminous United States from 1930 to 2012. Sci. Total Environ. 541, 1592–1602. https://doi.org/10.1016/j.scitotenv.2015.10.044

Yu, Z., Lu, C., 2018. Historical cropland expansion and abandonment in the continental U.S. during 1850 to 2016. Glob. Ecol. Biogeogr. 27, 322–333. https://doi.org/10.1111/geb.12697

Zanon, J.A., Favaretto, N., Goularte, G.D., Dieckow, J., Barth, G., 2019. Manure application at long-term in no-till: Effects on runoff, sediment and nutrients losses in high rainfall events. Agric. Water Manag. 105908.

Zhang, B., Tian, H., Lu, C., Dangal, S.R.S., Yang, J., Pan, S., 2017. Global manure nitrogen production and application in cropland during 1860–2014: a 5 arcmin gridded global dataset for Earth system modeling. Earth Syst. Sci. Data 9, 667–678. https://doi.org/10.5194/essd-9-667-2017

Zhang, X., Davidson, E.A., Zou, T., Lassaletta, L., Quan, Z., Li, T., Zhang, W., 2020. Quantifying Nutrient Budgets for Sustainable Nutrient Management. Glob. Biogeochem. Cycles 34, e2018GB006060. https://doi.org/10.1029/2018GB006060

Chapter 4. Century-long changes and drivers of P loading across land-ocean interface: A case study in the Mississippi River Basin

Abstract

Phosphorus (P) control is critical to mitigating eutrophication in aquatic ecosystems, but the effectiveness of controlling P export from soils has been limited by our poor understanding of P dynamics along the land-ocean aquatic continuum as well as the lack of well-developed process models that effectively couple terrestrial and aquatic biogeochemical P processes. Here, we coupled riverine P biogeochemical processes and water transport with terrestrial processes within the framework of the Dynamic Land Ecosystem Model (DLEM) to assess how multiple environmental changes, including fertilizer and manure P uses, land use, climate, and atmospheric CO_2, have affected the long-term dynamics of P loading and export from the Mississippi River Basin to the Gulf of Mexico during 1901-2018. Simulations show that riverine exports of dissolved inorganic phosphorus (DIP), dissolved organic phosphorus (DOP), particulate organic phosphorus (POP), and particulate inorganic phosphorus (PIP) increased by 42%, 33%, 59%, and 54%, respectively, since the 1900s. Riverine DIP and PIP exports were the dominant components of the total P flux. DIP export was mainly enhanced by the growing mineral P fertilizer use in croplands, while increased PIP and POP exports were a result of the intensified soil erosion due to increased precipitation. Climate variability resulted in substantial interannual and decadal variations in P loading and export. Soil legacy P continues to contribute to P loading. Our findings highlight the necessity to adopt effective P management strategies to control P losses through reductions in soil erosion, and additionally, to improve P use efficiency in crop production.

1. Introduction

Since the middle of the 20th century, a substantial amount of geological phosphorus (P) has entered terrestrial ecosystems as fertilizer to stimulate crop production (Elser and Bennett, 2011). Global mobilization of P has roughly tripled compared to its natural state (Smil, 2000) and the riverine P flux from land to ocean has accelerated (Carpenter, 2005). As the P cycle is a largely one-way flow from rock to soil and finally to streams, lakes, and oceans, the growing use

of industrial P fertilizer is rapidly depleting the supply of mineable deposits of P rock which are in limited supply and unevenly distributed around the world (Amundson et al., 2015). Furthermore, the increasing amount of P entering water bodies can disturb the ecological balance of aquatic systems, cause eutrophication and water quality degradation, and threaten human health and economic activities (Garnier et al., 2015). Freshwater lakes, reservoirs, and streams are typically P limited and vulnerable to P enrichment (Colborne et al., 2019; Correll, 1998). While coastal and oceanic hypoxia is commonly associated with nitrogen (N) loading (Ryther and Dunstan, 1971), the impact of P on coastal areas can also be detrimental to the headwaters of estuaries (Correll, 1998) and coastal areas with historically excessive nutrient loading (Conley et al., 2009; Lohrenz et al., 2008). The increasing loading of N, relative to P, from the Mississippi River Basin (MRB) has been associated with periodic P limitation in river-influenced regions of the northern Gulf of Mexico, especially during the spring bloom period (Sylvan et al., 2007). As studies suggest the important role of P in the occurrence of Gulf hypoxia, there is a growing recognition of the need to control both N and P loading from the MRB (Fennel and Laurent, 2018; Scavia and Donnelly, 2007; Sylvan et al., 2006). Therefore, evaluating P loading and export from land to ocean is critical for sustainable nutrient management and water security.

Numerous statistical and mechanistic models have been used to estimate P losses from terrestrial ecosystems to waterways. For example, the SPARROW model (Alexander et al., 2008) and the IMAGE-GNM (Beusen et al., 2015) have been used to estimate riverine P loading from the MRB. However, models that can comprehensively couple P processes across the land–aquatic interface are still lacking. In particular, previous studies based on limited observational data and over-simplified models have not adequately addressed how climate and human activities could interactively impact P export at a century-long time scale. Connecting P transformation and transport between the terrestrial and aquatic ecosystems can provide a new perspective to evaluate the P dynamic along the terrestrial-aquatic continuum and its response to environmental changes. In this study, our objectives were: (1) use the MRB as a testbed to evaluate the performance of the improved DLEM in simulating P loading and export across the land–aquatic interface, (2) estimate the exports of dissolved inorganic phosphorus (DIP), dissolved organic phosphorus (DOP), particulate organic phosphorus (POP), and particulate inorganic phosphorus (PIP) from the MRB to the Gulf of Mexico during 1901–2018; and (3) further quantify the contributions of climate, anthropogenic P input, land-use change, and

atmospheric CO_2 concentration to changes in P loading over the study period. This work will improve our understanding of underlying mechanisms controlling P loading and provide valuable information for nutrient management and pollution mitigation in the MRB.

2. Material and methods

2.1. Wastewater P discharge

The P discharge to surface water from wastewater is estimated based on an empirical approach developed by Van Drecht et al. (2009). The P discharge from wastewater mainly consists of P in human waste, laundry detergents, and dishwasher detergents, which are calculated as:

$$SWP_{i,y} = Pop_{i,y}\left(Hum_{i,y} + Det_y\right)D_y\left(1 - R_y\right) \quad (1)$$

where $SWP_{i,y}$ is the P discharge to surface water from sewage (g P person^{-1} day^{-1}) in year *y* and grid cell *i*; $Pop_{i,y}$ is population (person); $Hum_{i,y}$ and Det_y (g P person^{-1} day^{-1}) are wastewater P from human excreta and P-based detergents (laundry and dishwater), respectively; D_y is the fraction of the total population that is connected to public sewage systems and R_y is the removal fraction of P through wastewater treatment. The large-scale usage of P-based detergents started in 1940 when synthetic detergents were newly introduced, and the banning of phosphates in detergents emerged in the early 1970s, which culminated in a nationwide voluntary ban in 1994 (Litke, 1999). The peak value of detergent P usage in 1970 was estimated as 0.82 g P person^{-1} day^{-1} (Van Drecht et al., 2009), and we assumed it linearly increased from 1940 to 1970 then linearly decreased until 1994. The fraction of households connected to sewage systems in the U.S. was around 75% after 2000 (van Puijenbroek et al., 2019). The construction of sewage systems in industrialized countries started from the year 1870 onward, and a linear increase in D_y could be assumed for the period 1870-2000 (Morée et al., 2013). The general P removal fractions of primary treatment, secondary treatment, and tertiary treatment were estimated as 10%, 45%, and 90%, respectively (Van Drecht et al., 2009). The large-scale secondary treatment in the U.S. began around 1920 and tertiary treatment started to grow rapidly since 1970 (Hale et al., 2015). Thus we assumed R_y value were linearly increased to 0.1 in 1920, and to 0.45 in 1970, then it increased at a rate of 0.9% per year until 1990, and 0.3% afterwards according to the change rate of R estimated by Van Drecht et al. (2009). Hum was calculated as:

$$Hum_{i,y} = HumN_{i,y} f_{NP} \quad (2)$$

$$HumN_{i,y} = 0.365 \left[4 + 14 \left(\frac{GDP_{i,y}}{33{,}000} \right)^{0.3} \right] \quad (3)$$

where $HumN_{i,y}$ is the protein N intake (g N person^{-1} day^{-1}) and is estimated according to empirical relationships with per capita gross domestic product (GDP) (Van Drecht et al., 2009); f_{NP} is the ratio between human P and N waste and set as 1:10 (mass basis) (Morée et al., 2013). The TP estimated in this approach is divided into DIP (57.0%), DOP (0.5%), POP (2.3%), and PIP (40.2%) according to the information provided by Gu et al. (2011). The wastewater P directly enters surface water within each grid, and the simulated total wastewater P is presented in Figure 4-1d.

2.2. Data sources

Several datasets were developed or collected to characterize natural and human forcing in the MRB (Table 4-1). Based on the datasets, all the required input data for the model simulation (e.g., climate, land use, river network, soil properties, atmospheric CO_2, N inputs, P inputs, etc.) were developed at a spatial resolution of 5×5 arc-min. The daily climate data from 1979–2018, including precipitation, temperature, etc., were obtained from GRIDMET (Abatzoglou, 2013), and climate data before 1979 were downscaled from the CRUNCEP dataset (Viovy, 2018) and bias-corrected to GRIDMET. P fertilizer application data were developed based on crop-specific application data from the USDA National Agricultural Statistics Service (https://quickstats.nass.usda.gov/) and combined with cropland distribution maps. Since USDA only provided P fertilizer data after 1960, we assumed the changing trend of P fertilizer in the U.S. during 1860–1960 was consistent with global agricultural P fertilizer usage (Cordell et al., 2009). Manure P data were derived from the gridded manure P production and application dataset in the U.S. developed by Bian et al. (2021). Both P fertilizer and manure application increased rapidly from the 1940s to the 1970s (Figure 4-1b). Yearly P deposition data were extracted from a global P deposition map (Mahowald et al., 2008). P deposition only accounted for a small share (around 1% in 2000) of the total P input to terrestrial ecosystems compared to other sources. For land-use change, cropland expanded rapidly from 1901 to 1930 but decreased dramatically during 1955-1965 due to cropland abandonment; thereafter, cropland area increased again and stayed relatively stable after the 1980s (Figure 4-1c).

The MRB, draining 4.76 million km^2, encompasses 41% of the contiguous U.S. and is the largest contributor of fresh water and nutrients to the Gulf of Mexico. The MRB consists of seven major sub-basins, including Upper Mississippi, Ohio, Missouri, Arkansas, Red, Tennessee, and Lower Mississippi River basins (Figure 4-2). River discharge and water quality data of four USGS sites in the MRB at the outlet of major sub-basins were selected to calibrate and validate the DLEM–Terrestrial/Aquatic scheme simulated results. Near the outlet of the Lower Mississippi River basin, around 30% of the flow is diverted down the Atchafalaya River through the Old River Control Structure. The riverine transport in DLEM was simulated based on the river network and flow direction data derived from topographic data (Wu et al., 2012) and cannot capture this human-controlled flow diversion. Instead of validating P fluxes at USGS sites inside the Lower Mississippi River basin, we validated the riverine P export from the whole basin by comparing the simulated P exports from the MRB with the annual P exports data reported by USGS (https://nrtwq.usgs.gov/nwqn/#/GULF), which combined the observed loading data from sites on both the Mississippi River and Atchafalaya River (Lee et al., 2017).

To obtain continuous monthly P flux data based on water quality data from the four USGS sites, the Weighted Regressions on Time, Discharge, and Season (WRTDS) method was applied to calculate monthly DIP, total dissolved P (TDP), and TP loading from 1979 to 2018 (Hirsch et al., 2010). However, the WRTDS method cannot be directly applied at two sites (USGS 03612600 in Ohio/Tennessee, 07263620 in Arkansas) where long-term daily discharge data were not available from the USGS National Water Information System. So, we acquired the long-term monthly P loading data (DIP and TP) at these three sites from the USGS National Water Quality Network where monthly P loading in MRB has been assessed. The model outputs have four P components (DIP, DOP, POP, and PIP), but only three major P variables (DIP, TDP, and TP) can be provided by the USGS for validation. TDP (only available at USGS 06934500 in Missouri and 07022000 in Upper Mississippi) is the sum of DOP and DIP, and the difference between TP and TDP is particulate form P (PP), including POP and PIP. Simulated DOP can be indirectly validated according to the accuracy of simulated DIP and TDP; similarly, simulated PP can be validated by combining TP and TDP. However, the USGS data cannot support the validation of POP and PIP separately. To address this issue, we assumed the riverine POP had a stable ratio relationship with particulate organic carbon (POC). By verifying simulated riverine POC and PP, the simulated POP and PIP were validated indirectly (Yao et al., 2021). The USGS

data before 2000 were used for model calibration and the data after 2000 were used for model validation.

Table 4-1. Model input data and validation data.

Data variables	Time period/step	Reference/source
Model input data/Environmental Drivers		
Climate (Temperature, Precipitation)	1901–2018/ daily	GRIDMET (1979–2018) (http://www.climatologylab.org/gridmet.html) CRUNCEP (1901–1978) (https://doi.org/10.5065/PZ8F-F017)
Land Cover and Land Use (Crop density)	1901–2016/ yearly	(Yu and Lu, 2018)
P fertilizer application rate	1901–2018/ yearly	USDA National Agricultural Statistics Service (https://quickstats.nass.usda.gov/)
Manure P production	1901–2017 yearly	(Bian et al., 2021)
P deposition rate	Annual average	(Mahowald et al., 2008)
Model Calibration and Validation data		
River discharge, Water quality (DIP, TDP, TP) in USGS sites: 07022000, 06934500,	1979–2018 daily	USGS National Water Information System (https://waterdata.usgs.gov/nwis)
P loads (DIP, TP) in USGS sites: 03612600, 07263620	1979–2018 monthly	USGS National Water Quality Network (https://nrtwq.usgs.gov/nwqn/#/)
P loads (DIP, TP) from the whole MRB to the Gulf of Mexico	1980-2018 annually	USGS National Water Quality Network (https://nrtwq.usgs.gov/nwqn/#/GULF)

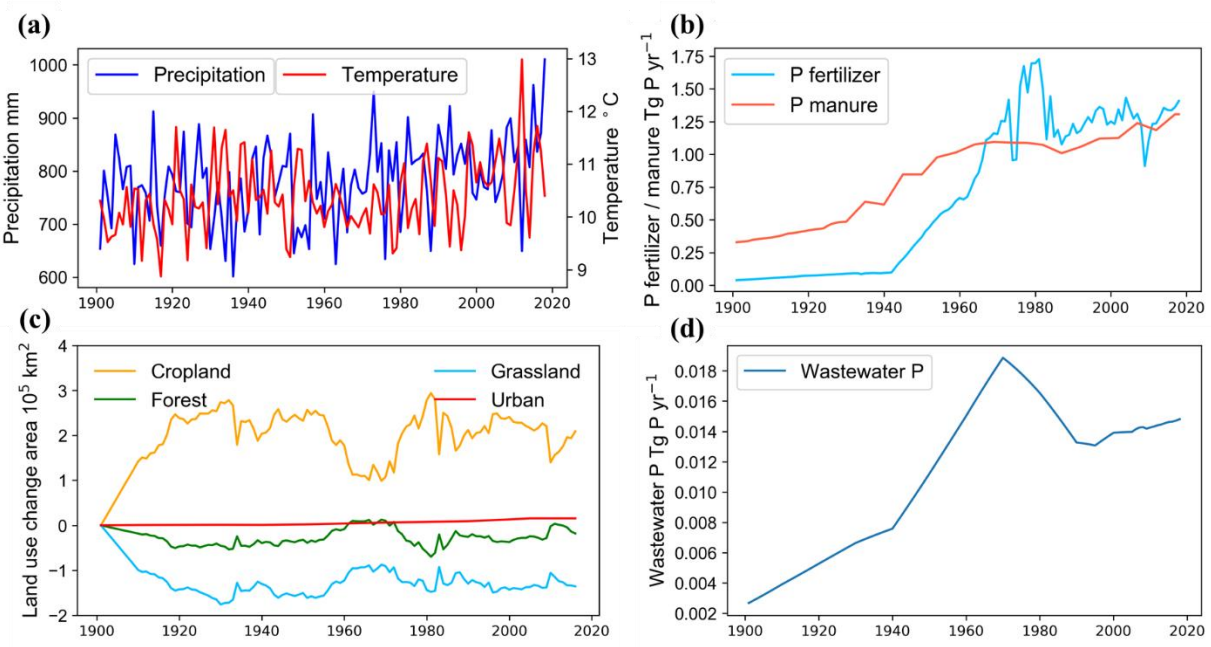

Figure 4-1. Interannual variation and trend of (a) climate, (b) fertilizer and manure P inputs, (c) land-use change area, and (d) wastewater P in the Mississippi River Basin.

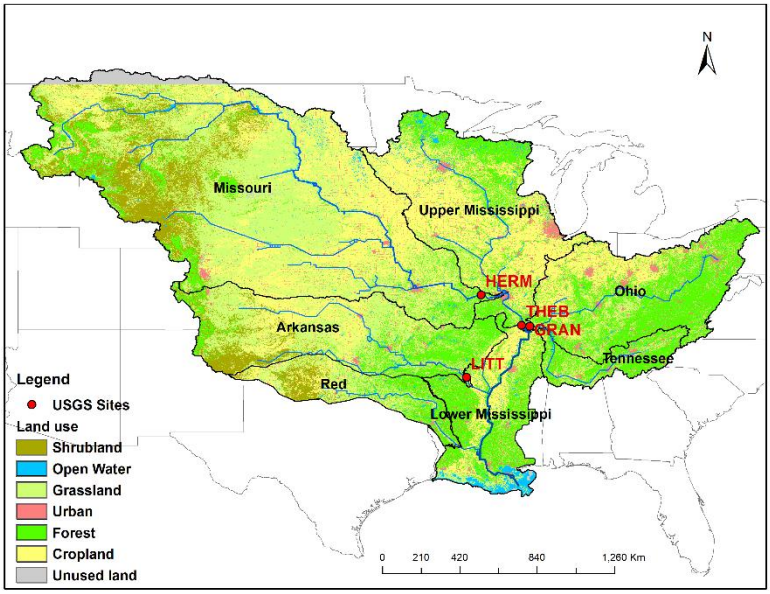

Figure 4-2. The Mississippi River Basin. USGS sites used for model calibration/validation include HERM (06934500), THEB (07022000), GRAN (03612600), LITT (07263620). Land use condition is derived from the National Land Cover Database (NLCD) 2016.

2.3. Simulation experiments

The DLEM simulations included three steps: 1) an equilibrium run that used 40-year (1861–1900) mean climate datasets to develop the initial state under the pre-1900 conditions; 2) a spin-up simulation that was performed to eliminate noise caused by the simulation shift from the equilibrium to the transient simulation; 3) a transient simulation using 118 years of forcings to generate results. Six simulation experiments (S1-S6), following a "without" strategy, were designed to study natural and anthropogenic impacts on riverine P loading (Table 4-2). All the simulations started from the same baseline equilibrium state. S1 (All combined) is the reference simulation with all the dynamic forcings. In experiment S2, the climate variables were fixed as the annual averages of climate data from 1901 to 1920. In experiments S3–S6, one of the forcings (CO_2, P fertilizer, P manure, and Land-use) was fixed in 1901, while other forcings varied with time. The differences between S2–S6 and S1 were taken as the impacts of the corresponding factors.

Table 4-2. Simulation experiments with the DLEM.

Experiments	Climate	CO_2	P fertilizer	P manure	Land-use
S1 (All combined)	1901–2018	1901–2018	1901–2018	1901–2018	1901–2018
S2 (Constant climate)	1901–1920 mean	1901–2018	1901–2018	1901–2018	1901–2018
S3 (Constant CO_2)	1901–2018	1901	1901–2018	1901–2018	1901–2018
S4 (Constant fertilizer)	1901–2018	1901–2018	1901	1901–2018	1901–2018
S5 (Constant manure)	1901–2018	1901–2018	1901–2018	1901	1901–2018
S6 (Constant land-use)	1901–2018	1901–2018	1901–2018	1901–2018	1901

3. Results

3.1. Model performance

The coefficient of determination (R^2) and Nash–Sutcliffe efficiency (*NSE*) were used to compare the simulated monthly results and USGS observed data. Target diagrams (Jolliff et al., 2009) provide information regarding the bias and Root–Mean–Square Difference (*RMSD*) of the simulated results (Table 4-3 and Figure 4-5). The DLEM-simulated discharge in the MRB has been validated and reported in a previous study (Figure 4-3, Tian et al., 2020). As for nutrient

fluxes, model performance at the watershed scale can be evaluated as "satisfactory" if monthly R^2>0.40, and *NSE*>0.35 (Moriasi et al., 2015). Generally, the DLEM could catch the variations and magnitudes of riverine DIP, TDP, and TP fluxes in the major sub-basins of MRB. For riverine DIP flux, the R^2 values ranged from 0.33 to 0.63, and *NSE* ranged from 0.32 to 0.59. The target diagram shows that the simulated results slightly overestimated DIP flux in the Ohio River, but slightly underestimated DIP flux in the Upper Mississippi River. The temporal variation of DIP fluxes agreed well with USGS data in most rivers except the Arkansas, where simulated DIP underestimated the peaks (Figure 4-4). For riverine TDP flux, the model performed well in the Missouri and Upper Mississippi Rivers, with low biases (Figures 4-4 and 4-5) and R^2 values ranging from 0.43 to 0.61 and *NSE* ranging from 0.23 to 0.57. The simulated riverine TP flux was overestimated in the Arkansas River but had very slight biases for other rivers, with R^2 values ranging from 0.26 to 0.70, and *NSE* ranging from 0.21 to 0.65. It was noted that the simulated results underestimate the numerous peaks of TP fluxes in Missouri and Upper Mississippi Rivers. The model performed better in the validation period than the calibration period for Missouri and Arkansas Rivers, and the opposite was seen for the Ohio River.

The average simulated DIP and TP exports from the MRB matched well with USGS observed data, though the interannual variation of P fluxes still showed discrepancies (Figure 4-6). The slope of simulated DIP export (0.14 Gg P yr^{-2}, p = 0.20) during 1980–2018 was similar to that of observed DIP export (0.15 Gg P yr^{-2}, p = 0.39), although the increasing trends were not significant (p >0.05). The simulated TP export increased at a rate of 1.03 Gg P yr^{-2} (p = 0.02) during 1980–2018, which was higher than the rate of observed TP export (slope = 0.77 Gg P yr^{-2}, p = 0.07). The simulated TP export slightly overestimated the increasing trend of TP export in recent decades.

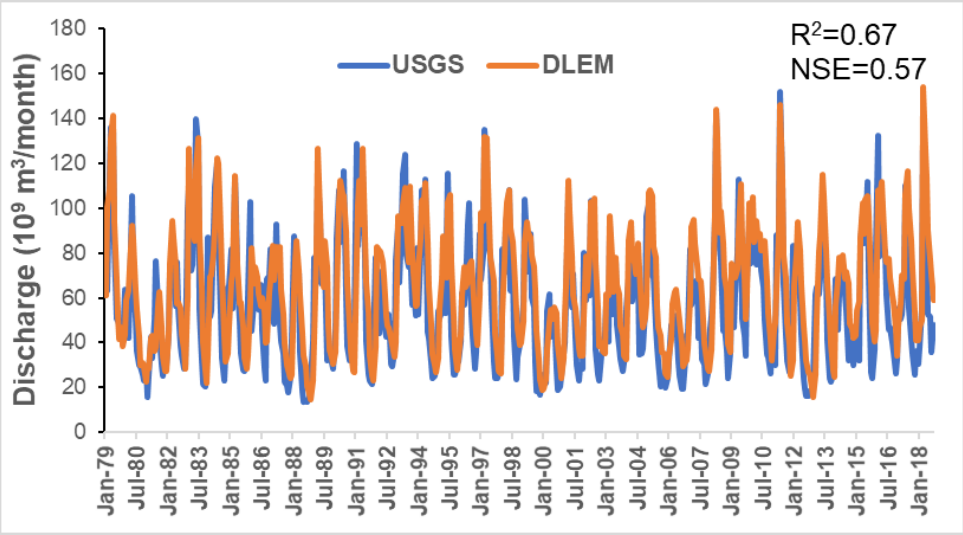

Figure 4-3. Comparison of monthly water flow between DLEM simulations and station observations from USGS stations. The USGS data are the sum of monthly flow at the Mississippi River at St. Francisville, Louisiana (site ID 07373420) and Atchafalaya River at Melville, Louisiana (site ID 07381495) gauging stations. The sum of water flow data at these two sites could approximately represent total water export from the MRB. More details of water discharge simulation by DLEM in the MRB can be found in Tao et al. (2014) and Tian et al. (2020).

Table 4-3. Evaluation of simulated results against field data.

Sub-basin (USGS Site ID)		TDP		DIP		TP	
		R^2	NSE	R^2	NSE	R^2	NSE
Missouri (USGS 06934500)	Calibration	0.43	0.23	0.46	0.37	0.26	0.21
	Validation	0.58	0.55	0.58	0.53	0.35	0.28
Upper Mississippi (USGS 07022000)	Calibration	0.57	0.57	0.59	0.57	0.47	0.46
	Validation	0.61	0.56	0.61	0.53	0.50	0.46
Ohio/Tennessee (USGS 03612600)	Calibration			0.63	0.59	0.60	0.59
	Validation			0.50	0.47	0.54	0.51
Arkansas (USGS 07263620)	Calibration			0.33	0.32	0.53	0.42
	Validation			0.49	0.44	0.70	0.65

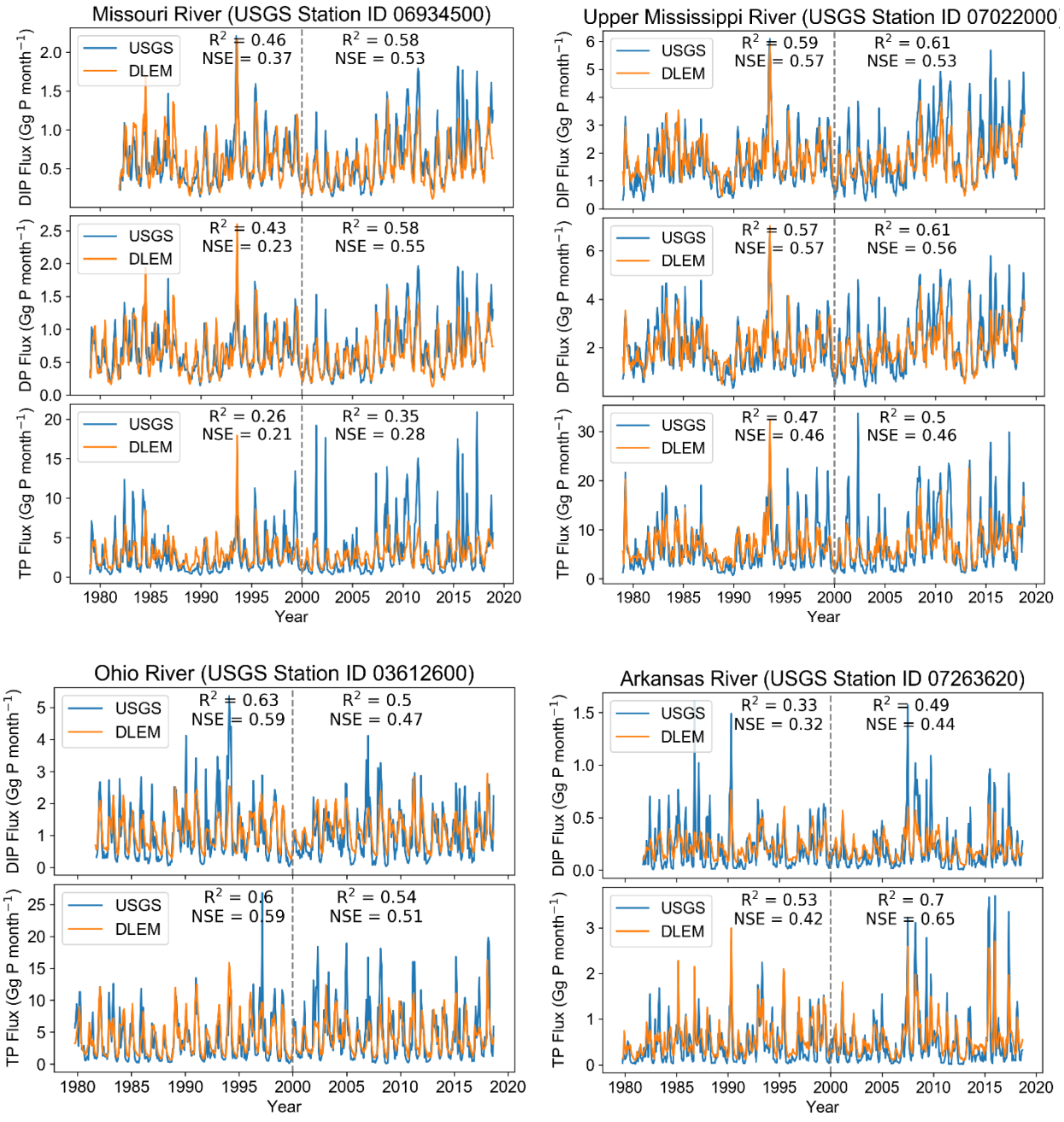

Figure 4-4. The comparison of monthly riverine DIP, DP, and TP fluxes between USGS data and DLEM results.

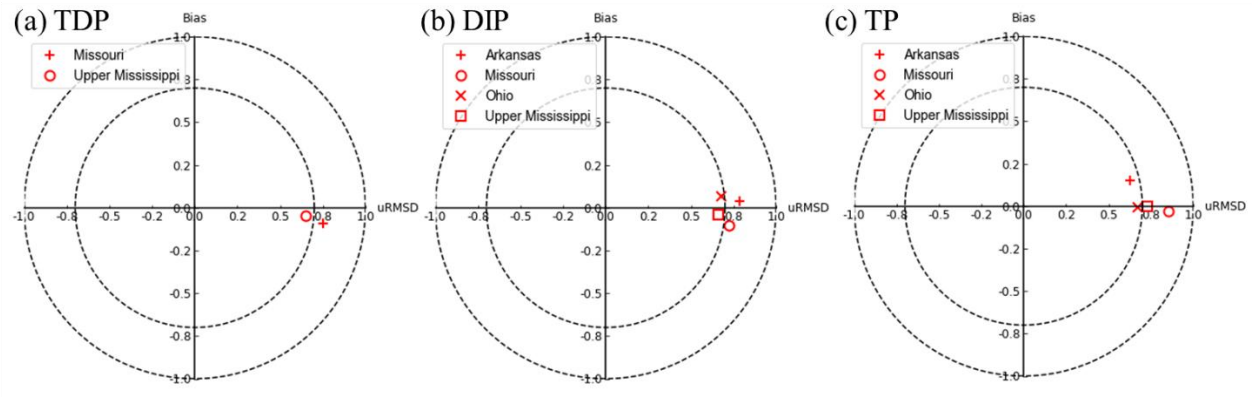

Figure 4-5. Normalized target diagrams for monthly (a) TDP, (b) DIP, and (c) TP comparisons between simulations and USGS data. (The X-axis is unbiased total Root–Mean–Square Difference (uRMSD), and Y-axis is normalized bias. Both axes are normalized by the standard deviation of USGS data)

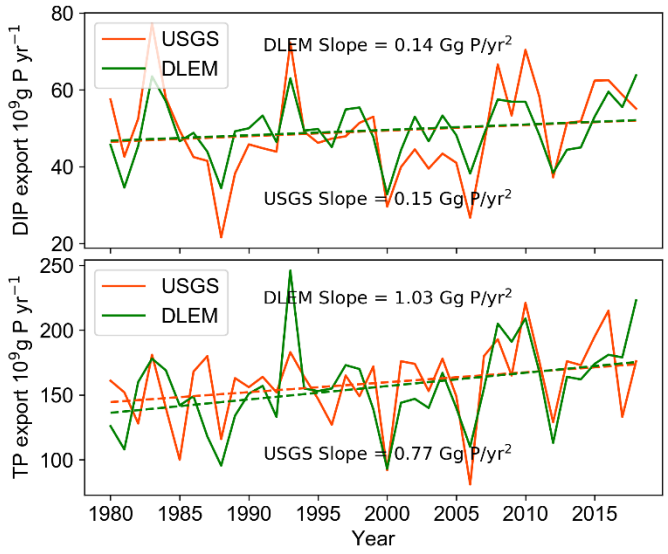

Figure 4-6. The comparison of USGS-observed and DLEM-simulated annual riverine DIP and TP exports from the MRB during 1980-2018.

3.2. Temporal pattern of P fluxes during 1901–2018

The simulated DIP, DOP, POP, and PIP exports from the MRB all exhibited obvious inter-annual fluctuations (Figure 4-7). Simulated riverine DIP export increased by 42%, from 36.3 Gg P yr^{-1} in the 1900s (1901–1909) to 51.6 Gg P yr^{-1} in the post-2010s (2010–2018). The fastest

growth of simulated DIP occurred during 1963–1973, at a rate of 2.0 Gg P yr^{-2}. After the 1970s, simulated DIP fluctuated around a stable value. Simulated riverine DOP export experienced a drop around the 1950s and 1960s, then increased in the 1970s, and leveled off thereafter, reaching 10.8 Gg P yr^{-1} in the post-2010s. Simulated POP and PIP exports, which exhibited a similar interannual variation pattern, increased by 59% (from 10.8 to 17.1 Gg P yr^{-1}) and by 54% (from 62.0 to 95.2 Gg P yr^{-1}), respectively, from the 1900s to the post-2010s. The growth rate of simulated POP and PIP had accelerated after the 1960s, at rates of 0.5 Gg P yr^{-2} and 0.1 Gg P yr^{-2}, respectively, during 1960-2018. The peak values of simulated P exports also became higher in some years of recent decades (e.g. 1993 and 2018). The PIP flux dominated the P export, accounting for 48-54% of TP export, followed by DIP flux, accounting for 30-35% (Figure 4-8). The POP and DOP fluxes contributed 9-10% and 6-8% to TP flux, respectively. The decadal average of TP export increased significantly since the 1960s and reached 163.1 Gg P yr^{-1} in the 1990s, then declined in the 2000s, but increased again to 174.8 Gg P yr^{-1} in the 2010s. From the 1960s to the post-2010s, DIP, DOP, POP, PIP, and TP increased by 42%, 53%, 60%, 53%, and 50%, respectively.

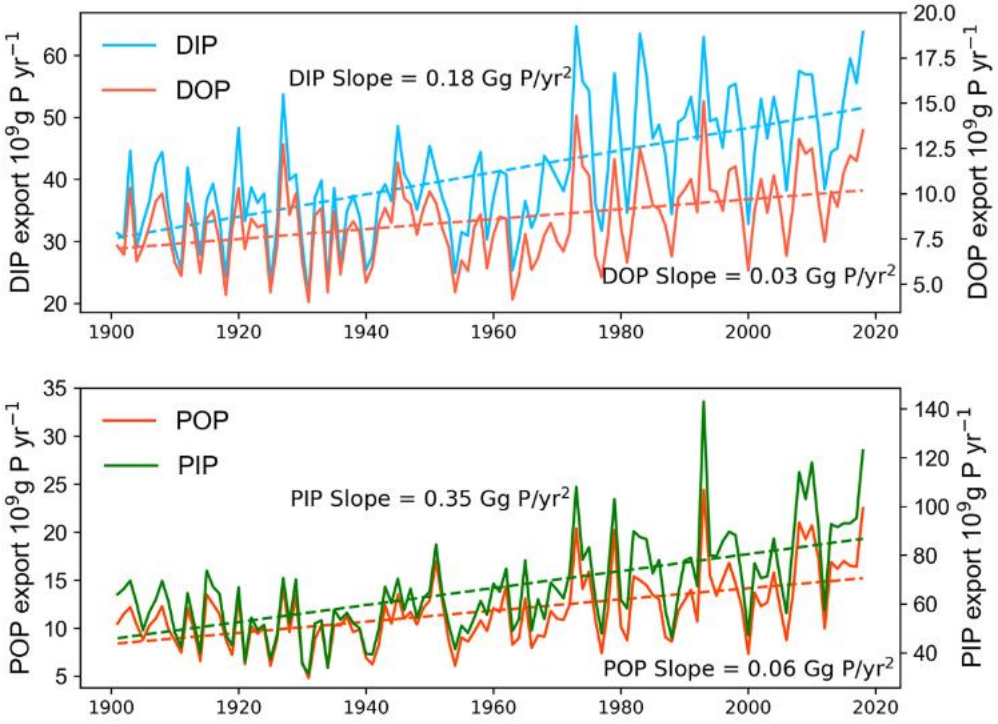

Figure 4-7. Interannual variation and trend in simulated DIP, DOP, POP, and PIP fluxes from the Mississippi River Basin during 1901–2018.

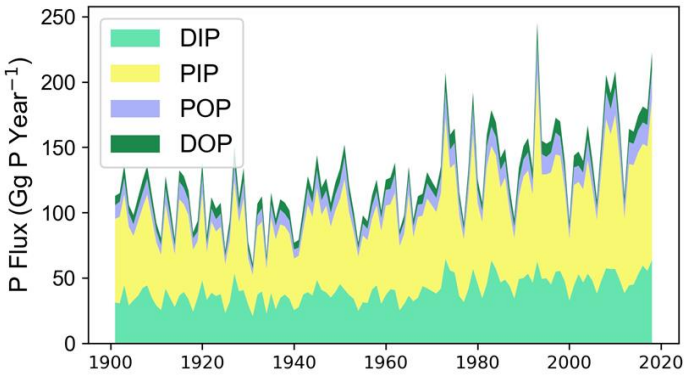

Figure 4-8. The annual variations and trends of riverine P fluxes from the MRB to the Gulf of Mexico.

3.3. Spatial variability of P yields

Yields of different P species showed different distribution characteristics which became noticeable, especially after 1980 (Figure 4-9). Simulated DIP yield decreased along a gradient from the central part of the MRB to both sides, and DOP yield was high in the central and eastern basin and low in the western part. With respect to change rates after 1980, DIP yield increased mostly in the cropland area (western Ohio, Upper Mississippi, and eastern Missouri) (Figures 4-2 and 4-10a). By contrast, DOP yield increased in almost the entire Ohio and slightly decreased in central Upper Mississippi and southern Lower Mississippi (Figure 4-10c). The distribution of simulated PIP and POP yields were similar, with high-yield regions concentrating on several hot spots (e.g. eastern Ohio, Upper Mississippi, western Missouri) (Figure 4-9). However, the change rates of PIP and POP yields were distributed more evenly (Figures 4-10b and 4-10d), with an increasing trend across most of the MRB except western Missouri. Compared to the other three P species, the change rate of DIP yield showed large spatial variability. It showed the fastest increase (>0.0006 g P m^{-2} yr^{-2}, p<0.05) in some regions like western Ohio and Upper Mississippi but the most rapid decrease (<–0.0004 g P m^{-2} yr^{-2}, p<0.05) in southeastern of Missouri, southern Lower Mississippi, and eastern Tennessee.

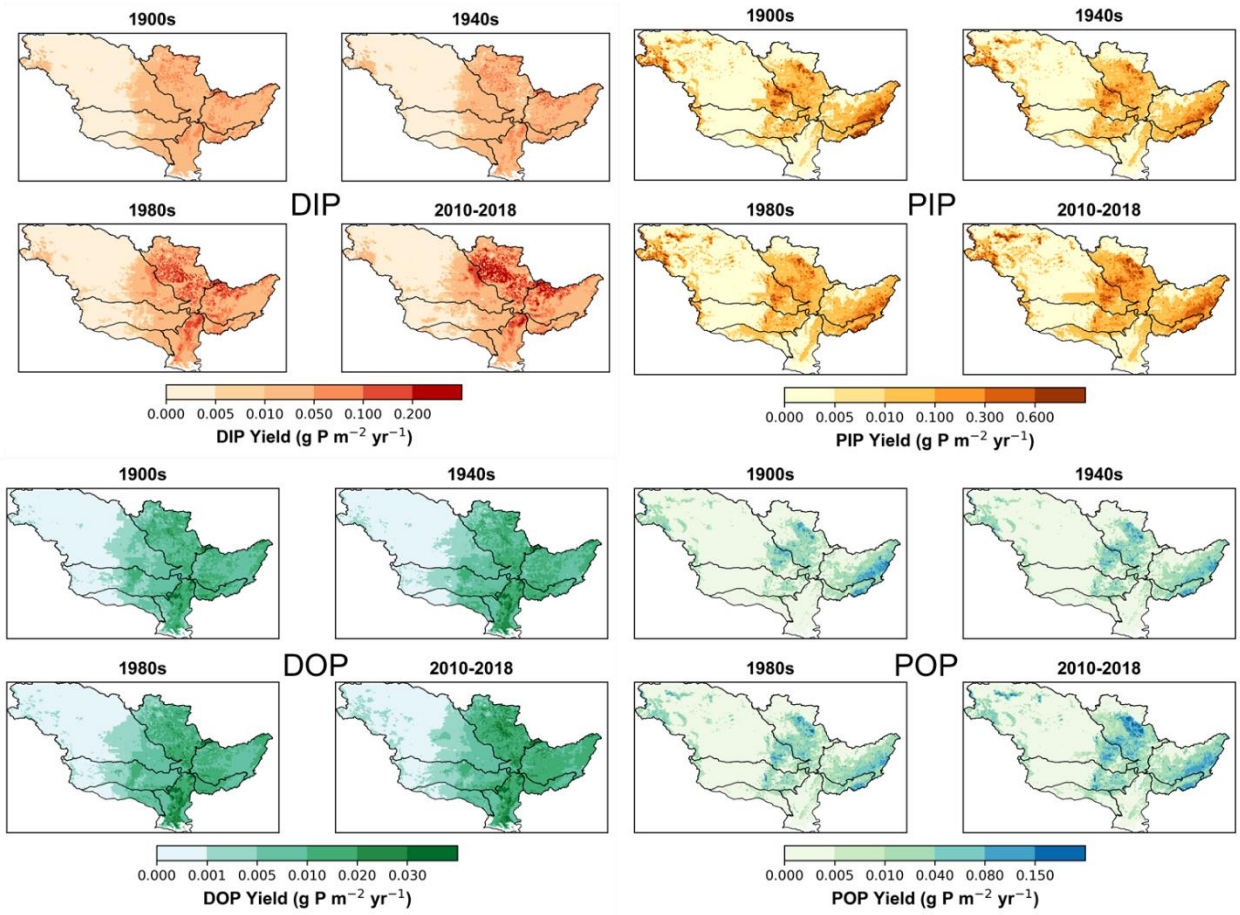

Figure 4-9. The spatial distributions of DIP, PIP, DOP, and POP yields across the MRB in the periods of the 1900s, 1940s, 1980s, and 2010-2018.

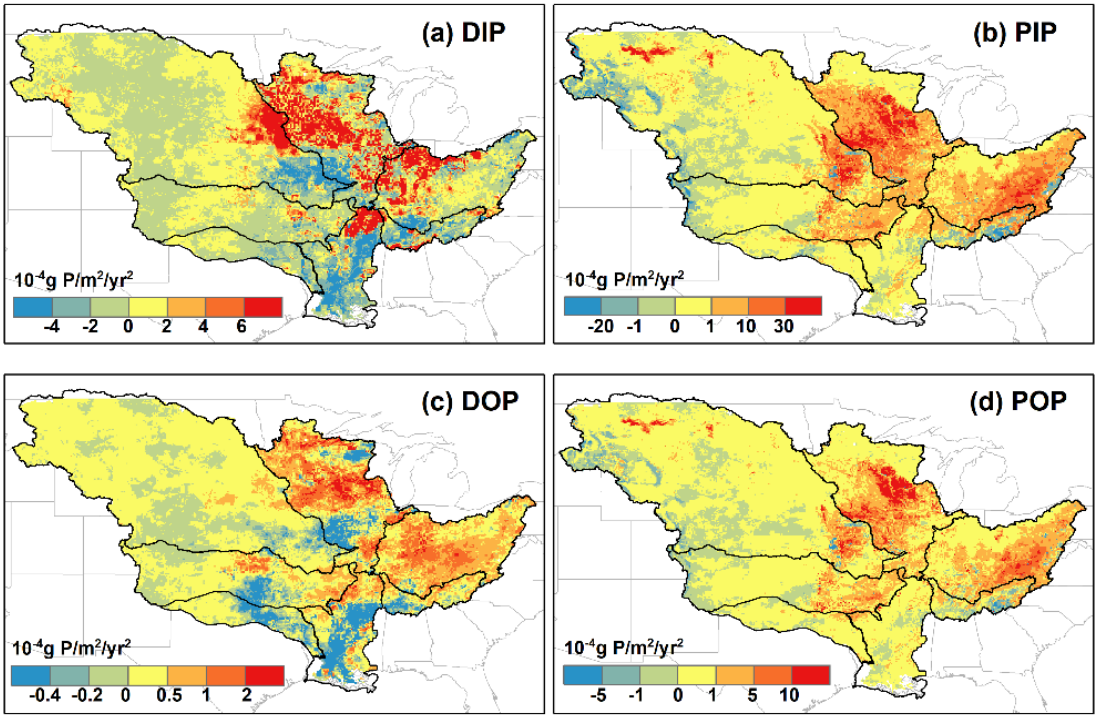

Figure 4-10. Annual change rates (1980–2018) in P yields: (a) DIP, (b) PIP, (c) DOP, and (d) POP. (Change rates of P yields were calculated based on the Mann–Kendall test)

3.4. Contributions of multiple environmental factors to changes in P loading

The increasing trends of different P components were dominated by different environmental factors (climate, fertilizer, manure, atmospheric CO_2, and land use), and the same factor might have opposite impacts on different P components (Figure 4-11). Riverine DIP loading is dominated by the increasing application of P fertilizer and manure after the 1950s. The simulated DIP export from 2010–2018 in S1 (reference simulation) is 27% higher than S4 ("constant fertilizer" simulation), and 17% higher than S5 ("constant manure" simulation). The land-use change (LUC) is the second important contributor to DIP export. Compared to S6 ("constant LUC" simulation), DIP export in S1 was 33% higher in the 1980s and 26% higher during 2010–2018. Climate variability and P fertilizer are two primary contributors to PIP export since the 1970s. Averaged over 2010–2018, the simulated export of PIP in S1 was higher than that in S2 ("constant climate" simulation) by 32% and S4 by 23%. LUC decreased the PIP export through the study period, and its impact was more pronounced before the 1940s but weakened thereafter. The changes in DOP and POP exports were dominated by two major factors, climate and LUC. The contributions of climate to DOP and POP exports magnified in recent decades,

and during 2010–2018, the exports of simulated riverine DOP and POP in S1 increased by 31% and 43%, respectively, compared with S2. LUC decreased DOP and POP exports by around 3% and 16% over 2010–2018, respectively. Since the 1970s, the rising atmospheric CO_2 concentration gradually increased the DOP export and played an increasingly important role in decreasing DIP and PIP exports.

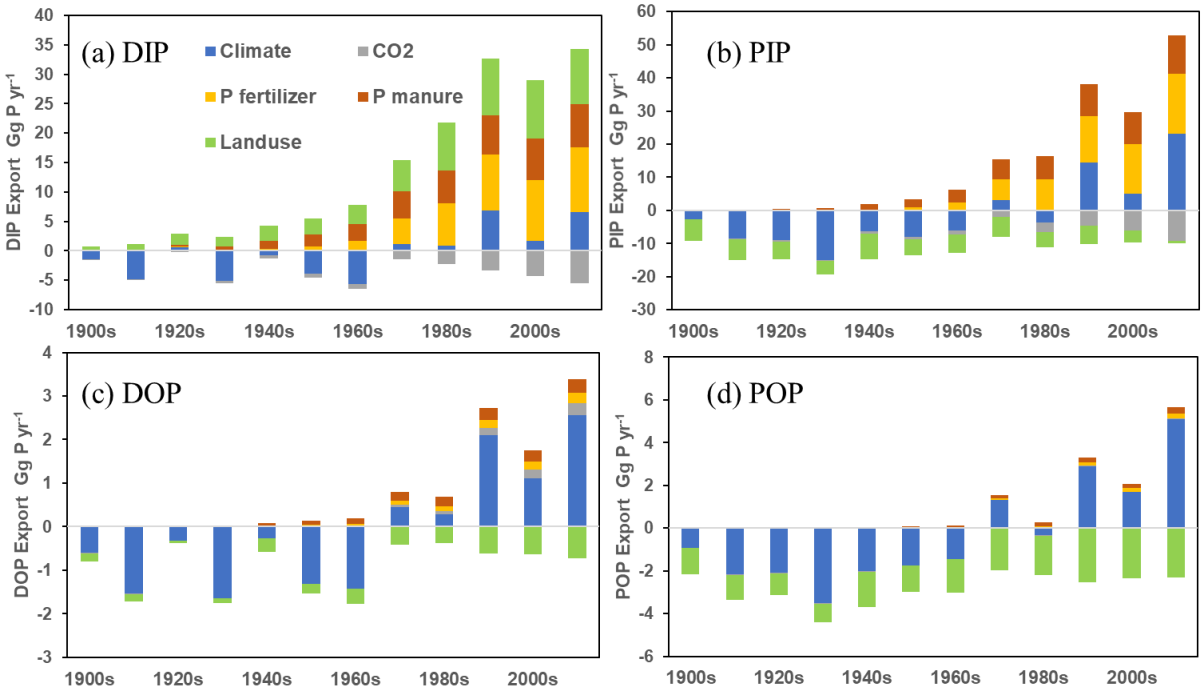

Figure 4-11. Decadal changes in the contributions of environmental factors on riverine (a) DIP, (b) PIP, (c) DOP, and (d) POP exports. Contributions were the cumulative difference between the reference simulation (S1) and counterfactual scenario (S2–S6) (see section 2.3).

In summary, climate (precipitation and temperature) variability and P fertilizer usage were the two key factors that increased TP loading since the 1970s (Table 4-4). The impacts of fertilizer application and animal manure on TP export continually increased throughout the study period, and climate induced the highest TP export (37.50 Gg P yr^{-1}) after 2010. Atmospheric CO_2 was the only factor that declined TP export since 1901, decreasing around 14.35 Gg P yr^{-1} export during 2010–2018. LUC first decreased TP export until the 1970s, and then started to increase TP export thereafter.

Table 4-4. Decadal changes in the differences of riverine TP export between the reference simulation (S1) and factorial experiments (S2–S6). Unit: Gg P yr^{-1}.

Year	Climate	CO_2	P fertilizer	P manure	LUC
1900s	-5.74	-0.05	0.00	0.02	-7.17
1910s	-17.13	-0.24	0.05	0.17	-6.71
1920s	-10.86	-0.63	0.16	0.66	-4.40
1930s	-25.20	-0.85	0.24	1.25	-3.31
1940s	-9.25	-1.46	0.59	3.11	-7.06
1950s	-14.81	-1.56	1.73	4.59	-3.36
1960s	-14.61	-2.04	4.25	6.80	-4.20
1970s	6.10	-3.40	10.69	11.14	-3.03
1980s	-2.80	-5.10	16.99	12.85	1.32
1990s	26.16	-7.79	23.95	16.78	1.06
2000s	9.56	-10.17	25.61	17.28	3.12
2010s	37.50	-14.35	29.51	19.47	5.52

4. Discussion

4.1. Importance of integrating terrestrial and aquatic processes

One of the essential advantages of the DLEM–Terrestrial/Aquatic scheme is having the ability to estimate the export of four riverine P species: DIP, DOP, PIP, and POP. DIP, as reactive P, is available for biological uptake and links the P and C cycles (Compton et al., 2000). DIP in fresh waters and coastal waters directly impacts the primary productivity of aquatic ecosystems and excessive DIP leads to eutrophication. The riverine DIP concentration is not only shaped by its abundance in local rocks and soils, but also by physical and biochemical transformations between different P species. In the soil environment, P ions are easily adsorbed to particles and colloids and co-precipitate with chemicals such as iron and calcium. As P enters the river in particulate form, P ions could be released and become bio-available if changes in iron/aluminum/calcium concentrations, temperature, pH, salinity, and redox conditions favor desorption process (Bai et al., 2017). Generally, DIP can be regarded as an immediately available nutrient source to aquatic biota, while particulate form P represents a longer-term source (McDowell et al., 2004). Meanwhile, the settling of PP is a major P detention process and riverine PP has the largest share in TP, thus the removal of P in water column may be enhanced

if the settling process is favored. The turnover rate of P between organic and inorganic forms is closely related to primary productivity and varies both spatially and seasonally (Heidel et al., 2006). Therefore, the concentrations and distributions of different P species in aquatic systems can change rapidly due to both biogeochemical cycling processes and local P loading. Additionally, considering the behavior of different forms of P in aquatic systems, the assessment of riverine export of multiple P species can provide detailed information for the further study of coastal ocean ecosystem processes.

4.2. Climate and anthropogenic control over P loading

In this study, the factorial experiments provided an evaluation of the individual contributions of multiple environmental factors to riverine P exports and offered insight into the mechanisms behind the responses. The major reasons for the increases of different P species in the MRB varied. Riverine DIP export was mainly driven by the increased usage of fertilizer while PIP, DOP, and POP exports were primarily driven by increased precipitation. The joint effect of climate and anthropogenic activities shaped temporal and spatial patterns of P loading.

4.2.1. Climate control over P loading

The magnitude and variation of P losses from land are directly influenced by climate, especially precipitation (Jennings et al., 2009). Climate impacts the reaction rates of biogeochemical transformations, such as weathering, decomposition, mineralization, and plant uptake. Climate also regulates the hydrological processes that modify the yield and transport of P across terrestrial and aquatic systems. The inter-annual variations of riverine DIP, PIP, DOP, and POP exports were strongly influenced by inter-annual variations in precipitation (Figures 4-1a and 4-6). The peaks of P exports consistently occurred in wet years (e.g. 1993 and 2008), while the lowest P exports occurred in dry years (e.g. 2000, 2006, and 2012). At the decadal scale, the 1950s drought was associated with low P exports, while rising precipitation and warming enhanced the exports of TP in recent decades (Figure 4-10). The intensified weathering under the condition of wetting and warming facilitated the transformation of P from mineral to biologically available form (Goll et al., 2014). The increasing P involved in the mobilization associated with the rising runoff contributed to the increasing trends of P exports. With regard to spatial patterns of P loading, conditions of relatively high precipitation contributed to high P yields in the central and eastern portion of the basin, especially for DOP yield (Figure 4-8). High precipitation

stimulated plant growth and ecosystem productivity, which could then further promote the accumulation of soil organic matter and modify the allocation of P in soil. High rates of leaching and organic P storage contributed to the high DOP yield in the eastern basin. Except for agricultural areas, climate-related factors dominated the change in P loading in most regions.

4.2.2. Anthropogenic control over P loading

In most agricultural soils, weathering results in slow release of P that is readily absorbed by crops or combined with aluminum, iron, calcium, and manganese, whereas application of mineral fertilizer can temporarily enhance the dissolved form of P. According to McDowell et al., (2004), application of P increased DIP that was subsequently lost to overland flow at levels 4–26 times greater than that of unamended soil. Meanwhile, around 28% of P may remain in agricultural soil and become legacy P (Kleinman et al., 2011; MacDonald et al., 2012). For DLEM, the legacy P in agricultural soil was from the accumulated labile P, secondary mineral P, and occluded P pools after fertilizer application (Figure 2-3). The soil legacy P, which can be a continuous source of soluble and particulate P released into waters, has raised concern in recent years (Rowe et al., 2016; Sabo et al., 2021). In this study, the consumption of P fertilizer was relatively stable after the 1980s (Figure 4-1b), but the contribution of fertilizer to TP loading continued to increase into the 2010s (Table 4-4). The soil legacy P has been shown to weaken the efficacy of conservation measures across watersheds and thus more effective nutrient management strategies may be required (Sharpley et al., 2013). Additionally, the P use efficiency (PUE) of crops has increased in some regions of the MRB as crop yields continued increasing while P fertilizer application keep relatively stable during the post-1980 period (Swaney and Howarth, 2019). The improved PUE in crop production could reduce the DIP yield in several agricultural areas (Figure 4-9).

Land-use change influences P loading by modifying the allocation of P inputs to soil and the resistance of soil to erosion. Croplands receives most mineral P fertilizer and are vulnerable to soil erosion, while harvested crops transfer P out of the agricultural systems. With regard to other land cover types, such as forest, the majority of P circulates inside the vegetation–microbe–soil system (Sohrt et al., 2017). Before the wide use of mineral P fertilizers (around the 1940s), the expansion of cropland consumed the P storage in soil and decreased P loading. According to Tiessen et al. (1992), soil organic P storage can drop significantly in response to long-term

cultivation and crop removal. After the 1940s, the application of mineral P fertilizer increased quickly and the P losses from cropland were intensified. By contrast, extensive cropland abandonment (Figure 4-1c) may, to some extent, alleviate P loss (Yu and Lu, 2018). Therefore, the impact of LUC on P loading varied with different types of land-use conversion and changed in different periods.

Elevated atmospheric CO_2 stimulates the plant growth and uptake of inorganic P (Terrer et al., 2019). Increased ecosystem primary production and C accumulation enhanced P immobilization into plant biomass and soil organic pools. As a result, inorganic P exports decreased while organic P exports increased in response to elevated atmospheric CO_2. As CO_2 emission continues rising, changing C cycle can potentially exert more influence on P cycle in terrestrial ecosystems and ultimately alter P export.

4.2.3. Interactive effect of climate and anthropogenic factors on soil erosion and P loss

As the major portion of soil P is tightly adsorbed to mineral particles, bound within organic matter or precipitated as weakly soluble salts, soil erosion is the most crucial factor driving potential P loss from ecosystems (Alewell et al., 2020; Carpenter and Bennett, 2011). Soil erosion is influenced by many factors (including rainfall, land use condition, soil type, topography, and management), and large amounts of soil loss can happen rapidly (Quinton et al., 2010). PP loss does not occur from the entire catchment but rather from many critical source areas where serious soil erosion occurs or soil P content is high (McDowell et al., 2004). From a temporal perspective, the increased precipitation in recent decades in the MRB would have accelerated soil erosion and PP loss (Lu et al., 2020; Tan et al., 2021). Furthermore, in extreme precipitation events, higher rainfall intensity can exacerbate soil erosion and potentially cause huge soil P loss on short time scales (Carpenter et al., 2018; Li and Fang, 2016). Anthropogenic management activities (e.g., overgrazing, intensive agriculture, and tile drainage) combined with related LUC are another primary cause of gradual change in soil erosion (Borrelli et al., 2017; Turner and Rabalais, 2003). Historically, erosion increased when forest cover was converted to cropland and declined when farms were abandoned (Turner and Rabalais, 2003). Cropland received most of the P inputs but also was vulnerable to erosion. Soil erosion accompanied by P loss has been recognized as a threat to soil P storage and food security, especially in places with low or no P fertilizer inputs (Bouwman et al., 2013; MacDonald et al., 2011). Due to the strong

interaction between climate and anthropogenic factors, land management options for erosion control and soil P retention need to consider climate change adaptation.

4.3. Uncertainty and limitation

In this study, the simulated results with DLEM–Terrestrial/Aquatic scheme can generally depict the magnitude and variation of P loading from the MRB on long-time scales. However, uncertainties remain due to limitations in the model structure and input datasets. The major component in riverine TP is the particulate form of P, which is derived from erosion and gradual settling during river transport process. Landscape soil erosion through overland flow is estimated in the model, but bank erosion and other geological hazards, like mass wasting, were not considered in this study. It is understood that historical soil erosion has left significant sediments within river valleys and floodplains that are an important source for modern sediment in the MRB (Hassan et al., 2017). However, our simulated results may underestimate the sediment and PIP yields from river valleys in the Lower Mississippi.

From a temporal perspective, the peak values of P loading in Missouri and Upper Mississippi were underestimated in our simulations and may result from the underestimation of peak flows and the lack of accounting for resuspension processes in river channels. Extreme precipitation events and peak flow can potentially cause a higher magnitude of erosion. In this study, we assumed each grid represents a hydrological unit, and the peak flow calculated in grid cells may be underestimated compared to estimates for actual catchments.

We also did not account for the interaction between bottom sediment and water column due to the unsound representation of biogeochemical processes inside river sediment in the current model. Some of the P in sediments in stream bottom can be introduced to the water column through resuspension (particulate form) or by diffusion (dissolved inorganic forms) (Vilmin et al., 2015). Resuspension can be significant when flow rate is high (Pulley et al., 2016). Therefore, the omission of resuspended P as source in our model leads to an underestimation of riverine P exports in the simulation, especially during peak flow.

Additionally, PP is more likely to be sequestered in dam reservoirs as the abundance of dams in the MRB may have enhanced the retention of P loads (Maavara et al., 2015). Sediment loads transported down the Lower Mississippi were reported to fall by more than half over the

last century due to the trapping characteristic of dam and reservoir construction and in-channel storage (Li et al., 2020; Meade and Moody, 2010; Remo et al., 2017), and PP loads may experience a similar decline process. Considering the DLEM results were validated against observed data only in the recent decades, the simulated results may underestimate the P loading before the 1950s when reservoirs initially started to play a key role in reducing riverine sediment.

Moreover, the lock-and-dam systems construction, channel straightening, bank stabilization, the loss of wetlands, and occlusion of floodplain swamps in the basin during the 20th century would affect P delivery to the Gulf but were not considered in this study. The neglecting of these physical changes may limit the efficacy of in-stream processes and introduce considerable uncertainty in the estimate of long-term P loading, especially during the early to middle part of the 20th century. In the future, we plan to develop a process-based dam module within DLEM and build a more robust hydrological module to estimate the impact of dam and reservoir on nutrient loading.

The century-scale simulation is heavily dependent on a sizeable number of input datasets. Many assumptions were made to extend the datasets back to the preindustrial period. For example, P fertilizer data in the U.S. are only available after 1960, and the data before 1960 were estimated according to the global change trend of P fertilizer consumption, which brought uncertainties to the simulated P exports before 1960. Furthermore, several input datasets, such as P deposition and lithology data, were extracted from global datasets at 0.5 degree-arc resolution, and these were resampled to arc 5-min resolution to match other input data, potentially introducing spatial biases. Due to the unavailability of the dynamic and spatially explicit P point sources data in the MRB, we estimated P emissions from wastewater by applying an empirical method based on population and GDP. However, variations in wastewater P, especially those associated with reductions due to policy and technological changes, were hard to accurately estimate without specific data. Additionally, the annual P inputs, such as fertilizer and manure, were allocated on each day equally within the crop growing seasons, which ignored the impact of fertilizer and manure application timing on P dynamics at daily or seasonal scale.

5. Conclusion

This study developed a riverine P module coupled with a terrestrial biogeochemical model, the DLEM–Terrestrial/Aquatic scheme, to simulate P dynamics across the land-ocean

aquatic continuum. The model was applied in the MRB and performed relatively well to simulate the magnitudes and variations of riverine P exports. The simulated results suggest that riverine PIP dominated the TP flux, while DOP had the smallest contribution. The estimated riverine DIP, DOP, PIP, and POP exports all increased over 1901-2018, but DIP and DOP exports leveled off after the 1970s. The increase in DIP export was mainly driven by elevated usage of P fertilizer and manure and increases in the other three P species were driven by increasing precipitation. The intense soil erosion accompanied by PP loss during extreme precipitation events appears to dominate the TP flux. LUC contributed to the increase of DIP load, but reduced loads of DOP, POP, and PIP. Rising atmospheric CO_2 concentrations played an increasingly important role in decreasing DIP and PIP exports. This study highlights the impacts of changes in terrestrial ecosystems on P loading to aquatic systems, which is critical for sustainable nutrient management and water security in a changing global environment.

References

Abatzoglou, J.T., 2013. Development of gridded surface meteorological data for ecological applications and modelling. Int. J. Climatol. 33, 121–131. https://doi.org/10.1002/joc.3413

Alewell, C., Ringeval, B., Ballabio, C., Robinson, D.A., Panagos, P., Borrelli, P., 2020. Global phosphorus shortage will be aggravated by soil erosion. Nat. Commun. 11, 4546. https://doi.org/10.1038/s41467-020-18326-7

Alexander, R.B., Smith, R.A., Schwarz, G.E., Boyer, E.W., Nolan, J.V., Brakebill, J.W., 2008. Differences in Phosphorus and Nitrogen Delivery to The Gulf of Mexico from the Mississippi River Basin. Environ. Sci. Technol. 42, 822–830. https://doi.org/10.1021/es0716103

Amundson, R., Berhe, A.A., Hopmans, J.W., Olson, C., Sztein, A.E., Sparks, D.L., 2015. Soil and human security in the 21st century. Science 348, 1261071–1261071. https://doi.org/10.1126/science.1261071

Bai, J., Ye, X., Jia, J., Zhang, G., Zhao, Q., Cui, B., Liu, X., 2017. Phosphorus sorption-desorption and effects of temperature, pH and salinity on phosphorus sorption in marsh soils from coastal wetlands with different flooding conditions. Chemosphere 188, 677–688. https://doi.org/10.1016/j.chemosphere.2017.08.117

Beusen, A.H.W., Van Beek, L.P.H., Bouwman, A.F., Mogollón, J.M., Middelburg, J.J., 2015. Coupling global models for hydrology and nutrient loading to simulate nitrogen and phosphorus retention in surface water – description of IMAGE–GNM and analysis of performance. Geosci. Model Dev. 8, 4045–4067. https://doi.org/10.5194/gmd-8-4045-2015

Bian, Z., Tian, H., Yang, Q., Xu, R., Pan, S., Zhang, B., 2021. Production and application of manure nitrogen and phosphorus in the United States since 1860. Earth Syst. Sci. Data 13, 515–527. https://doi.org/10.5194/essd-13-515-2021

Borrelli, P., Robinson, D.A., Fleischer, L.R., Lugato, E., Ballabio, C., Alewell, C., Meusburger, K., Modugno, S., Schütt, B., Ferro, V., Bagarello, V., Oost, K.V., Montanarella, L., Panagos, P., 2017. An assessment of the global impact of 21st century land use change on soil erosion. Nat. Commun. 8, 2013. https://doi.org/10.1038/s41467-017-02142-7

Bouwman, L., Goldewijk, K.K., Van Der Hoek, K.W., Beusen, A.H.W., Van Vuuren, D.P., Willems, J., Rufino, M.C., Stehfest, E., 2013. Exploring global changes in nitrogen and phosphorus cycles in agriculture induced by livestock production over the 1900-2050 period. Proc. Natl. Acad. Sci. 110, 20882–20887. https://doi.org/10.1073/pnas.1012878108

Carpenter, S.R., 2005. Eutrophication of aquatic ecosystems: Bistability and soil phosphorus. Proc. Natl. Acad. Sci. 102, 10002–10005. https://doi.org/10.1073/pnas.0503959102

Carpenter, S.R., Bennett, E.M., 2011. Reconsideration of the planetary boundary for phosphorus. Environ. Res. Lett. 6, 014009. https://doi.org/10.1088/1748-9326/6/1/014009

Carpenter, S.R., Booth, E.G., Kucharik, C.J., 2018. Extreme precipitation and phosphorus loads from two agricultural watersheds. Limnol. Oceanogr. 63, 1221–1233. https://doi.org/10.1002/lno.10767

Colborne, S.F., Maguire, T.J., Mayer, B., Nightingale, M., Enns, G.E., Fisk, A.T., Drouillard, K.G., Mohamed, M.N., Weisener, C.G., Wellen, C., 2019. Water and sediment as sources

of phosphate in aquatic ecosystems: The Detroit River and its role in the Laurentian Great Lakes. Sci. Total Environ. 647, 1594–1603.
Compton, J., Mallinson, D., Glenn, C.R., Filippelli, G., Föllmi, K., Shields, G., Zanin, Y., 2000. Variations in the global phosphorus cycle.
Conley, D.J., Paerl, H.W., Howarth, R.W., Boesch, D.F., Seitzinger, S.P., Havens, K.E., Lancelot, C., Likens, G.E., 2009. Controlling Eutrophication: Nitrogen and Phosphorus. Science 323, 1014–1015. https://doi.org/10.1126/science.1167755
Cordell, D., Drangert, J.-O., White, S., 2009. The story of phosphorus: Global food security and food for thought. Glob. Environ. Change, Traditional Peoples and Climate Change 19, 292–305. https://doi.org/10.1016/j.gloenvcha.2008.10.009
Correll, D.L., 1998. The Role of Phosphorus in the Eutrophication of Receiving Waters: A Review. J. Environ. Qual. 27, 261–266. https://doi.org/10.2134/jeq1998.00472425002700020004x
Elser, J., Bennett, E., 2011. A broken biogeochemical cycle. Nature 478, 29–31. https://doi.org/10.1038/478029a
Fennel, K., Laurent, A., 2018. N and P as ultimate and proximate limiting nutrients in the northern Gulf of Mexico: implications for hypoxia reduction strategies. Biogeosciences 15, 3121–3131. https://doi.org/10.5194/bg-15-3121-2018
Garnier, J., Lassaletta, L., Billen, G., Romero, E., Grizzetti, B., Némery, J., Le, T.P.Q., Pistocchi, C., Aissa-Grouz, N., Luu, T.N.M., 2015. Phosphorus budget in the water-agro-food system at nested scales in two contrasted regions of the world (ASEAN-8 and EU-27). Glob. Biogeochem. Cycles 29, 1348–1368.
Goll, D.S., Moosdorf, N., Hartmann, J., Brovkin, V., 2014. Climate-driven changes in chemical weathering and associated phosphorus release since 1850: Implications for the land carbon balance. Geophys. Res. Lett. 41, 3553–3558. https://doi.org/10.1002/2014GL059471
Gu, A.Z., Liu, L., Neethling, J.B., Stensel, H.D., Murthy, S., 2011. Treatability and fate of various phosphorus fractions in different wastewater treatment processes. Water Sci. Technol. 63, 804–810.
Hale, R.L., Grimm, N.B., Vörösmarty, C.J., Fekete, B., 2015. Nitrogen and phosphorus fluxes from watersheds of the northeast U.S. from 1930 to 2000: Role of anthropogenic nutrient inputs, infrastructure, and runoff. Glob. Biogeochem. Cycles 29, 341–356. https://doi.org/10.1002/2014GB004909
Hassan, M.A., Roberge, L., Church, M., More, M., Donner, S.D., Leach, J., Ali, K.F., 2017. What are the contemporary sources of sediment in the Mississippi River? Geophys. Res. Lett. 44, 8919–8924.
Heidel, K., Sujoy Roy, Creager, C., Chih-Fang Chung, Grieb, T., 2006. Conceptual Model for Nutrients In the Central Valley and Sacramento-San Joaquin Delta. https://doi.org/10.13140/RG.2.2.13466.13769
Hirsch, R.M., Moyer, D.L., Archfield, S.A., 2010. Weighted Regressions on Time, Discharge, and Season (WRTDS), with an Application to Chesapeake Bay River Inputs. J. Am. Water Resour. Assoc. 46, 857–880. https://doi.org/10.1111/j.1752-1688.2010.00482.x
Jennings, E., Allott, N., Pierson, D.C., Schneiderman, E.M., Lenihan, D., Samuelsson, P., Taylor, D., 2009. Impacts of climate change on phosphorus loading from a grassland catchment: Implications for future management. Water Res. 43, 4316–4326. https://doi.org/10.1016/j.watres.2009.06.032

Jolliff, J.K., Kindle, J.C., Shulman, I., Penta, B., Friedrichs, M.A., Helber, R., Arnone, R.A., 2009. Summary diagrams for coupled hydrodynamic-ecosystem model skill assessment. J. Mar. Syst. 76, 64–82.

Kleinman, P., Sharpley, A., Buda, A., McDowell, R., Allen, A., 2011. Soil controls of phosphorus in runoff: Management barriers and opportunities. Can. J. Soil Sci. 91, 329–338.

Lee, C.J., Murphy, J.C., Crawford, C.G., Deacon, J.R., 2017. Methods for computing water-quality loads at sites in the U.S. Geological Survey National Water Quality Network (USGS Numbered Series No. 2017–1120), Methods for computing water-quality loads at sites in the U.S. Geological Survey National Water Quality Network, Open-File Report. U.S. Geological Survey, Reston, VA. https://doi.org/10.3133/ofr20171120

Li, T., Wang, S., Liu, Y., Fu, B., Zhao, W., 2020. A retrospective analysis on changes in sediment flux in the Mississippi River system: trends, driving forces, and implications. J. Soils Sediments 20, 1719–1729. https://doi.org/10.1007/s11368-019-02495-0

Li, Z., Fang, H., 2016. Impacts of climate change on water erosion: A review. Earth-Sci. Rev. 163, 94–117. https://doi.org/10.1016/j.earscirev.2016.10.004

Litke, D.W., 1999. Review of phosphorus control measures in the United States and their effects on water quality. US Department of the Interior, US Geological Survey.

Lohrenz, S.E., Redalje, D.G., Cai, W.-J., Acker, J., Dagg, M., 2008. A retrospective analysis of nutrients and phytoplankton productivity in the Mississippi River plume. Cont. Shelf Res. 28, 1466–1475. https://doi.org/10.1016/j.csr.2007.06.019

Lu, C., Zhang, J., Tian, H., Crumpton, W.G., Helmers, M.J., Cai, W.-J., Hopkinson, C.S., Lohrenz, S.E., 2020. Increased extreme precipitation challenges nitrogen load management to the Gulf of Mexico. Commun. Earth Environ. 1, 1–10. https://doi.org/10.1038/s43247-020-00020-7

Maavara, T., Parsons, C.T., Ridenour, C., Stojanovic, S., Dürr, H.H., Powley, H.R., Van Cappellen, P., 2015. Global phosphorus retention by river damming. Proc. Natl. Acad. Sci. 112, 15603–15608. https://doi.org/10.1073/pnas.1511797112

MacDonald, G.K., Bennett, E.M., Carpenter, S.R., 2012. Embodied phosphorus and the global connections of United States agriculture. Environ. Res. Lett. 7, 044024. https://doi.org/10.1088/1748-9326/7/4/044024

MacDonald, G.K., Bennett, E.M., Potter, P.A., Ramankutty, N., 2011. Agronomic phosphorus imbalances across the world's croplands. Proc. Natl. Acad. Sci. 108, 3086–3091.

Mahowald, N., Jickells, T.D., Baker, A.R., Artaxo, P., Benitez-Nelson, C.R., Bergametti, G., Bond, T.C., Chen, Y., Cohen, D.D., Herut, B., Kubilay, N., Losno, R., Luo, C., Maenhaut, W., McGee, K.A., Okin, G.S., Siefert, R.L., Tsukuda, S., 2008. Global distribution of atmospheric phosphorus sources, concentrations and deposition rates, and anthropogenic impacts: GLOBAL ATMOSPHERIC PHOSPHORUS. Glob. Biogeochem. Cycles 22, n/a-n/a. https://doi.org/10.1029/2008GB003240

McDowell, R.W., Biggs, B.J.F., Sharpley, A.N., Nguyen, L., 2004. Connecting phosphorus loss from agricultural landscapes to surface water quality. Chem. Ecol. 20, 1–40. https://doi.org/10.1080/02757540310001626092

Meade, R.H., Moody, J.A., 2010. Causes for the decline of suspended-sediment discharge in the Mississippi River system, 1940–2007. Hydrol. Process. 24, 35–49. https://doi.org/10.1002/hyp.7477

Morée, A.L., Beusen, A.H.W., Bouwman, A.F., Willems, W.J., 2013. Exploring global nitrogen and phosphorus flows in urban wastes during the twentieth century. Glob. Biogeochem. Cycles 27, 836–846. https://doi.org/10.1002/gbc.20072

Moriasi, D.N., Gitau, M.W., Pai, N., Daggupati, P., 2015. Hydrologic and water quality models: Performance measures and evaluation criteria. Trans. ASABE 58, 1763–1785.

Pulley, S., Foster, I., Antunes, P., 2016. The dynamics of sediment-associated contaminants over a transition from drought to multiple flood events in a lowland UK catchment. Hydrol. Process. 30, 704–719.

Quinton, J.N., Govers, G., Van Oost, K., Bardgett, R.D., 2010. The impact of agricultural soil erosion on biogeochemical cycling. Nat. Geosci. 3, 311–314. https://doi.org/10.1038/ngeo838

Remo, J., Ryherd, J.K., Ruffner, C., Therrell, M., 2017. Temporal and spatial patterns of sedimentation within the batture lands of the middle Mississippi River, USA. https://doi.org/10.1016/J.GEOMORPH.2018.02.010

Rowe, H., Withers, P.J.A., Baas, P., Chan, N.I., Doody, D., Holiman, J., Jacobs, B., Li, H., MacDonald, G.K., McDowell, R., Sharpley, A.N., Shen, J., Taheri, W., Wallenstein, M., Weintraub, M.N., 2016. Integrating legacy soil phosphorus into sustainable nutrient management strategies for future food, bioenergy and water security. Nutr. Cycl. Agroecosystems 104, 393–412. https://doi.org/10.1007/s10705-015-9726-1

Ryther, J.H., Dunstan, W.M., 1971. Nitrogen, Phosphorus, and Eutrophication in the Coastal Marine Environment. Science 171, 1008–1013. https://doi.org/10.1126/science.171.3975.1008

Sabo, R.D., Clark, C.M., Gibbs, D.A., Metson, G.S., Todd, M.J., LeDuc, S.D., Greiner, D., Fry, M.M., Polinsky, R., Yang, Q., Tian, H., Compton, J.E., 2021. Phosphorus Inventory for the Conterminous United States (2002–2012). J. Geophys. Res. Biogeosciences 126, e2020JG005684. https://doi.org/10.1029/2020JG005684

Scavia, D., Donnelly, K.A., 2007. Reassessing Hypoxia Forecasts for the Gulf of Mexico. Environ. Sci. Technol. 41, 8111–8117. https://doi.org/10.1021/es0714235

Sharpley, A., Jarvie, H.P., Buda, A., May, L., Spears, B., Kleinman, P., 2013. Phosphorus Legacy: Overcoming the Effects of Past Management Practices to Mitigate Future Water Quality Impairment. J. Environ. Qual. 42, 1308–1326. https://doi.org/10.2134/jeq2013.03.0098

Smil, V., 2000. Phosphorus in the environment: natural flows and human interferences. Annu. Rev. Energy Environ. 25, 53–88.

Sohrt, J., Lang, F., Weiler, M., 2017. Quantifying components of the phosphorus cycle in temperate forests. WIREs Water 4, e1243. https://doi.org/10.1002/wat2.1243

Swaney, D.P., Howarth, R.W., 2019. Phosphorus use efficiency and crop production: Patterns of regional variation in the United States, 1987–2012. Sci. Total Environ. 685, 174–188. https://doi.org/10.1016/j.scitotenv.2019.05.228

Sylvan, J.B., Dortch, Q., Nelson, D.M., Maier Brown, A.F., Morrison, W., Ammerman, J.W., 2006. Phosphorus Limits Phytoplankton Growth on the Louisiana Shelf During the Period of Hypoxia Formation. Environ. Sci. Technol. 40, 7548–7553. https://doi.org/10.1021/es061417t

Sylvan, J.B., Quigg, A., Tozzi, S., Ammerman, J.W., 2007. Eutrophication-induced phosphorus limitation in the Mississippi River plume: Evidence from fast repetition rate fluorometry. Limnol. Oceanogr. 52, 2679–2685. https://doi.org/10.4319/lo.2007.52.6.2679

Tan, Z., Leung, L.R., Li, H.-Y., Tesfa, T., Zhu, Q., Yang, X., Liu, Y., Huang, M., 2021. Increased extreme rains intensify erosional nitrogen and phosphorus fluxes to the northern Gulf of Mexico in recent decades. Environ. Res. Lett. 16, 054080. https://doi.org/10.1088/1748-9326/abf006

Terrer, C., Jackson, R.B., Prentice, I.C., Keenan, T.F., Kaiser, C., Vicca, S., Fisher, J.B., Reich, P.B., Stocker, B.D., Hungate, B.A., Peñuelas, J., McCallum, I., Soudzilovskaia, N.A., Cernusak, L.A., Talhelm, A.F., Van Sundert, K., Piao, S., Newton, P.C.D., Hovenden, M.J., Blumenthal, D.M., Liu, Y.Y., Müller, C., Winter, K., Field, C.B., Viechtbauer, W., Van Lissa, C.J., Hoosbeek, M.R., Watanabe, M., Koike, T., Leshyk, V.O., Polley, H.W., Franklin, O., 2019. Nitrogen and phosphorus constrain the CO 2 fertilization of global plant biomass. Nat. Clim. Change 9, 684–689. https://doi.org/10.1038/s41558-019-0545-2

Tiessen, H., Salcedo, I.H., Sampaio, E., 1992. Nutrient and soil organic matter dynamics under shifting cultivation in semi-arid northeastern Brazil. Agric. Ecosyst. Environ. 38, 139–151.

Turner, R.E., Rabalais, N.N., 2003. Linking Landscape and Water Quality in the Mississippi River Basin for 200 Years. BioScience 53, 563–572. https://doi.org/10.1641/0006-3568(2003)053[0563:LLAWQI]2.0.CO;2

Van Drecht, G., Bouwman, A.F., Harrison, J., Knoop, J.M., 2009. Global nitrogen and phosphate in urban wastewater for the period 1970 to 2050. Glob. Biogeochem. Cycles 23. https://doi.org/10.1029/2009GB003458

van Puijenbroek, P.J.T.M., Beusen, A.H.W., Bouwman, A.F., 2019. Global nitrogen and phosphorus in urban waste water based on the Shared Socio-economic pathways. J. Environ. Manage. 231, 446–456. https://doi.org/10.1016/j.jenvman.2018.10.048

Vilmin, L., Aissa-Grouz, N., Garnier, J., Billen, G., Mouchel, J.-M., Poulin, M., Flipo, N., 2015. Impact of hydro-sedimentary processes on the dynamics of soluble reactive phosphorus in the Seine River. Biogeochemistry 122, 229–251. https://doi.org/10.1007/s10533-014-0038-3

Viovy, N., 2018. CRUNCEP Version 7 - Atmospheric Forcing Data for the Community Land Model. https://doi.org/10.5065/PZ8F-F017

Wu, H., Kimball, J.S., Li, H., Huang, M., Leung, L.R., Adler, R.F., 2012. A new global river network database for macroscale hydrologic modeling. Water Resour. Res. 48. https://doi.org/10.1029/2012WR012313

Yao, Y., Tian, H., Pan, S., Najjar, R.G., Friedrichs, M.A.M., Bian, Z., Li, H.-Y., Hofmann, E.E., 2021. Riverine Carbon Cycling Over the Past Century in the Mid-Atlantic Region of the United States. J. Geophys. Res. Biogeosciences 126, e2020JG005968. https://doi.org/10.1029/2020JG005968

Yu, Z., Lu, C., 2018. Historical cropland expansion and abandonment in the continental U.S. during 1850 to 2016. Glob. Ecol. Biogeogr. 27, 322–333. https://doi.org/10.1111/geb.12697

Chapter 5. Quantification of N and P budgets and legacy soil nutrients in the Mississippi River Basin.

Abstract

Legacy soil nutrients can act as a long-term nutrient source for aquatic systems and may prevent the achievement of water quality goals. Estimating the sources and sinks of soil legacy nitrogen (N) and phosphorus (P) is essential for sustainable nutrient management and understanding biogeochemical cycles. While several efforts have been conducted to quantify one single nutrient budget in the Mississippi River Basin (MRB), no study has estimated both N and P budgets under the same modeling framework. Here, we quantified major N and P inputs (synthetic fertilizer N and P, livestock manure N and P, atmospheric N deposition, biological N fixation, and weathering P) and outputs (harvest crop N and P, N and P loading, and N_2O, NO, N_2 and NH_3 gases emissions) across the MRB during 1901-2018. The estimated total N inputs and outputs increased from 5.05 and 3 .09 Tg N yr^{-1} in the 1900s to 20.57 and 16.68 Tg N yr^{-1} in the 2010s, respectively. The increased nutrient inputs are associated with intensive agricultural activities and fossil fuel consumption within the basin. Meanwhile, Total P inputs and outputs increased from 0.44 and 0.57 Tg P yr^{-1} in the 1900s to 2.59 and 1.96 Tg P yr^{-1} in the 2010s, respectively. The crop harvest nutrient, the largest nutrient output, continually increased over the study period even when nutrient inputs stopped increasing, reflecting the enhanced nutrient use efficiency of crops in the MRB. Both N and P balance increased substantially from 1930 to 1980, then P balance decreased dramatically within the 1980s while N balance showed a slight decline. The legacy N and P storage increased 423.80 Tg N and 54.80 Tg P, respectively, during 1901-2018. Better utilizing legacy soil nutrients can bring both economic and environmental benefits through reducing fertilizer inputs and nutrient loading. This study highlights the importance of quantifying the N and P budgets at the watershed scale for efficient nutrient management and pollution reduction.

1. Introduction

Nitrogen (N) and phosphorus (P) are fundamental nutrients for life growth, but the intensive usage of N and P in agriculture and increasing fossil fuel consumption have largely disturbed nutrient cycles and brought environmental concerns (Steffen et al., 2015). Overloading

anthropogenic nutrients received by agricultural systems stimulated the loss of nutrients from land to atmosphere and water through the biogeochemical cycles. N dominates the vertical pathway (into the atmosphere) of nutrient losses, while both N and P can leave the system through the lateral pathway (into the aquatic system). N in fertilizer and manure could rapidly volatilize into the atmosphere as ammonia that can react with other air pollutants and form aerosols to reduce visibility and threaten human health (Bouwman et al., 2002; Xu et al., 2018). Additionally, N can be converted to nitrous oxide (N_2O), one of the most important greenhouse gasses, in nitrification and denitrification processes (Davidson, 2009; Tian et al., 2019). Increased N and P loading from land have resulted in harmful algal blooms, eutrophication, and hypoxia in aquatic ecosystems, which degraded drinking water and impaired public health (Conley et al., 2009). Efficient nutrient usage and allocation strategies are necessary for minimizing undesirable environmental impacts while still producing sufficient food to feed the population.

Measuring and monitoring nutrient budgets, including N and P inputs and outputs of ecosystems, is the first step toward better nutrient management (Zhang et al., 2020). Nutrient surplus and nutrient use efficiency (NUE) can be further evaluated based on nutrient inputs and outputs of a system (Oenema et al., 2003; Zhang et al., 2015). Nutrient losses from plant-soil systems to the atmosphere and aquatic ecosystem cause most of the nutrient-related environmental issues (Fowler et al., 2013; Gruber and Galloway, 2008). Assessing nutrient usage and loss under the same framework can inform stakeholders on the trade-offs between food production for growing population and nutrient pollution (Scoones and Toulmin, 1998). Additionally, estimating the regional variability of legacy soil nutrients, the remaining N or P accumulated in the soil from historical fertilizer and manure application, also needs the establishment of nutrient budgets (Meter et al., 2017). Evidence has suggested that legacy nutrient sources continue to impair water quality even after agricultural inputs have ceased (Meter et al., 2016; Motew et al., 2017; Sharpley et al., 2013). Assessing legacy nutrients based on nutrient inputs and outputs change can help to set realistic targets and timelines for water environment restoration and assist with making management strategies to utilize legacy soil nutrient resources in agriculture (Sabo et al., 2021).

Given the benefits for nutrient management, nutrient budgets have been estimated on multiple spatial and temporal scales. The net anthropogenic nitrogen inputs (NANI) or net anthropogenic phosphorus inputs (NAPI) method is one of the approaches to quantify nutrient budget in landscape systems (Howarth et al., 1996). The NANI or NAPI approach has been successfully applied to evaluate riverine nutrient export and the impact of human activities on nutrient balance across watersheds (Hu et al., 2020; Metson et al., 2017; Sabo et al., 2019). However, the inventory-based nutrient budget quantifications often collect or calculate nutrient inputs and outputs according to different data sources, making nutrients difficult to balance (Oenema and Heinen, 1999). In contrast, a process-based biogeochemical model is capable of simulating nutrient flux within or across a system under the same framework, and nutrient dynamics inside the system usually follow the principle of conservation of mass (Lawrence et al., 2019; Wang et al., 2020). The model-based quantification also has an advantage in estimating long-term continuous changes in nutrient budget, especially when datasets of some budget terms are limited available. Although nutrient budgeting approaches have been developed and widely applied in previous studies, accurately quantifying nutrient budgets at regional or global scale remains a challenge (Zhang et al., 2020). Large uncertainties exist in measuring many budget terms and potentially some nutrient flows have not been considered, such as nutrient leaching, ammonia volatilization, and denitrification (Duncan et al., 2013; Oenema et al., 2003).

The "dead zone" in the northern Gulf of Mexico has expanded since the 1950s, as large amounts of nutrients are loaded into Gulf from the Mississippi River Basin (MRB). An action plan was launched in 2001 to reduce hypoxia in the Gulf, but the water quality goals still haven't been met despite investments in wetland restoration and improving nutrient management (Rabalais and Turner, 2019). Legacy nutrient in the MRB is suggested as the major factor preventing the achievement of water quality goals in the Gulf (Meter et al., 2018; Sharpley et al., 2013). Many methods have been used to estimate the nutrient sources in the MRB, and these methods typically focus on the inputs of nutrients (synthetic fertilizer, livestock manure, atmospheric deposition, and biological fixation) and their related impacts on riverine loading. David et al. (2010) applied NANI approaches to assess agricultural and human inputs and outputs of N across the MRB from 1940 to 2010 by utilizing both state and county scale survey databases. Meter et al. (2017) combined survey data and a process-based model to quantify both N inputs and outputs in the MRB at two-century scale and estimated the impact of legacy N on

riverine N loading. However, in these budget studies, crop harvest removal N was the only calculated N output while N gaseous form losses (NH_3, N_2O, NO, and N_2) from terrestrial ecosystems were not explicitly taken into account. Moreover, none of these studies estimated both N and P inputs and outputs in the MRB under the same framework.

Investigating the impact of legacy soil nutrients on nutrient loading from the MRB calls for the establishment of nutrient budgets. In this study, we applied a process-based biogeochemical model, Dynamic Land Ecosystem Model (DLEM) to simulate the major N and P inputs and outputs, including harvest crop N and P, N and P loading, biological N fixation, NH_3, N_2O, NO, and N_2 emissions, and P weathering driving by multiple forcing datasets, including N and P fertilizer and livestock manure N and P in the MRB. The dynamics of N and P fluxes across the land-water-atmosphere system during 1901-2018 were estimated under the same modeling framework. The estimated N and P budgets allow us to more accurately quantify changes in legacy soil nutrients at long-term scale and synthetically understand the biogeochemical processes at the whole basin scale.

2. Methods

The DLEM is a processes-based biogeochemical model coupling water, C, N, P cycles across the plant-soil-aquatic continuum (Figure 5-1). The model is capable of simulating the long-term dynamics of N and P fluxes and storages in terrestrial and aquatic ecosystems and their interactions with the atmosphere driven by multiple environmental forces (i.e., climate, atmospheric CO_2 concentration, land-use change, synthetic fertilizer, livestock manure, and atmospheric deposition). Within the model framework, the nutrients from terrestrial ecosystems enter into aquatic ecosystems through surface and subsurface runoff, leaching, and erosion, then are transported from headwaters to mainstreams and finally to coastal oceans. During our years of research, the DLEM has been developed, improved, and applied to estimate century-long dynamics of nutrient loading (Tian et al., 2020; Yang et al., 2015), N_2O emission (Lu et al., 2021; Tian et al., 2015), NH_3 emission (Xu et al., 2019), and crop yield (Ren et al., 2012; Zhang et al., 2018). For nutrient budgets established in this study, N and P fertilizer, manure N and P, and N deposition are input variables. N fixation, harvest N and P, NH_3 emission, N_2O emission, N_2 emission, NO emission, and N and P loading are simulated variables. The soil legacy effect is represented by the accumulation of nutrients in all soil N and P pools, and N is primarily stored

in soil organic pools (e.g. NOM and PSOM), while P is stored in both organic pools and inorganic pools (e.g. Secondary Mineral P and Occluded P) (Figure 5-1).

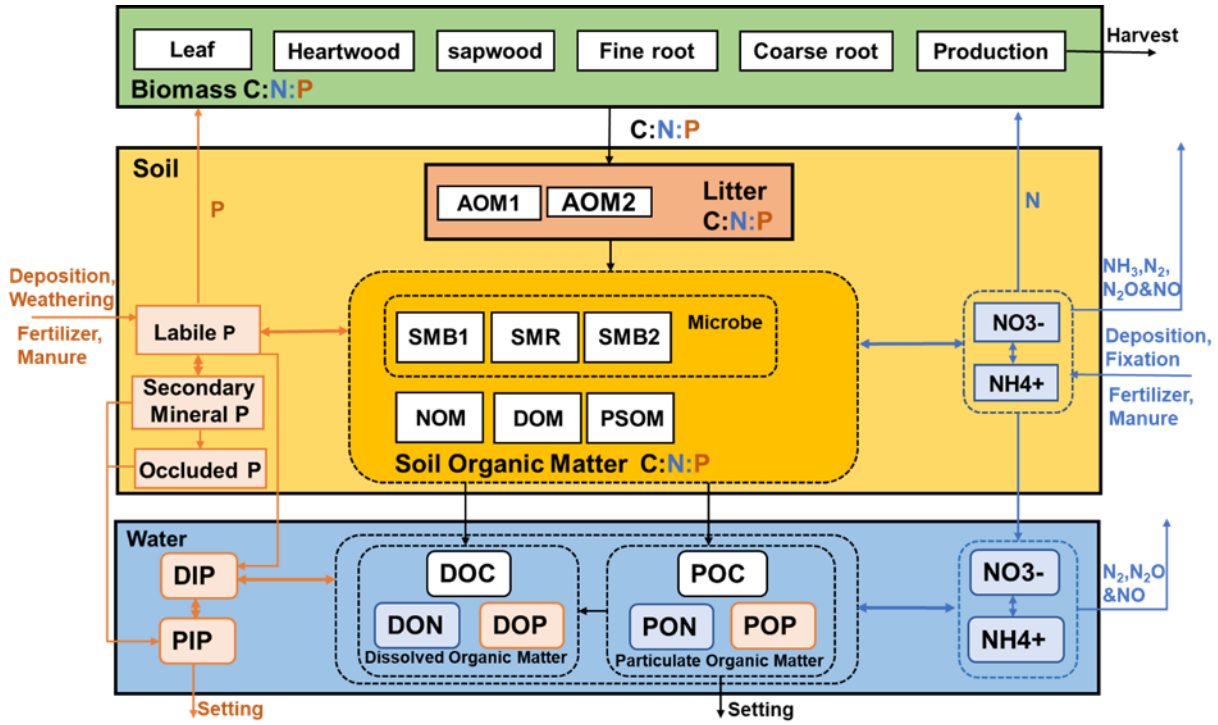

Figure 5-1. The major N and P pools and fluxes in the DLEM-Terrestrial/Aquatic scheme. Blue arrows and boxes represent unique N processes and orange ones represent unique P processes. Organic matter pools interact with each other with coupled C, N and P. AOM1 and AOM2 are litter pools with different residence time. Soil organic matter consists of six pools: autochthonous microbial pool (SMB1), zymogenous microbial (SMB2), soil microbial residues (SMR), native organic matter (NOM), passive soil organic matter (PSOM), and dissolved organic matter (DOM).

2.1. Photosynthesis and crop removal

The N and P fluxes are coupled with C flux in plant growth processes, and the gross primary productivity (GPP) of plant determines the dynamics of plant biomass and nutrient uptake. The DLEM uses a modified Farquhar's model to simulate GPP (Bonan, 1996; Farquhar et al., 1980). The canopy is divided into sunlit and shaded layers. GPP (g C m^{-2} day^{-1}) is calculated by scaling leaf assimilation rates up to the whole canopy (Tian et al., 2010):

$$GPP_{sun} = 12.01 \times 10^{-6} \times A_{sun} \times plai_{sun} \times dayl \times 3600 \quad (1)$$

$$GPP_{shade} = 12.01 \times 10^{-6} \times A_{shade} \times plai_{shade} \times dayl \times 3600 \quad (2)$$

$$GPP = GPP_{sun} + GPP_{shade} \quad (3)$$

where GPP_{sun} and GPP_{shade} (g C m^{-2} day^{-1}) are the GPP of sunlit and shaded canopy, respectively; A_{sun} and A_{shade} (μmol/m^2/s) are assimilation rates of the sunlit and shaded canopy; $plai_{sum}$ and $plai_{shade}$ are sunlit and shaded leaf area indices, estimated as equations 4 and 5, respectively; $dayl$ is daytime length (second) in a day (h). 12.01×10^{-6} is a constant to change the unit from μmol CO_2 to gram C.

$$plai_{sun} = 1 - EXP(-proj_{LAI}) \quad (4)$$

$$plai_{shade} = proj_{LAI} - plai_{sun} \quad (5)$$

where $proj_{LAI}$ is the projected leaf area index, which is calculated as the product of leaf carbon content (g C m^{-2}) and plant type function (PFT) specific leaf area (SLA, m^2 g C^{-1}). Using similar methods to Collatz et al. (1991), DLEM determines the C assimilation rate (*A*) as the minimum of three limiting rates, w_c , w_j, w_e, which are functions that represent the assimilation rates as limited by the efficiency of the photosynthetic enzymes system (Rubisco-limited), the amount of photosynthetically active radiation (PAR) captured by leaf chlorophyll (light-limited), and the capacity of leaves to export or utilize photosynthesis products (export-limited) for C_3 species, respectively. For C_4 species, w_e refer to the phosphoenolpyruvate (PEP) carboxylase limited rate of carboxylation. The sunlit and the shaded canopy C assimilation rate can be estimated as:

$$A = \min(w_c, w_j, w_e) \times Index_{gs} \quad (6)$$

$$w_c = \begin{cases} \frac{(c_i - \Gamma_*)V_{max}}{c_i + K_c(1+o_i/K_0)} & for\ C_3\ plants \\ V_{max} & for\ C_4\ plants \end{cases} \quad (7)$$

$$w_j = \begin{cases} \frac{(c_i - \Gamma_*)4.6\emptyset\alpha}{c_i + 2\Gamma_*} & for\ C_3\ plants \\ 4.6\emptyset\alpha & for\ C_4\ plants \end{cases} \quad (8)$$

$$w_j = \begin{cases} 0.5V_{max} & for\ C_3\ plants \\ 4000V_{max}\frac{c_i}{P_{atm}} & for\ C_4\ plants \end{cases} \quad (9)$$

where c_i is the internal leaf CO_2 concentration (Pa); o_i is the O_2 concentration (Pa); Γ_* is the CO_2 compensation point (Pa); K_c and K_0 (Pa) are the Michaelis-Menten constants for CO_2 and O_2 at 25 ^oC, respectively; α is the quantum efficiency; $\emptyset$ is the absorbed photosynthetically active radiation ($W\cdot M^{-2}$); V_{max} (µmol CO_2 m^{-2} s^{-1}) is the maximum rate of carboxylation varies with temperature,

foliage nitrogen and phosphorus concentration, and soil moisture (Bonan, 1996), calculated as:

$$V_{max} = V_{max25} a_{vmax}^{\frac{T_{ave}-25}{10}} f(NP) f(T_{ave}) \beta_t \quad (10)$$

where V_{max25} is the maximum rate of carboxylation at 25 °C (μmol CO_2 m^{-2} s^{-1}) and a_{vmax} is the maximum temperature sensitivity parameter. $f(NP)$ adjusts the rate of photosynthesis, calculated as:

$$f_{sun}(NP) = \frac{2}{\frac{1}{f_{sun}(N)} + \frac{1}{f_{sun}(P)}} \quad (11)$$

$$f_{shade}(NP) = \frac{2}{\frac{1}{f_{shade}(N)} + \frac{1}{f_{shade}(P)}} \quad (12)$$

where $f_{sun}(N)$ and $f_{shade}(N)$ are sunlit and shaded leaves N limitation coefficients, and $f_{sun}(P)$ and $f_{shade}(P)$ are sunlit and shaded leaves P limitation coefficients. Leaf nutrient limitation coefficients are applied to impact V_{cmax}, through which J_{max} is also affected.

$f(T_{ave})$ is a function of temperature-related metabolic processes as the following:

$$f(T_{ave}) = \left[1 + \exp\left(\frac{-220000 + 710(T_{ave}+273.16)}{8.314(T_{ave}+273.16)}\right)\right]^{-1} \quad (13)$$

β_t is a function (0-1) that represents the soil moisture and the lower temperature effects on stomatal resistance and photosynthesis.

$$\beta_t = \beta(T_{min}) \times \beta(w) \quad (14)$$

$$\beta(T_{min}) = \begin{cases} 0 & for\ T_{min} < -8\ ℃ \\ 1 + 0.125 T_{min} & for -8\ ℃ \le T_{min} \le 0\ ℃ \\ 1 & for \quad T_{min} > 0\ ℃ \end{cases} \quad (15)$$

$$\beta(w) = \sum_{i=1}^{10} w_i\, r_i \quad (16)$$

$$w_i = \begin{cases} 0 & for\ ps_i > psi_{close} \\ \frac{psi_{close} - ps_i}{psi_{close} - psi_{open}} & for\ psi_{open} \le ps_i \le psi_{close} \\ 1 & for\ ps_i < psi_{close} \end{cases} \quad (17)$$

where T_{min} is the daily minimum temperature; w_i is the soil water stress of soil layer i; ps_i is the soil water potential of soil layer i, estimated from Saxton & Rawls (2006). r_i is the root fractions distributed in soil layer i; psi_{close} and psi_{open} are the plant functional specific tolerance of the soil water potential for stomata overall close and open. The water stress in plants is a function of soil

water potential, which ranges from 0 to 1. Under no water limitations, the soil water stress of soil layer i (w_i) is equal to 1 where the soil water potential is at its maximum i.e., soil water potential when the stomata is opened (psi_{open}). Under frequent water stress, however, w_i is calculated based on wilting point potential of specific plant functional types and depends on the balance between psi_{close} and psi_{open}.

Crop yield formation is determined by the relation of biomass supply to the grains and the actual demand of the grains. In DLEM, crop yield is estimated as the product of total aboveground biomass and harvest index (Ren et al., 2012). The potential GPP of crops can be adjusted by adding a technique-related parameter that changes V_{cmax} over the study period and could reflect the increased yield caused by the improvement of the breed of crops and farming technologies. More details regarding the crop module in the DELM can be found in Zhang et al. (2018).

2.2. Biological N fixation

The Biological N fixation (BNF) via legume plants is simulated by following the methods in Yu & Zhuang (2020), which considering (1) the accessible N concentration in soils, (2) the limitation of temperature, (3) soil water status, (4) the carbon demand for N2 fixation and (5) the percentage of N2 fixing plants for each ecosystem type.

$$N_{fix} = N_{fixpot} f_B(T) f_B(W) f_B(N) f_B(C) \tag{18}$$

where N_{fix} is the nitrogen fixation rate of each PFT. N_{fixpot} is the potential N_2 fixation rate (g N d^{-1}). $f_B(T)$ is the influence function of soil temperature. $f_B(W)$ is the soil water function. $f_B(N)$ is the function of root substrate N concentration. $f_B(C)$ is the function of plant carbon availability.

BNF increases as the temperature rises from a minimum temperature (0–5 ℃) for N fixation to the optimal temperature; the maximum rate (1) occurs within an optimal range (15–25 ℃) and decreases from the optimal to the maximum temperature, above which BNF will stop at 35–40 ℃:

$$f_B(T) = \begin{cases} 0 \quad for \;\; T > T_{max} \;\; or \; T < T_{min} \\ \frac{T - T_{min}}{T_{optL} - T_{min}} \quad for \;\; T_{min} \le T \le T_{optL} \\ \frac{T_{max} - T}{T_{max} - T_{optH}} \quad for \;\; T_{optH} \le T \le T_{max} \end{cases} \tag{19}$$

Soil water deficit and flood dramatically inhibit N_2 fixation because of drought stress and oxygen deficit. The impact of soil water is calculated as:

$$f_B(W) = \begin{cases} 0 & for \;\; W < W_a \\ \varphi_1 + \varphi_2 & for \;\; W_a \le W \le W_b \\ 1 & for \;\; W > W_b \end{cases} \quad (20)$$

where W is the available soil water, which is defined as the ratio of water content to that at the field capacity. W_a is the bottom threshold below which N_2 fixation is restricted by soil moisture. W_b is the upper threshold above which nitrogen fixation is not limited by soil moisture. φ_1 and φ_2 are parameters representing the linear relationship between soil water content and its effect on N_2 fixation, respectively.

The N_2 fixation is only considered to occur when the direct N uptake from soil cannot meet the plant N demand. The inhibition effect of N is defined as:

$$f_B(N) = \begin{cases} 1 - f_{Nup} ln(1000 - N_s) & for \; N_s \ge 0.001 \\ 1 & for \; N_s < 0.001 \end{cases} \quad (21)$$

where f_{Nup} is a parameter related to legume biological N_2 fixation and soil N. N_s is the soil mineral N (g N m^{-2}).

The carbon effect is modeled following a Michaelis–Menten equation:

$$f_B(C) = \frac{1}{1 + K_C / C_r} \quad (22)$$

where C_r is the dissolved soil organic carbon content (g C m^{-2}) to represent carbon availability from plants to N_2 fixers. K_C is the Michaelis–Menten constant, which is plant species dependent.

2.3. N_2O, NO, and N_2 gases emissions

The N_2O, NO, and N_2 gases are generated in nitrification and denitrification processes and we estimated emissions of these three gases based on the methods in Chatskikh et al. (2005). Firstly, the N gas production potential is determined from the simulated nitrification and denitrification.

$$Ngas_{nit} = k_{np} f_{nT}(T) wfpNit \quad (23)$$

where $Ngas_{nit}$ is potential N gas emission (g N d^{-1}) from nitrification. k_{np} represents the proportion of N intermediates resulting in N_2O emissions from nitrification. $f_{nT}(T)$ represents the effect of temperature on nitrification. wfp is water-filled porosity which is the ratio of soil water content and total soil porosity. Nit is soil nitrification which is described by first-order kinetics modified by soil temperature and soil water potential.

$$Ngas_{denit} = Denf_d(T)f(wfp)f(NO3) \quad (24)$$

where $Ngas_{denit}$ is the potential N gases emission from denitrification (g N d^{-1}). Den is the denitrification potential (g N d^{-1}) which is assumed to be proportional to the soil organic matter mineralization rate, and to depend on soil clay content. $f_d(T)$ represents the temperature effect and $f(wfp)$ defines the dependency of denitrification on water-filled porosity. $f(NO3)$ describes the dependency of the denitrification rate on nitrate concentration.

Secondly, the potential N gas emission is divided into N_2O, NO, and N_2 emissions according to the effects of soil physical properties on the efficiency by which denitrification reduces N_2O to N_2. N_2O from nitrification and denitrification is calculated as:

$$N_2O = (Ngas_{nit} + Ngas_{denit})f_{NT}(T)(1 - f(wfp))f(clay)f(depth) \quad (25)$$

where $f_{NT}(T)$ represents the impact of temperature on actual N2O emission. $f(clay)$ is the effect of clay content in soil, and $f_2(depth)$ is the effect of soil depth (m).

NO is calculated according to an empirical equation that sets up the relationship with N_2O.

$$NO = N_2O/10^{(2.6wfp-1.66)} \quad (26)$$

And the left fraction of nitrogen gas is N_2,

$$N_2 = Ngas_{nit} + Ngas_{denit} - N_2O - NO \quad (27)$$

2.4. NH_3 emission

The NH_3 emission consists of direct emission from manure and indirect emission from soil. The indirect emission from soil is simulated in DLEM by coupling the Bidirectional NH_3 exchange module (Bi-NH_3) from the Community Multi-scale Air Quality model with the DLEM (Xu et al.,

2018, 2019). The soil emission of NH_3 varies daily after chemical N fertilizer was applied to soils and is calculated as follows:

$$NH_3 = C_c / (R_a + 0.5\ R_{inc}) \quad (28)$$

where C_c is the canopy NH_3 compensation point as calculated in equation 30, R_a is the aerodynamic resistance ranging from 30 to 200, and R_{inc} is the aerodynamic resistance within the canopy. Units of NH_3 fluxes are μg m^{-3} s^{-1}, units of all compensation points are μg m^{-3}, and units of all the above resistances are s m^{-1}. For R_{inc}, the following equation was used:

$$R_{inc} = b_0 \times LAI \times \frac{h_{can}}{\mu_*} \quad (29)$$

where b_0 is an empirical constant taken as 14 m^{-1}, LAI is the leaf area index, h_{can} is the canopy height (m), and μ_* is the fraction velocity ranging from 0.2 to 0.5 (m s^{-1}). For C_c, the following equation was used:

$$C_c = \frac{\frac{C_{st}}{R_b+R_{st}}+\frac{C_g}{0.5R_{inc}+R_{bg}+R_{soil}}}{(R_a+0.5R_{inc})^{-1}+(R_b+R_{st})^{-1}+(R_b+R_w)^{-1}+(0.5R_{inc}+R_{bg}+R_{soil})^{-1}} \quad (30)$$

where R_b is the quasi laminar boundary layer resistance at the leaf surface, R_{st} is the stomatal resistance, R_{bg} is the quasi laminar boundary layer resistance at the ground surface, R_w is the cuticular resistance, and R_{soil} is the resistance to diffusion through the soil layer(Cooter et al., 2012; Sakaguchi & Zeng, 2009).

The soil emission potential of NH_3 is regulated by the ratio of NH_4^+ concentration ($[NH_4^+]$) to H^+ concentration ($[H^+]$), which is defined as

$$\Gamma_g = \frac{N_{fer}/(\theta_s M_N d_l)}{10^{-\mathrm{pH}}} \quad (31)$$

where N_{fer} is the fertilizer application rate (g N m^{-2}), d_l is the depth of soil layer (m), and pH is the pH of the soil after N fertilizer application (pH = 7.5), M_N is the molar mass of N (14 g mol^{-1}), θ_s is the soil volumetric water content in m^3 m^{-3}. The maximum emission potential was found in the first time of fertilization and decreased with passing time. The DLEM deals with loss of N fertilizer at daily step including plant and microbial uptake, nitrification, or N leaching/runoff resulting in variable amounts of NH_4^+ over time.

The ground layer (C_g) compensation points are defined as follows:

$$C_g = M_n/V_m \frac{161500}{T_s} e^{(-\frac{10380}{T_s})} \Gamma_g \quad (32)$$

where M_n = 1.7×10^7 μg mol^{-1}, V_m = 1×10^{-3} (convert L to m^3), T_s is soil temperature in °K.

The stomatal compensation points are defined as follows:

$$C_{st} = M_n/V_m \frac{161500}{T_{can}} e^{(-\frac{10380}{T_{can}})} \Gamma_s \quad (33)$$

where T_{can} is the canopy temperature in °K, Γ_s is the ratio of [NH_4^+] to [H^+] in the apoplast parametrized in Massad et al. (2010).

Emission factors for estimating NH_3 emissions from livestock excreta were adopted from previous studies. Bouwman et al. (2002) provided a median value of EF (23%) to estimate the global NH_3 loss from animal manure. The range of EF in Bouwman et al. (2002) was 19−29%. Based on the work by Beusen et al. (2008) and Riddick et al. (2016) applied a revised EF (17%) to estimate NH_3 emissions from animal manure. In DELM, livestock manure N can be divided into urine and feces, and we adopted the EF of 26% on urine and 12% on feces (Laubach et al., 2013). to estimate NH_3 loss from livestock manure.

2.5. P weathering

Parent material weathering is the primary source of soil inorganic P. Here, we used the method proposed by Hartmann et al. (2014) to calculate the P release from rock weathering, which considers the influences of lithology, temperature, and soil properties:

$$f_{weath,i} = (b_{carbonate,i} + b_{silicate,i})q \quad (34)$$

$$P_w = f_{weath,i} w_i F_{T,i} F_{S,i} \quad (35)$$

$$F_{T,i} = exp(-\frac{E_{a,i}}{R}\left(\frac{1}{T} - \frac{1}{T_0}\right)) \quad (36)$$

where f_{weath} represents the chemical weathering flux of lithology i (g m^{-2} day^{-1}), $b_{carbonate,i}$ and $b_{silicate,i}$ are parameters given the relative contribution from carbonate and silicate weathering, q is the runoff (mm day^{-1}), w_i is the P contents in lithological classes relative to the SiO2 and the major cation, $F_{T,i}$ represents the effect of soil temperature on weathering, $F_{S,i}$ represents a reduction effect of certain soil types on weathering, $E_{a,i}$ is the activation energy for lithology (kJ/mol) and R is the gas constant, T is temperature in Kelvin and T_0 is reference

temperature (284.15 K). The lithology-specific values of $b_{carbonate,i}$, $b_{silicate,i}$, $F_{S,i}$ and $E_{a,i}$ are derived from Hartmann et al. (2014).

3. Results

3.1. Nitrogen budget

The major N inputs in terrestrial ecosystems include N fertilizer, manure N, atmospheric N deposition, and N fixation, and major N outputs include harvest N, N gases (NH_3, N_2O, NO, N_2) emissions, and N loading. The decadal average total N inputs in the MRB increased from 5.05 Tg N yr^{-1} in the 1900s to 20.57 Tg N yr^{-1} in the 2010s (Table 5-1 and Figure 5-2). N fertilizer started to increase rapidly (at a speed of 0.12 Tg N yr^{-2}, $p < 0.01$) since the 1940s to 7.97 Tg N yr^{-1} in 2004, then it slightly decreased during 2005-2010 and increased again in the 2010s. N fertilizer became the largest N input (over 30%) since the 1980s, before which N fixation is the dominant N input. N fixation steadily increased at a speed of 0.04 Tg N yr^{-2} during 1901-2018, and it still contributed 31% (6.43 Tg N yr^{-1}) of total N inputs in the 2010s. The manure N and atmospheric N deposition, accounting for 19% (3.92 Tg N yr^{-1}) and 16% (3.20 Tg N yr^{-1}) of total N input in the 2010s respectively, are also important N sources. Manure N increased significantly from 1901 to 1960 and became relatively stable thereafter, similarly, atmospheric N deposition first increased but slightly decreased after the 1980s.

The decadal average total N outputs increased from 3.09 to 16.68 Tg N yr^{-1} during the 1900s-2010s. Harvest crop N which is the primary N output increased at a speed of 0.10 Tg N yr^{-2} over 1901-2018, and its share in total N outputs increased from 36% (1.11 Tg N yr^{-1}) to 68% (11.43 Tg N yr^{-1}) from the 1900s to the 2010s. Meanwhile, Simulated NH_3 emissions have increased over fourfold (from 0.26 to 1.43 Tg N yr^{-1}) and emissions of N_2O (from 0.32 to 0.60 Tg N yr^{-1}), NO (from 0.24 to 0.43 Tg N yr^{-1}), and N_2 (from 0.60 to 1.17 Tg N yr^{-1}) have almost doubled due to the enhanced anthropogenic N inputs and climate warming. Riverine N loading also increased dramatically from 0.56 Tg N yr^{-1} in the 1900s to 1.63 Tg N yr^{-1} in the 2010s. As the proportion of harvest crop N in total N outputs increased significantly, the proportions of N_2O, N_2, and NO emissions and N loading have seen a decrease since the 1900s, and that of NH_3 emission started to decrease after the 1960s. The proportions of N gas emissions and N loading in total N inputs, however, were relatively stable from the 1960s to the 2010s, with total gas emission accounting for 18-19% and riverine N loading accounting for 8-9% of N inputs.

Table 5-1. The decadal average N inputs and outputs in the MRB (Tg N yr^{-1}).

Year	N Fertilizer	Manure N	N Deposition	N Fixation	Harvest N	NH_3 Emission	N_2O Emission	N_2 Emission	NO Emission	N Loading
1900s	0.03	1.44	1.27	2.31	-1.11	-0.26	-0.32	-0.60	-0.24	-0.56
1910s	0.07	1.63	1.28	2.38	-1.22	-0.31	-0.33	-0.61	-0.25	-0.55
1920s	0.28	1.88	1.37	2.50	-1.46	-0.38	-0.36	-0.67	-0.27	-0.65
1930s	0.36	2.31	1.39	2.74	-2.13	-0.48	-0.41	-0.73	-0.33	-0.69
1940s	0.65	2.88	1.55	3.72	-2.84	-0.61	-0.43	-0.79	-0.32	-0.95
1950s	1.71	3.31	1.85	3.94	-3.62	-0.82	-0.43	-0.78	-0.32	-0.99
1960s	2.95	3.58	2.35	4.31	-4.64	-1.00	-0.43	-0.74	-0.31	-1.05
1970s	4.72	3.57	2.92	5.16	-6.57	-1.17	-0.49	-0.88	-0.35	-1.50
1980s	5.85	3.38	3.29	5.50	-8.53	-1.25	-0.56	-0.99	-0.41	-1.63
1990s	6.55	3.51	3.39	5.51	-9.17	-1.34	-0.58	-1.08	-0.41	-1.78
2000s	7.16	3.89	3.34	5.78	-10.65	-1.45	-0.60	-1.11	-0.43	-1.57
2010s	7.02	3.92	3.20	6.43	-11.43	-1.43	-0.60	-1.17	-0.43	-1.63

Note: The N inputs are in positive number and N outputs are in negative number.

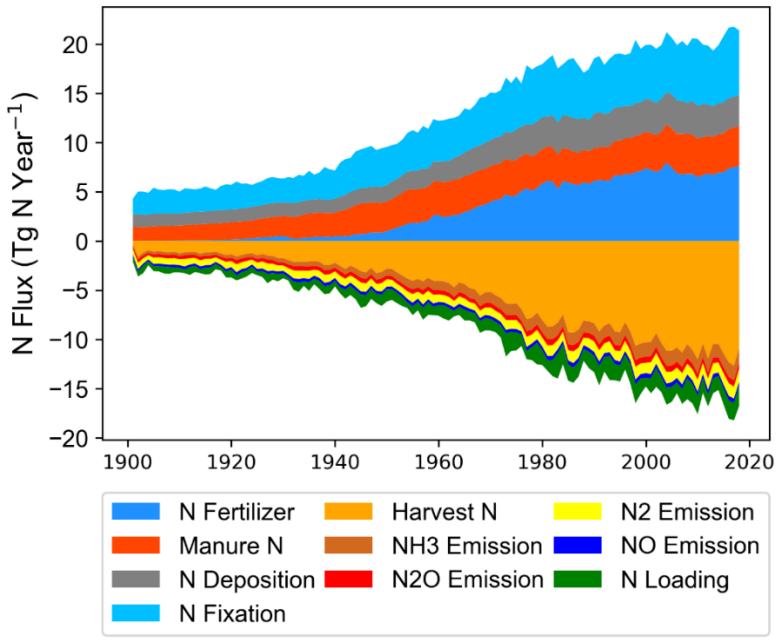

Figure 5-2. The N budget in the Mississippi River Basin during 1901-2018.

3.2. Nitrogen loading

With respect to the change in N loading during 1901-2018, the four N species all exhibit increasing trends with different magnitudes (Figure 5-3). Riverine nitrite (NO_3^-) export increased at a rate of 9.79 Gg yr^{-1} over the study period, and decadal average NO_3^- export in the 2010s (1054 Gg yr^{-1}) was 285% higher compared to the 1900s (274 Gg yr^{-1}). The most substantial increase in NO_3^- export occurred during the 1960s and 1970s, and NO_3^- export peaked in 1983 then slightly decreased. Riverine ammonia (NH_4^+) increased 116% from the 1900s (13 Gg yr^{-1}) to the 2010s (27 Gg yr^{-1}). The NH_4^+ export also increased significantly since 1960 and began to level off after 1980. Riverine dissolved organic nitrogen (DON) and particulate organic nitrogen (PON) increased from 144 and 126 Gg yr^{-1} in the 1900s to 268 and 277 Gg yr^{-1} in the 2010s, respectively. The increase rate of PON export (120%) is higher than that of DON (85%), and PON export started to exceed DON export in the 2010s. Different from the other three N species, riverine PON export continued to increase slightly after 1980 with the highest amount occurring in 2018. Average NO_3^- export over 1901-2018 had the largest share (66%) in TN export, followed by DON (17%) and PON (16%), and NH_4^+ only accounted for 2% of TN export.

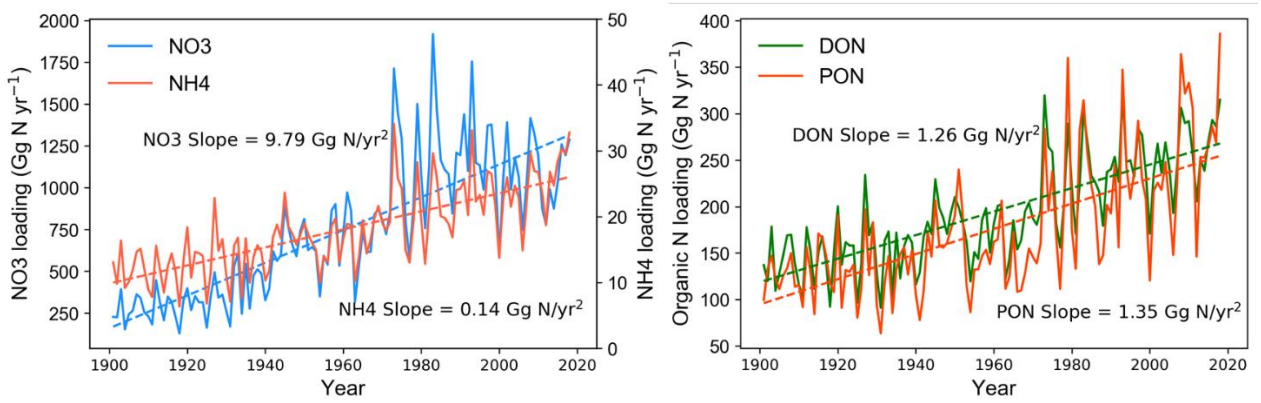

Figure 5-3. The interannual variations and trends of inorganic N (NO_3^- and NH_4^+) and organic N (DON and PON) loading from the Mississippi River Basin during 1901-2018.

3.2. Phosphorus budget

The major P inputs include P fertilizer, livestock manure P and weathering P, and P outputs consist of harvest crop P and P loading. Total P inputs and outputs increased from 0.42 and 0.56 Tg P yr^{-1} in the 1900s to 2.57 and 1.90 Tg P yr^{-1} in the 2010s, respectively (Table 5-2

and Figure 5-4). Manure P was the dominant P input (over 50%) and increased significantly before the 1960s, thereafter, the P fertilizer input exceed manure P and became the largest P input. Synthetic P fertilizer increased rapidly since the 1940s, and reached 1.34 Tg P yr^{-1} in the 1970s, but it experienced a decrease within the 1980s and then fluctuated around 1.30 Tg P yr^{-1}. Weathering P only accounted for a small share (< 8%) of total P inputs over the study period, so does the atmospheric P deposition which only contributed around 1% in total P inputs after the 1960s. The average annual harvest P was 0.47 Tg P yr^{-1} in the 1900s, accounting for around 82% of P outputs, and increased to 1.78 Tg P yr^{-1} in the 2010s, accounting for 91% of P outputs. Average riverine P loading increased from 0.10 Tg P yr^{-1} (account for 18% of P outputs) in the 1900s to 0.19 Tg P yr^{-1} (account for 9% of P outputs) in the 2010s. The crop harvest removal P in total P inputs increased from 45% to 68% from the 1960s to the 2010s, meanwhile, that of P loading was stable, accounting for 6-7% in total P inputs.

Table 5-2. The decadal average P inputs and outputs in the MRB (Tg P yr^{-1}).

Year	P Fertilizer	Manure P	Weathering P	P deposition	Harvest P	P Loading
1900s	0.05	0.34	0.03	0.02	-0.47	-0.10
1910s	0.06	0.39	0.03	0.02	-0.53	-0.10
1920s	0.08	0.45	0.03	0.02	-0.58	-0.10
1930s	0.09	0.59	0.02	0.02	-0.62	-0.09
1940s	0.19	0.78	0.03	0.02	-0.68	-0.11
1950s	0.52	0.96	0.02	0.02	-0.78	-0.11
1960s	0.88	1.07	0.02	0.02	-0.89	-0.11
1970s	1.34	1.09	0.03	0.02	-1.14	-0.15
1980s	1.32	1.04	0.03	0.02	-1.40	-0.15
1990s	1.26	1.09	0.03	0.02	-1.51	-0.17
2000s	1.26	1.18	0.03	0.02	-1.68	-0.16
2010s	1.30	1.24	0.04	0.02	-1.78	-0.19

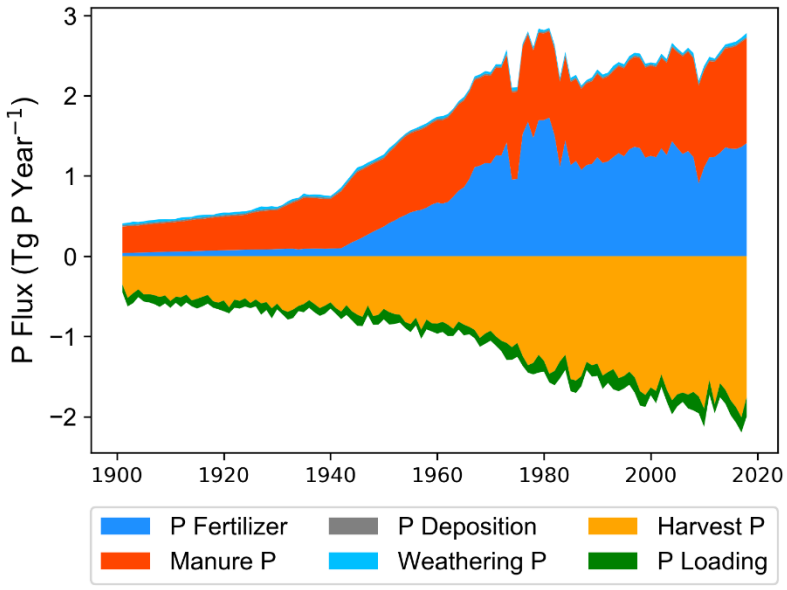

Figure 5-4. The P budget in the Mississippi River Basin during 1901-2018.

3.4. Changes in legacy soil nutrients

The nutrient balance, the difference between inputs and outputs of N and P, can reflect the accumulation speed of legacy nutrients. The N balance first increased from 1.96 Tg N yr^{-1} in the 1900s to 5.41 Tg N yr^{-1} in the 1970s, then decreased to 3.89 Tg N yr^{-1} in the 2010s (Figure 5-5). The legacy N, represented by the N accumulation, increased 423.80 Tg N during 1901-2018. The accumulation of N in terrestrial ecosystems slowed down as N balance experienced a decreasing trend since the 1980s. The average P balance was -0.13 Tg P yr^{-1} in the 1900s, and became positive after the 1930s, then it reached the peak of 1.18 Tg P yr^{-1} in the 1970s, and slightly decreased to 0.68 Tg P yr^{-1} in the 2010s. The legacy P storage first decreased 3.78 Tg P during 1901-1934 due to the higher P outputs compared with P inputs, then it shifted to increase and reached back to the 1901 level after 1951. The accumulation of legacy P also slowed down after 1980 and P storage in ecosystems in 2018 was 54.80 Tg P higher than in 1901.

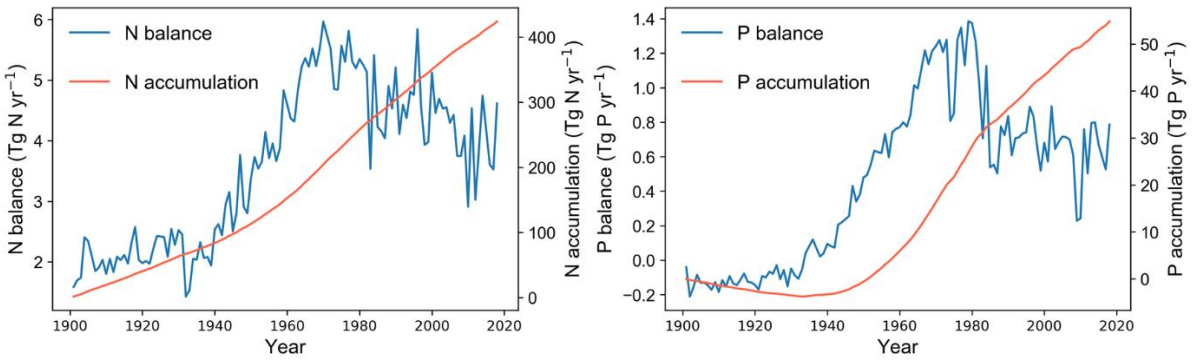

Figure 5-5. The N and P balance and accumulation in the MRB. Nutrient balance is the difference between nutrient inputs and outputs and nutrient accumulation is the sum of the historical nutrient balance.

4. Discussion

This study quantified the N and P budgets under the same modeling framework in the MRB during 1901-2018. The major N and P inputs and outputs estimated in this study are comparable with the estimation by David et al. (2010) and Stackpoole et al. (2021). The increases in synthetic fertilizer N and P, the most important nutrient inputs, were mainly driven by the intensive application on cropland in the Midwest U.S. (Cao et al., 2018). The increase in manure nutrient input was contributed by both increasing livestock numbers and body weights (Bian et al., 2021). The steady increase in N fixation was related to the growing soybean productivity (David et al., 2010). Atmospheric N deposition increased as a result of high N oxide emissions from fossil fuel consumption, but has begun to decline in recent decades due to the successful implementation of Clean Air Act Amendments in 1990 (Lloret and Valiela, 2016). The major N and P outputs, including harvest crop N and P, N and P loading, and N gases emissions all increased over the last century driven by the intensified application of synthetic fertilizer and livestock manure in agricultural systems. The proportion of harvest crop nutrients in total nutrients inputs increased significantly over the study period in the MRB. Moreover, crop harvest N and P continually increased even when the N fertilizer stopped increasing after the 1990s and P fertilizer decreased in the 1980s. Swaney & Howarth (2019) reported that as crop yields have increased, nutrient use efficiency has increased in some regions of the MRB. The

enhanced nutrient use efficiency explained the increased harvest crop nutrient output even when nutrient inputs stopped increasing.

The nutrient surplus that is stored in soils as organic matter or inorganic matter can serve as a long-term source of soluble and particulate nutrients that can be potentially released into waters, which has raised concern in recent years (Rowe et al., 2016; Sabo et al., 2021). The N surplus could be stored in plant and soil, and mostly exist in soil organic matter, because inorganic form of N is easily lost to water or atmosphere and unlikely to establish high storage amount. The P surplus, by comparison, could be prone to store in plant and soil, because P is less mobile and occurs largely as particulate inorganic form by attaching to clay and metal particles (McDowell et al., 2004). Both soil legacy N and P in the MRB have been built up due to the overuse of fertilizer, especially from 1930-to 1980 (Figure 5-4). Legacy nutrients can persist for many decades to more than a century after the termination of anthropogenic input (Fraterrigo et al., 2005; Sabo et al., 2021). The legacy nutrients that remain within soil and groundwater still serve as long-term nutrient sources for coastal oceans (Meter et al., 2018; Stackpoole et al., 2019). Therefore, the reduction of non-point source nutrient loads from the MRB is hindered, especially in regions with long histories of crop cultivation and nutrient application (Goyette et al., 2019). On the other hand, legacy soil nutrients can act as a potential nutrient source for crops and be integrated into sustainable nutrient management strategies for future food production (Rowe et al., 2016). Better utilizing legacy soil nutrients can bring both economic and environmental benefits. Improving soil nutrient acquisition and crop nutrient utilization efficiency is necessary for future nutrient management.

Nutrient budgets have been increasingly adopted by various stakeholders for a variety of applications, such as evaluating crop NUE, managing fertilizer and manure application, and controlling water pollution, air pollution, and greenhouse gas emissions. Based on the information from nutrient budgets, farmers and policymakers can make strategies to optimize fertilizer application and monitor the environmental impacts of agricultural production based on nutrient budget information. This nutrient budget study could advance our knowledge of biogeochemical processes and provide a full picture of the dynamics of N and P fluxes across the MRB. The legacy soil nutrient estimated in this study may inspire stakeholders to efficiently utilize this valuable resource and control its negative environmental impacts.

5. Conclusion

The legacy nutrients result from the balance between inputs and outputs of N and P in a long historical period. The N and P outputs in the Mississippi River Basin, including harvest removal, gas emission, and riverine loading, all increased over the last century following the sharp growth of the anthropogenic N and P inputs. The proportions of harvested N and P in total nutrient inputs increased from the 1960s to the 2010s, reflecting the increased NUE of crops. Both N and P balances substantially increased from the 1930s to the 1970s, after which N balance decreased slightly since the 1970s, while P balance dramatically decreased in the 1980s due to the reduction in P fertilizer usage. The legacy soil nutrients, represented by nutrient accumulation, continued to increase but had slowed down since the 1980s in the MRB.

References

Beusen, A.H.W., Bouwman, A.F., Heuberger, P.S.C., Van Drecht, G., Van Der Hoek, K.W., 2008. Bottom-up uncertainty estimates of global ammonia emissions from global agricultural production systems. Atmos. Environ. 42, 6067–6077. https://doi.org/10.1016/j.atmosenv.2008.03.044

Bian, Z., Tian, H., Yang, Q., Xu, R., Pan, S., Zhang, B., 2021. Production and application of manure nitrogen and phosphorus in the United States since 1860. Earth Syst. Sci. Data 13, 515–527. https://doi.org/10.5194/essd-13-515-2021

Bonan, G.B., 1996. Land surface model (LSM version 1.0) for ecological, hydrological, and atmospheric studies: Technical description and users guide. Technical note. National Center for Atmospheric Research, Boulder, CO (United States ….

Bouwman, A.F., Boumans, L.J.M., Batjes, N.H., 2002. Estimation of global NH3 volatilization loss from synthetic fertilizers and animal manure applied to arable lands and grasslands. Glob. Biogeochem. Cycles 16, 8-1-8–14.

Cao, P., Lu, C., Yu, Z., 2018. Historical nitrogen fertilizer use in agricultural ecosystems of the contiguous United States during 1850–2015: application rate, timing, and fertilizer types. Earth Syst. Sci. Data 10, 969–984. https://doi.org/10.5194/essd-10-969-2018

Chatskikh, D., Olesen, J.E., Berntsen, J., Regina, K., Yamulki, S., 2005. Simulation of Effects of Soils, Climate and Management on N2O Emission from Grasslands. Biogeochemistry 76, 395–419. https://doi.org/10.1007/s10533-005-6996-8

Collatz, G.J., Ball, J.T., Grivet, C., Berry, J.A., 1991. Physiological and environmental regulation of stomatal conductance, photosynthesis and transpiration: a model that includes a laminar boundary layer. Agric. For. Meteorol. 54, 107–136. https://doi.org/10.1016/0168-1923(91)90002-8

Conley, D.J., Paerl, H.W., Howarth, R.W., Boesch, D.F., Seitzinger, S.P., Havens, K.E., Lancelot, C., Likens, G.E., 2009. Controlling Eutrophication: Nitrogen and Phosphorus. Science 323, 1014–1015. https://doi.org/10.1126/science.1167755

Cooter, E.J., Bash, J.O., Benson, V., Ran, L., 2012. Linking agricultural crop management and air quality models for regional to national-scale nitrogen assessments. Biogeosciences 9, 4023–4035. https://doi.org/10.5194/bg-9-4023-2012

David, M.B., Drinkwater, L.E., McIsaac, G.F., 2010. Sources of Nitrate Yields in the Mississippi River Basin. J. Environ. Qual. 39, 1657–1667. https://doi.org/10.2134/jeq2010.0115

Davidson, E.A., 2009. The contribution of manure and fertilizer nitrogen to atmospheric nitrous oxide since 1860. Nat. Geosci. 2, 659.

Duncan, J.M., Groffman, P.M., Band, L.E., 2013. Towards closing the watershed nitrogen budget: Spatial and temporal scaling of denitrification. J. Geophys. Res. Biogeosciences 118, 1105–1119.

Farquhar, G.D., von Caemmerer, S., Berry, J.A., 1980. A biochemical model of photosynthetic CO2 assimilation in leaves of C3 species. Planta 149, 78–90. https://doi.org/10.1007/BF00386231

Fowler, D., Coyle, M., Skiba, U., Sutton, M.A., Cape, J.N., Reis, S., Sheppard, L.J., Jenkins, A., Grizzetti, B., Galloway, J.N., Vitousek, P., Leach, A., Bouwman, A.F., Butterbach-Bahl, K., Dentener, F., Stevenson, D., Amann, M., Voss, M., 2013. The global nitrogen cycle in the twenty-first century. Philos. Trans. R. Soc. B Biol. Sci. 368, 20130164. https://doi.org/10.1098/rstb.2013.0164

Fraterrigo, J.M., Turner, M.G., Pearson, S.M., Dixon, P., 2005. Effects of past land use on spatial heterogeneity of soil nutrients in southern Appalachian forests. Ecol. Monogr. 75, 215–230.

Goyette, J.-O., Bennett, E.M., Maranger, R., 2019. Differential influence of landscape features and climate on nitrogen and phosphorus transport throughout the watershed. Biogeochemistry 142, 155–174. https://doi.org/10.1007/s10533-018-0526-y

Gruber, N., Galloway, J.N., 2008. An Earth-system perspective of the global nitrogen cycle. Nature 451, 293–296. https://doi.org/10.1038/nature06592

Hartmann, J., Moosdorf, N., Lauerwald, R., Hinderer, M., West, A.J., 2014. Global chemical weathering and associated P-release — The role of lithology, temperature and soil properties. Chem. Geol. 363, 145–163. https://doi.org/10.1016/j.chemgeo.2013.10.025

Howarth, R.W., Billen, G., Swaney, D., Townsend, A., Jaworski, N., Lajtha, K., Downing, J.A., Elmgren, R., Caraco, N., Jordan, T., 1996. Riverine inputs of nitrogen to the North Atlantic Ocean: fluxes and human influences. Biogeochemistry 35, 75–139.

Hu, M., Liu, Y., Zhang, Y., Shen, H., Yao, M., Dahlgren, R.A., Chen, D., 2020. Long-term (1980–2015) changes in net anthropogenic phosphorus inputs and riverine phosphorus export in the Yangtze River basin. Water Res. 177, 115779. https://doi.org/10.1016/j.watres.2020.115779

Laubach, J., Taghizadeh-Toosi, A., Gibbs, S.J., Sherlock, R.R., Kelliher, F.M., Grover, S.P.P., 2013. Ammonia emissions from cattle urine and dung excreted on pasture. Biogeosciences 10, 327–338. https://doi.org/10.5194/bg-10-327-2013

Lawrence, D.M., Fisher, R.A., Koven, C.D., Oleson, K.W., Swenson, S.C., Bonan, G., Collier, N., Ghimire, B., van Kampenhout, L., Kennedy, D., Kluzek, E., Lawrence, P.J., Li, F., Li, H., Lombardozzi, D., Riley, W.J., Sacks, W.J., Shi, M., Vertenstein, M., Wieder, W.R., Xu, C., Ali, A.A., Badger, A.M., Bisht, G., van den Broeke, M., Brunke, M.A., Burns, S.P., Buzan, J., Clark, M., Craig, A., Dahlin, K., Drewniak, B., Fisher, J.B., Flanner, M., Fox, A.M., Gentine, P., Hoffman, F., Keppel-Aleks, G., Knox, R., Kumar, S., Lenaerts, J., Leung, L.R., Lipscomb, W.H., Lu, Y., Pandey, A., Pelletier, J.D., Perket, J., Randerson, J.T., Ricciuto, D.M., Sanderson, B.M., Slater, A., Subin, Z.M., Tang, J., Thomas, R.Q., Val Martin, M., Zeng, X., 2019. The Community Land Model Version 5: Description of New Features, Benchmarking, and Impact of Forcing Uncertainty. J. Adv. Model. Earth Syst. 11, 4245–4287. https://doi.org/10.1029/2018MS001583

Lloret, J., Valiela, I., 2016. Unprecedented decrease in deposition of nitrogen oxides over North America: the relative effects of emission controls and prevailing air-mass trajectories. Biogeochemistry 129, 165–180.

Lu, C., Yu, Z., Zhang, J., Cao, P., Tian, H., Nevison, C., 2021. Century-long changes and drivers of soil nitrous oxide (N2O) emissions across the contiguous United States. Glob. Change Biol. n/a. https://doi.org/10.1111/gcb.16061

Massad, R.-S., Nemitz, E., Sutton, M.A., 2010. Review and parameterisation of bi-directional ammonia exchange between vegetation and the atmosphere. Atmospheric Chem. Phys. 10, 10359–10386. https://doi.org/10.5194/acp-10-10359-2010

McDowell, R.W., Biggs, B.J.F., Sharpley, A.N., Nguyen, L., 2004. Connecting phosphorus loss from agricultural landscapes to surface water quality. Chem. Ecol. 20, 1–40. https://doi.org/10.1080/02757540310001626092

Meter, K.J.V., Basu, N.B., Cappellen, P.V., 2017. Two centuries of nitrogen dynamics: Legacy sources and sinks in the Mississippi and Susquehanna River Basins. Glob. Biogeochem. Cycles 31, 2–23. https://doi.org/10.1002/2016GB005498

Meter, K.J.V., Basu, N.B., Veenstra, J.J., Burras, C.L., 2016. The nitrogen legacy: emerging evidence of nitrogen accumulation in anthropogenic landscapes. Environ. Res. Lett. 11, 035014. https://doi.org/10.1088/1748-9326/11/3/035014

Meter, K.J.V., Cappellen, P.V., Basu, N.B., 2018. Legacy nitrogen may prevent achievement of water quality goals in the Gulf of Mexico. Science 360, 427–430. https://doi.org/10.1126/science.aar4462

Metson, G.S., Lin, J., Harrison, J.A., Compton, J.E., 2017. Linking terrestrial phosphorus inputs to riverine export across the United States. Water Res. 124, 177–191. https://doi.org/10.1016/j.watres.2017.07.037

Motew, M., Chen, X., Booth, E.G., Carpenter, S.R., Pinkas, P., Zipper, S.C., Loheide, S.P., Donner, S.D., Tsuruta, K., Vadas, P.A., Kucharik, C.J., 2017. The Influence of Legacy P on Lake Water Quality in a Midwestern Agricultural Watershed. Ecosystems 20, 1468–1482. https://doi.org/10.1007/s10021-017-0125-0

Oenema, O., Heinen, M., 1999. Uncertainties in nutrient budgets due to biases and errors.

Oenema, O., Kros, H., de Vries, W., 2003. Approaches and uncertainties in nutrient budgets: implications for nutrient management and environmental policies. Eur. J. Agron. 20, 3–16.

Rabalais, N.N., Turner, R.E., 2019. Gulf of Mexico Hypoxia: Past, Present, and Future. Limnol. Oceanogr. Bull. 28, 117–124. https://doi.org/10.1002/lob.10351

Ren, W., Tian, H., Tao, B., Huang, Y., Pan, S., 2012. China's crop productivity and soil carbon storage as influenced by multifactor global change. Glob. Change Biol. 18, 2945–2957. https://doi.org/10.1111/j.1365-2486.2012.02741.x

Riddick, S., Ward, D., Hess, P., Mahowald, N., Massad, R., Holland, E., 2016. Estimate of changes in agricultural terrestrial nitrogen pathways and ammonia emissions from 1850 to present in the Community Earth System Model. Biogeosciences 13, 3397–3426. https://doi.org/10.5194/bg-13-3397-2016

Rowe, H., Withers, P.J.A., Baas, P., Chan, N.I., Doody, D., Holiman, J., Jacobs, B., Li, H., MacDonald, G.K., McDowell, R., Sharpley, A.N., Shen, J., Taheri, W., Wallenstein, M., Weintraub, M.N., 2016. Integrating legacy soil phosphorus into sustainable nutrient management strategies for future food, bioenergy and water security. Nutr. Cycl. Agroecosystems 104, 393–412. https://doi.org/10.1007/s10705-015-9726-1

Sabo, R.D., Clark, C.M., Bash, J., Sobota, D., Cooter, E., Dobrowolski, J.P., Houlton, B.Z., Rea, A., Schwede, D., Morford, S.L., Compton, J.E., 2019. Decadal Shift in Nitrogen Inputs and Fluxes Across the Contiguous United States: 2002–2012. J. Geophys. Res. Biogeosciences 124, 3104–3124. https://doi.org/10.1029/2019JG005110

Sabo, R.D., Clark, C.M., Gibbs, D.A., Metson, G.S., Todd, M.J., LeDuc, S.D., Greiner, D., Fry, M.M., Polinsky, R., Yang, Q., Tian, H., Compton, J.E., 2021. Phosphorus Inventory for the Conterminous United States (2002–2012). J. Geophys. Res. Biogeosciences 126, e2020JG005684. https://doi.org/10.1029/2020JG005684

Sakaguchi, K., Zeng, X., 2009. Effects of soil wetness, plant litter, and under-canopy atmospheric stability on ground evaporation in the Community Land Model (CLM3.5). J. Geophys. Res. Atmospheres 114. https://doi.org/10.1029/2008JD010834

Saxton, K.E., Rawls, W.J., 2006. Soil Water Characteristic Estimates by Texture and Organic Matter for Hydrologic Solutions. Soil Sci. Soc. Am. J. 70, 1569–1578. https://doi.org/10.2136/sssaj2005.0117

Scoones, I., Toulmin, C., 1998. Soil nutrient balances: what use for policy? Agric. Ecosyst. Environ. 71, 255–267.

Sharpley, A., Jarvie, H.P., Buda, A., May, L., Spears, B., Kleinman, P., 2013. Phosphorus Legacy: Overcoming the Effects of Past Management Practices to Mitigate Future Water Quality Impairment. J. Environ. Qual. 42, 1308–1326. https://doi.org/10.2134/jeq2013.03.0098

Stackpoole, S., Sabo, R., Falcone, J., Sprague, L., 2021. Long-Term Mississippi River Trends Expose Shifts in the River Load Response to Watershed Nutrient Balances Between 1975 and 2017. Water Resour. Res. 57, e2021WR030318. https://doi.org/10.1029/2021WR030318

Stackpoole, S.M., Stets, E.G., Sprague, L.A., 2019. Variable impacts of contemporary versus legacy agricultural phosphorus on US river water quality. Proc. Natl. Acad. Sci. 116, 20562–20567. https://doi.org/10.1073/pnas.1903226116

Steffen, W., Richardson, K., Rockstrom, J., Cornell, S.E., Fetzer, I., Bennett, E.M., Biggs, R., Carpenter, S.R., de Vries, W., de Wit, C.A., Folke, C., Gerten, D., Heinke, J., Mace, G.M., Persson, L.M., Ramanathan, V., Reyers, B., Sorlin, S., 2015. Planetary boundaries: Guiding human development on a changing planet. Science 347, 1259855–1259855. https://doi.org/10.1126/science.1259855

Swaney, D.P., Howarth, R.W., 2019. Phosphorus use efficiency and crop production: Patterns of regional variation in the United States, 1987–2012. Sci. Total Environ. 685, 174–188. https://doi.org/10.1016/j.scitotenv.2019.05.228

Tian, H., Chen, G., Liu, M., Zhang, C., Sun, G., Lu, C., Xu, X., Ren, W., Pan, S., Chappelka, A., 2010. Model estimates of net primary productivity, evapotranspiration, and water use efficiency in the terrestrial ecosystems of the southern United States during 1895–2007. For. Ecol. Manag. 259, 1311–1327.

Tian, H., Chen, G., Lu, C., Xu, X., Hayes, D.J., Ren, W., Pan, S., Huntzinger, D.N., Wofsy, S.C., 2015. North American terrestrial CO2 uptake largely offset by CH4 and N2O emissions: toward a full accounting of the greenhouse gas budget. Clim. Change 129, 413–426. https://doi.org/10.1007/s10584-014-1072-9

Tian, H., Xu, R., Pan, S., Yao, Y., Bian, Z., Cai, W.-J., Hopkinson, C.S., Justic, D., Lohrenz, S., Lu, C., Ren, W., Yang, J., 2020. Long-Term Trajectory of Nitrogen Loading and Delivery From Mississippi River Basin to the Gulf of Mexico. Glob. Biogeochem. Cycles 34, e2019GB006475. https://doi.org/10.1029/2019GB006475

Tian, H., Yang, J., Xu, R., Lu, C., Canadell, J.G., Davidson, E.A., Jackson, R.B., Arneth, A., Chang, J., Ciais, P., Gerber, S., Ito, A., Joos, F., Lienert, S., Messina, P., Olin, S., Pan, S., Peng, C., Saikawa, E., Thompson, R.L., Vuichard, N., Winiwarter, W., Zaehle, S., Zhang, B., 2019. Global soil nitrous oxide emissions since the preindustrial era estimated by an ensemble of terrestrial biosphere models: Magnitude, attribution, and uncertainty. Glob. Change Biol. 25, 640–659. https://doi.org/10.1111/gcb.14514

Wang, Z., Tian, H., Yang, J., Shi, H., Pan, S., Yao, Y., Banger, K., Yang, Q., 2020. Coupling of Phosphorus Processes With Carbon and Nitrogen Cycles in the Dynamic Land Ecosystem Model: Model Structure, Parameterization, and Evaluation in Tropical

Forests. J. Adv. Model. Earth Syst. 12, e2020MS002123. https://doi.org/10.1029/2020MS002123
Xu, R., Pan, S.F., Chen, J., Chen, G.S., Yang, J., Dangal, S.R.S., Shepard, J.P., Tian, H.Q., 2018. Half-century ammonia emissions from agricultural systems in Southern Asia: Magnitude, spatiotemporal patterns, and implications for human health. GeoHealth 2, 40–53.
Xu, R., Tian, H., Pan, S., Prior, S.A., Feng, Y., Batchelor, W.D., Chen, J., Yang, J., 2019. Global ammonia emissions from synthetic nitrogen fertilizer applications in agricultural systems: Empirical and process-based estimates and uncertainty. Glob. Change Biol. 25, 314–326.
Yang, Q., Tian, H., Friedrichs, M.A., Hopkinson, C.S., Lu, C., Najjar, R.G., 2015. Increased nitrogen export from eastern North America to the Atlantic Ocean due to climatic and anthropogenic changes during 1901–2008. J. Geophys. Res. Biogeosciences 120, 1046–1068.
Yu, T., Zhuang, Q., 2020. Modeling biological nitrogen fixation in global natural terrestrial ecosystems. Biogeosciences 17, 3643–3657. https://doi.org/10.5194/bg-17-3643-2020
Zhang, J., Tian, H., Yang, J., Pan, S., 2018. Improving Representation of Crop Growth and Yield in the Dynamic Land Ecosystem Model and Its Application to China. J. Adv. Model. Earth Syst. 10, 1680–1707. https://doi.org/10.1029/2017MS001253
Zhang, X., Davidson, E.A., Mauzerall, D.L., Searchinger, T.D., Dumas, P., Shen, Y., 2015. Managing nitrogen for sustainable development. Nature 528, 51–59. https://doi.org/10.1038/nature15743
Zhang, X., Davidson, E.A., Zou, T., Lassaletta, L., Quan, Z., Li, T., Zhang, W., 2020. Quantifying Nutrient Budgets for Sustainable Nutrient Management. Glob. Biogeochem. Cycles 34, e2018GB006060. https://doi.org/10.1029/2018GB006060

Chapter 6. The impact of legacy soil nutrients on nutrient loading and N:P stoichiometry from the Mississippi River Basin

Abstract

Human-induced imbalance of nitrogen (N) and phosphorus (P) in terrestrial ecosystems can lead to the disproportionate N and P loading, subsequently shifting the elemental stoichiometry in estuaries and coastal oceans and impacting the structure and functioning of aquatic ecosystems. The N:P ratio of nutrient loading from the Mississippi River Basin had increased before the late 1980s driven by the enhanced usage of N fertilizer over P fertilizer, whereafter it started to decrease while the N:P ratio of fertilizer application didn't exhibit a similar trend. Here, we hypothesized that legacy soil nutrients might contribute to the decreasing N:P loading ratio. For this, a coupled biogeochemical and hydrological model, in combination with long-term anthropogenic nutrients input, was used to evaluate the impact of soil nutrient legacy on N:P ratio of nutrient loading to the Gulf of Mexico. The results show that the longer resident time of P in soils contributes to much slower release of soil P to rivers than that of N. If anthropogenic nutrient surpluses were reduced or suspended, soil legacy inorganic N would decline quicker than soil inorganic legacy P, leading to the dramatic decrease in the ratio of inorganic N and P. As crop nutrient efficiency has increased in recent decades within the Mississippi River Basin, legacy soil nutrients have played a more important role in contributing to riverine nutrient loading. Extreme precipitation events have stimulated soil erosion which has facilitated more P loading than N. The increasingly dominant role of legacy nutrients as a source combined with more extreme precipitation may explain the decreasing N:P loading ratio in the Mississippi River. Our study suggests that legacy soil nutrient pools should be fully considered in resolving the eutrophication and nutrient imbalance issues, particularly in the context of global environmental changes.

1. Introduction

The global nitrogen (N) and phosphorus (P) cycles have been substantially disturbed by anthropogenic activities due to the growing demands for food and energy. Biologically available N and P inputs to the biosphere have doubled (Bouwman et al., 2009; Smil, 2000), bringing high risks to the stability and sustainability of the Earth system (Steffen et al., 2015). Moreover, the

higher proportion of anthropogenic inputs of reactive N relative to P inputs has led to a global increase in the N:P stoichiometric ratio (Peñuelas et al., 2013; Peñuelas and Sardans, 2022; Ptacnik et al., 2005). The altered environmental N:P ratios have been affecting the metabolism and growth rates of organisms, ecosystem functions and structures, and the global carbon cycle (Peñuelas et al., 2013; Sterner and Elser, 2017; Vitousek et al., 2009). For aquatic ecosystems, nutrient loading from terrestrial ecosystems, especially agricultural land, has stimulated eutrophication and degraded water quality (Cai et al., 2011; Howarth, 2008; Paerl et al., 2016).

Total N and total P are commonly used metrics of eutrophication, but they are not adequate for understanding the biodiversity and structure of aquatic communities (Glibert, 2017). A stoichiometric perspective can provide further insights into the aquatic nutrient imbalance and its effects on ecological processes, especially those associated with harmful algal bloom (Elser et al., 2007; Heil et al., 2007; Ptacnik et al., 2005). Stoichiometric N:P ratio has been widely used as an effective index to derive nutrient limitation of phytoplankton growth in both freshwater and marine systems (Guildford and Hecky, 2000; Justić et al., 1995; Qin et al., 2020). Nutrient limitation could vary in different aquatic systems and seasons (Howarth et al., 2021; Zhang et al., 2021). Specifically, lakes are generally limited by P due to the existence of N_2-fixing cyanobacteria while coastal oceans are limited by N as planktonic N_2 fixation is rarely observed in high salinity water (Conley et al., 2009).

The terrestrial-aquatic linkage in stoichiometric alterations plays a critical role in determining whether nutrients are balanced in aquatic ecosystems. When nutrient loads don't change in stoichiometric proportion to the "Redfield ratio", nutrient unbalanced conditions of receiving water may favor the proliferation of harmful algal blooms and the production of toxins (Glibert and Burkholder, 2011; Van de Waal et al., 2009). Globally, the excess use of N fertilizer over P fertilizer in agriculture has induced the increasing N:P stoichiometry of nutrient loads (Peñuelas et al., 2012), resulting in the proliferation of non-N_2-fixing cyanobacteria in freshwater and a shift towards more dinoflagellates in marine systems (Glibert, 2017; Lehman, 2007; Li et al., 2015). Stoichiometric analysis of nutrient loads and nutrient requirements of aquatic ecosystems can inform strategy and management efforts to control the most critical nutrient. Therefore, understanding the linkages between the stochiometric characterization of nutrient

loads and water quality is important and deserves more research, especially for estuaries and coastal oceans (Smith, 2006).

In the “dead zone” of the northern Gulf of Mexico, one of the largest hypoxic zones in the coastal ocean, the hypoxia is periodically limited by P but ultimately limited by N (Dodds, 2006; Lohrenz et al., 2008; Turner and Rabalais, 2013). In light of the heavy nutrient leakage from intensive agricultural activities within the Mississippi River Basin (MRB), action plans have been launched since 2001 to manage nutrients to reduce nutrient loading. However, the hypoxic zone area hasn’t exhibited a clear decreasing trend and the hypoxic area reached the recorded largest ever in 2017 (US EPA, 2021). Water quality monitoring data from stations (St, Francisville, Louisiana, observed by the USGS) near the outlet of the Mississippi River showed that the mean annual TN:TP ratio increased from the late 1970s to the 1980s, but then shifted to declined (Turner et al., 2006, Figure 6-1). The increase of the N:P ratio in nutrient loading was consistent with that of anthropogenic nutrient inputs to agricultural land. However, the recent decline of the N:P ratio has not been well explained yet.

Since legacy soil nutrients can reside within soil and groundwater for several decades and thus act as a long-term source to coastal oceans (Meter et al., 2018; Stackpoole et al., 2019), we hypothesized that they may contribute to the declining N:P ratio of nutrient loading from the MRB. Considering the legacy nutrients dynamics are difficult to be directly monitored, previous efforts mainly took advantage of statistical or watershed models that generally assumed a steady state of nutrient cycles at the annual timestep or ignored the accumulation of nutrients within soils (Chen et al., 2018). Long-term input datasets and process-based modeling can provide a reliable pathway to assess watershed legacy nutrient dynamics (Meter et al., 2018, 2017). However, few studies have estimated the impacts of both soil legacy N and P on nutrient loading under the same modeling framework. In this study, we explored the potential reasons for the declining stoichiometry ratio of N and P loading through synthesizing data and modeling to quantify long-term N and P dynamics along the terrestrial-aquatic continuum in the MRB. The specific workflow is listed as the following: (1) assessing the impacts of legacy soil nutrients on riverine N and P loadings by factorial simulations, and (2) investigating the response of N/P loading to environmental changes, such as climate, fertilizer, and manure application, groundwater, and land-use change. This work holds the potential to benefit strategy designing

and concentrating resources to better manage the nutrient exports from the MRB to estuaries and coastal oceans.

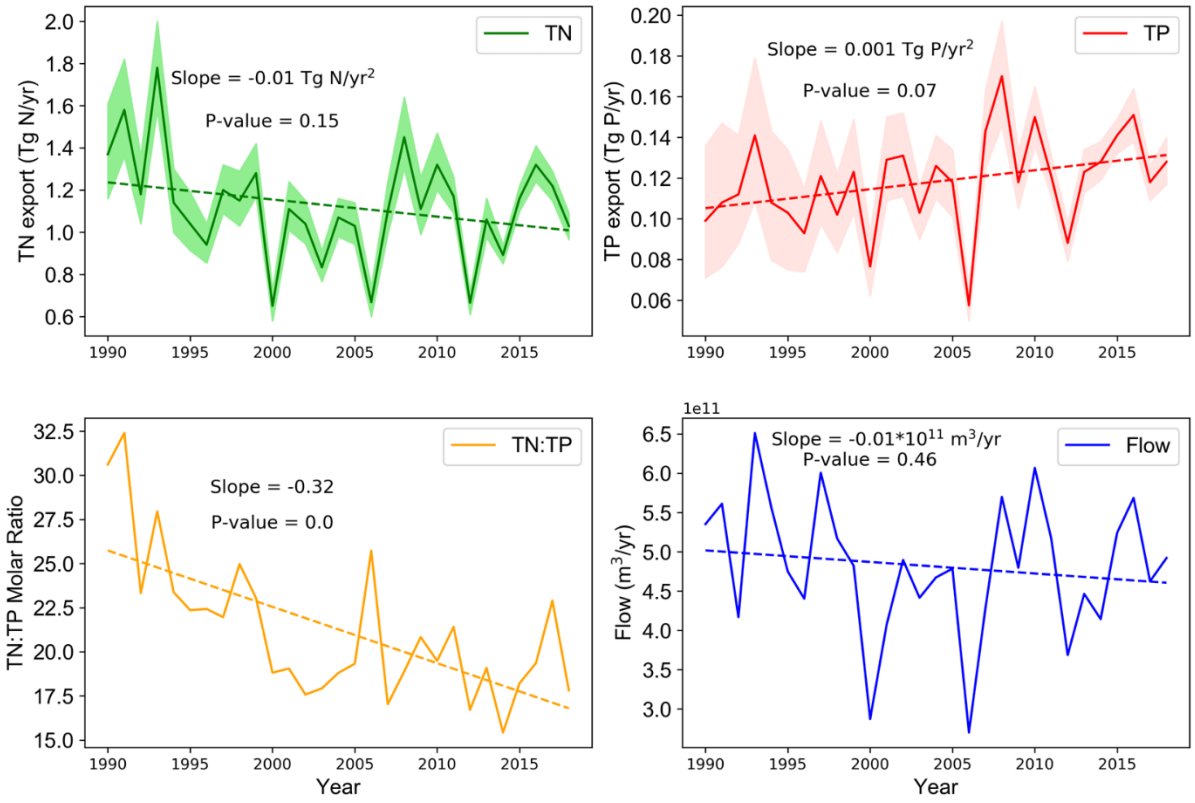

Figure 6-1. Interannual variations and trends of riverine N and P fluxes, TN:TP ratio in water, and flow from 1990 to 2018 at USGS site St, Francisville (USGS 07373420).

2. Methods

The process-based Dynamic Land Ecosystem Model (DLEM) (see Chapters 2 and 5) is applied in the MRB to investigate the impact of legacy nutrients on riverine nutrient loading. The dominant nutrient sources contributing riverine nutrient loading includes newly added nutrient and legacy nutrients. The legacy nutrient within the MRB has been estimated by establishing nutrient budgets in terrestrial ecosystems during 1901-2018 (Figures 6-2 and 6-4). Major N and P inputs in nutrient budgets include synthetic N and P fertilizer, livestock manure N and P, atmospheric N deposition, and biological N fixation (BNF). Meanwhile, the major N and P outputs include harvest removal N and P, N gases (NH_3, N_2O, NO, N_2) emissions, and riverine N

and P loading. The legacy soil nutrient continued to increase since 1940 but has slowed down after the 1970s.

Newly added nutrient source for nutrient loading could be indicated by nutrient surplus (calculated as total nutrient inputs – harvested removal nutrient in agricultural ecosystems). According to the nutrient budgets established by the model (see Chapter 5), both N and P surplus substantially increased from the 1930s to the 1970s, then N surplus leveled off and started to slightly decrease since the 1990s, while P surplus dramatically decreased in the 1980s due to the reduction in P fertilizer usage (Figure 6-2). Nutrient surplus in each year indicates the newly added nutrients that are available for loss to aquatic or atmospheric systems.

Two simulation scenarios were configured to investigate the impact of legacy soil nutrients on nutrient loading (Figure 6-3). The NORMAL scenario adopted historical nutrient inputs and outputs during 1901-2018. The simulation under LEGACY scenario was consistent with NORMAL scenario during 1901-1990, but assumed that there was no additional nutrient surplus on agricultural land thereafter, which means the nutrient use efficiency (NUE) of agricultural systems was 100% and the sum of nutrient inputs (fertilizer, manure, atmospheric deposition, weathering, and BNF) to agricultural systems was equal to harvest removal nutrient. Under the NORMAL scenario, the newly added nutrient and previous soil nutrient stock were both dominant nutrient sources for riverine nutrient loading over 1901-2018, while under the LEGACY scenario, the soil nutrient stock first accumulated during 1901-1990 and then became the only dominant nutrient source to riverine nutrient loading since 1991. The difference between the simulated results of the two scenarios since 1991 provided an indication of how legacy soil nutrients influenced the N:P ratio of riverine nutrient loading from the MRB.

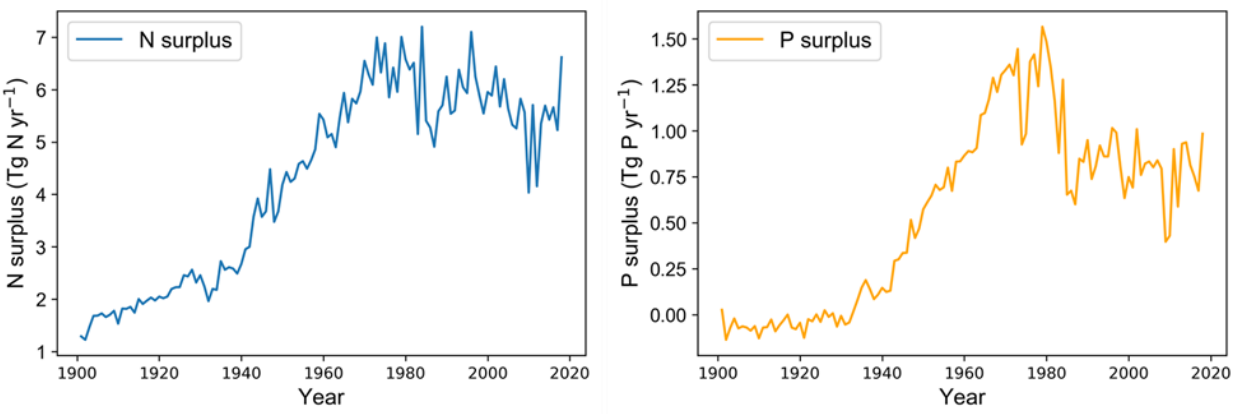

Figure 6-2. The annual variations of N and P surplus in the MRB during 1901-2018. Nutrient surplus is defined as the difference between N or P inputs (fertilizer, manure, BNF, deposition, and weathering) and harvest removal N or P in agricultural systems.

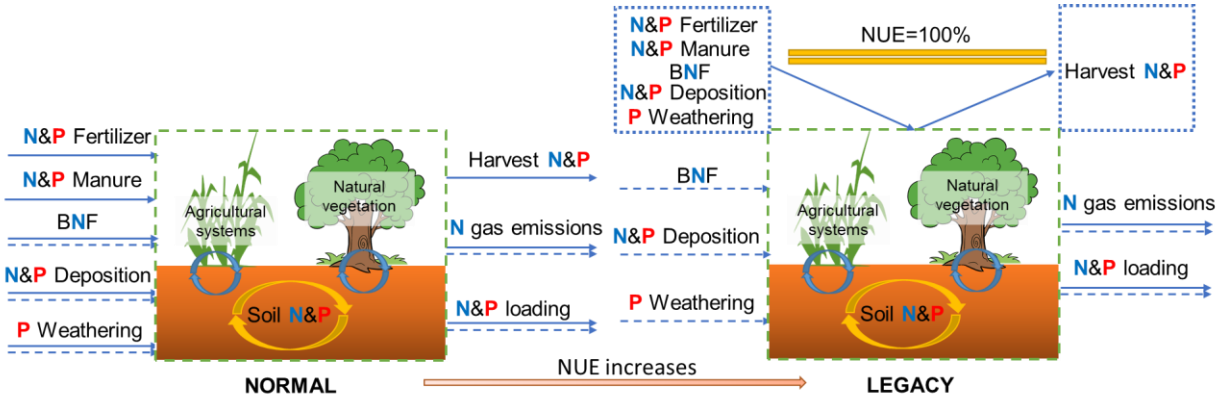

Figure 6-3. The N and P inputs and outputs in terrestrial ecosystems under NORMAL and LEGACY (after 1990) scenarios. The solid arrows represent fluxes in agricultural systems and the dash arrows represent fluxes in natural ecosystems.

3. Results and discussions

3.1. Impacts of legacy soil nutrients on N:P loading

In the NORMAL scenario, simulated riverine total nitrogen (TN) and total phosphorus (TP) loading increased by 219% and 62% from the 1900s to the 1990s, then TN loading decreased by 9% while TP loading increased by 9% from the 1990s to the 2010s (Figure 6-4a-b). In contrast, riverine TN loading decreased by 20%, and TP loading increased by 3% from the 1990s to the 2010s in the LEGACY scenario (Figure 6-4c-d). Compared with TP loading, TN

loading exhibit a distinct difference after 1990 between the two scenarios. The nutrient loading after 1990 in the LEGACY scenario was primarily contributed by agricultural legacy soil nutrient and background nutrient loss from natural ecosystems. Dissolved inorganic nutrients were major decreasing components for both N and P loads if there was no nutrient surplus on agricultural land. The proportions of dissolved inorganic nitrogen (DIN) and dissolved inorganic phosphorus (DIP) in TN and TP export decreased from 73% and 31% to 43% and 28% from the 1980s to the 2010s, respectively, and the reduction in DIN is more substantial than DIP under the LEGACY scenario (Figure 6-4c-d). The TN:TP molar ratio of nutrient loading caused by soil nutrients storage prior to 1991 decreased from 24 in 1991 to 11 in 2018 (LEGACY scenario), which mainly contributed by the decreasing DIN:DIP molar ratio (changed from 56 to 17) (Figure 6-5). As the DIN is the major component of TN loading while the proportion of DIP in TP export is less than half, the impact of decreasing DIN has a larger impact on TN compared with the impact of DIP on TP.

Nitrogen can leave terrestrial ecosystems through gas emission (vertical flux) and water transport (lateral flux), but the major pathway for P loss is the lateral flux to aquatic systems (Elser and Bennett, 2011). Compared with N which is highly soluble and can convert to gaseous form through volatilization, nitrification, and denitrification processes, P is less mobile and occurs largely as particulate form by attaching to clay surface, or combining with Fe, Al, Mg, and Ca (McDowell et al., 2004). The higher retention of P in soil compared with N decouples the N and P between soil and water, and the average N:P ratio of loading is usually higher than that of soil surpluses (Romero et al., 2021). The mean residence time of P in the terrestrial biosphere is estimated to be over 3.5 times that of N (Wang et al., 2010). If anthropogenic nutrient surpluses were reduced or suspended, soil labile N (inorganic N and organic N with short resident time) would decline quickly within a decade, and soil legacy organic N with long resident time would serve as a long-term N source but the mineralization rate would limit its contribution to DIN loading. Meanwhile, soil labile P would decrease much slower than N, and P loading derived from soil legacy P may also decrease slower than N. In the MRB, the usages of synthetic fertilizer and livestock manure nutrients have remained relatively stable since the 1990s, meanwhile, crop harvest continued to increase and the agroecosystem changed toward a high NUE system (Swaney and Howarth, 2019) (Figure 6-3). As newly added nutrient surpluses have begun to decrease (Figure 6-2), legacy nutrients started playing a more important role in

contributing to nutrient loading in recent decades. The long-term changes in the N:P ratio of nutrient loading, therefore, were more affected by legacy nutrient sources than newly added nutrient surpluses and declined in the recent three decades.

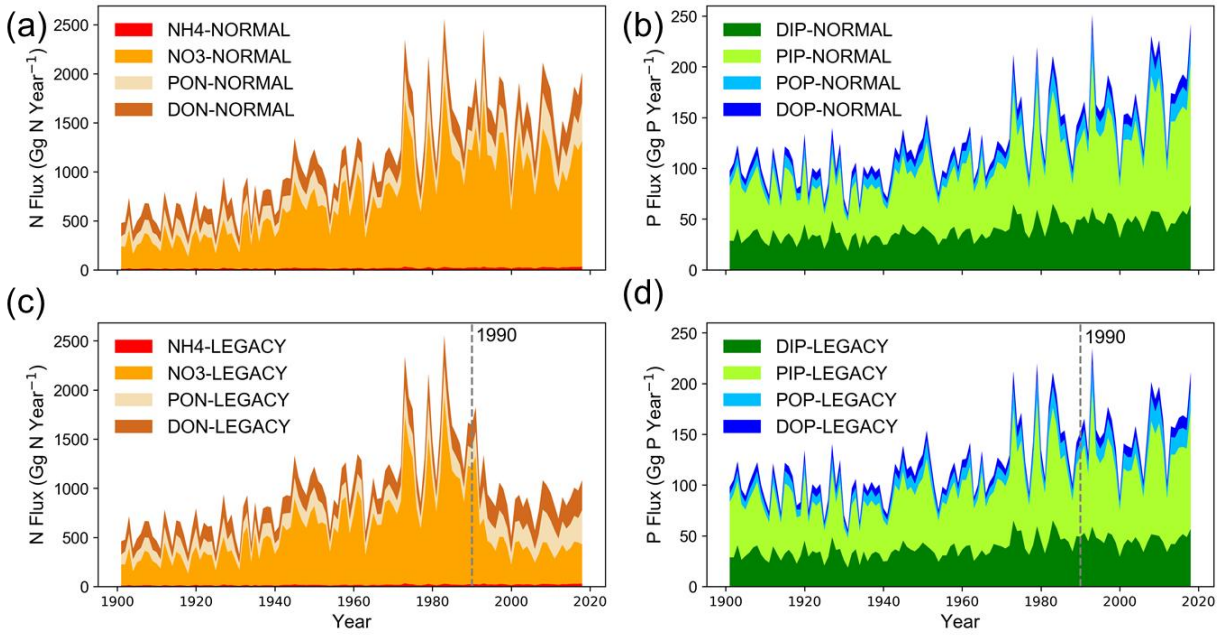

Figure 6-4. The interannual variations and trends of (a, c) simulated N exports, (b, d) simulated P exports, in the NORMAL and LEGACY scenarios during 1901-2018. NH4: ammonium; NO3: nitrate; PON: particulate organic nitrogen; DON: dissolved organic nitrogen; DIP: dissolved organic phosphorus; PIP: particulate inorganic phosphorus; POP: particulate organic phosphorus; DOP: dissolved organic phosphorus.

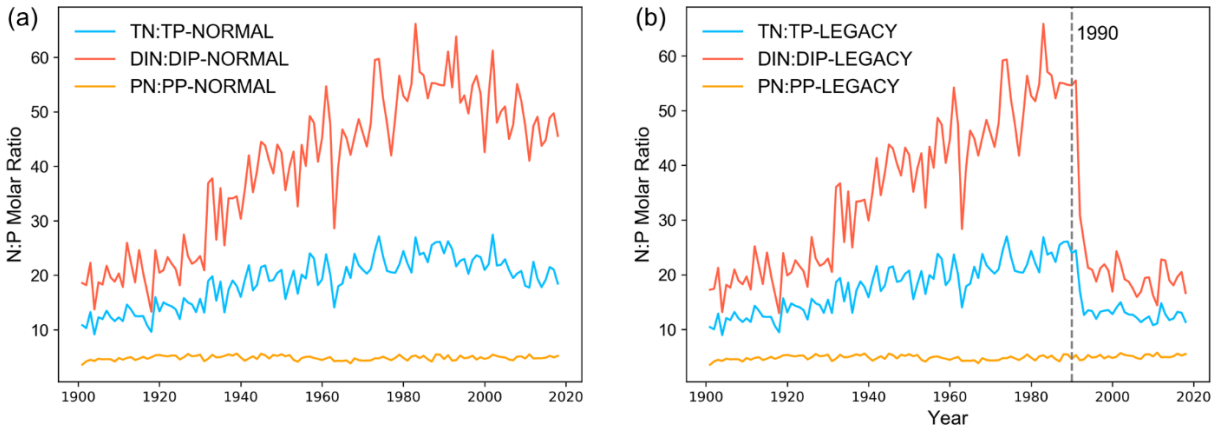

Figure 6-5. The interannual variations and long-term trends of simulated TN:TP, DIN:DIP, and PN:PP molar ratio of riverine exports in the (a) NORMAL and (b) LEGACY scenarios during 1901-2018. DIN: dissolved inorganic nitrogen (NH_4^+ and NO_3^-); PN: particulate nitrogen (PON); PP: particulate phosphorus (PIP and POP).

3.2. Impact of other environmental factors on N:P loading ratio

3.2.1. Fertilizer and manure application

Synthetic fertilizer and livestock manure are the two most important anthropogenic N and P inputs into agricultural land. The N:P molar ratio of fertilizer increased from around 8 to 12 from the 1960s to the 1990s, but it became relatively stable after 1990 except 2008-2010 when the price of P fertilizer highly increased and consumption was constrained (Figure 6-6). Meanwhile, the N:P molar ratio of manure slightly decreased from 7.4 to 6.8 from 1960 to 2018. The decreasing N:P ratio of manure was associated with the change in the structure of livestock populations (Bian et al., 2021), and may make a small contribution to the decreasing N:P ratio of nutrients loading. The nutrient surplus which is the major basis for many statistical methods or lumped watershed model to calculate the nutrient loading indicate the overall impact of agricultural activities on nutrient balance. The DLEM-simulated nutrient surplus N:P ratio in the MRB didn't exhibit a significant decreasing trend during 1990-2018. Several nutrient budget works based on survey data showed that the N:P ratio in cropland nutrient surplus has been increasing over the past three decades in the U.S (Jones and Bruulsema, 2021; Lu et al., 2021). Although the nutrients surplus decreased due to the increased crop harvest and steady application of fertilizer after the 1990s, the surplus decreased at a similar speed for N and P. Generally,

changes in fertilizer and manure application contributed to the increase in the N:P ratio of nutrient loading before the 1990s, but maybe not the major reason for the decreasing N:P loading ratio thereafter.

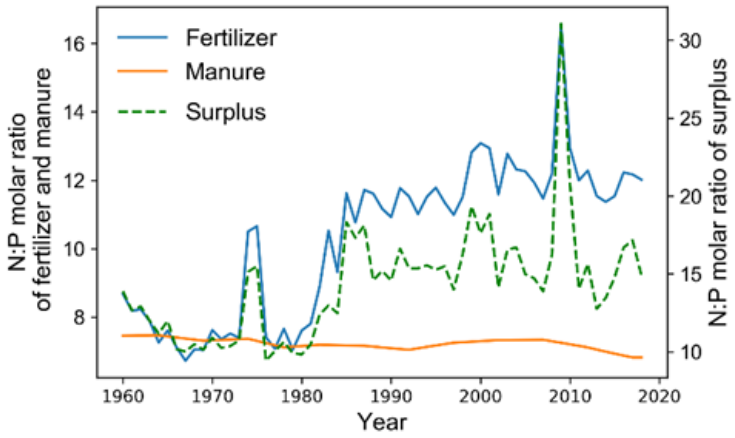

Figure 6-6. The interannual variations and trends of fertilizer, manure, and nutrients surplus in the MRB during 1960-2018. Note: the analysis period starts from 1960 when the fertilizer inventory data from USDA are available.

3.2.2. Climate

Changes in precipitation and temperature impact N and P loading not only by altering the timing and magnitude of runoff, but also through affecting biotic and abiotic mechanisms related to N and P cycles. The sensitivity of N:P loading ratio to climate variability largely depends on the difference in the response of N and P loading to hydrologic variability. Leong et al. (2014) indicated that N:P increases with discharge in subbasins with intensive crop agriculture and high fertilizer application rates but is less predictable in other subbasins of the MRB. In agricultural land where the leaching of DIN and DIP was the major pathway for nutrients entering aquatic systems, the high mobility of inorganic N compared with inorganic P may make DIN more sensitive to discharge than DIP. The erosion loss of particulate form N and P is the other major source of nutrient loading. The more frequent extreme precipitation in the MRB can enhance the erosion rate and the loss of nutrients. Tan et al. (2021) estimated that average erosional PN and PP fluxes into the northern Gulf of Mexico were 775 Gg N yr^{-1} and 328 Gg P yr^{-1} at increasing rates of about 15 Gg N yr^{-1} and 6 Gg P yr^{-1}, respectively, during 1991-2019. The molar ratio of

PN and PP fluxes (5.2) is close to that of increased rates of PN and PP (5.5), which means PN:PP ratio keep relatively stable under the condition of increasing extreme precipitation. PP (POP and PIP) is the dominant P species (over 55% of TP), while PN (mostly PON) only accounts for around 15% of the TN (Figure 6-3a-b). The increasing TP export to the Gulf of Mexico after the 1990s largely resulted from the enhanced PP loading due to the increased precipitation. In contrast, the increased PN cannot offset the decrease of DIN. The proportion of different N and P species matters in changing TN:TP loading ratio. Compared with DIN:DIP ratio, PN:PP ratio is much lower (Figure 6-4). Thus, if the proportion of particulate form nutrient components increased within the total nutrient loading, the TN:TP ratio may decrease even though the PP:PN ratio is not sensitive to discharge. For non-agricultural regions where soil inorganic nutrients supply is limited, the increase rate of erosional nutrients may become higher than that of leaching nutrients when precipitation increased, which can lead to the growing proportion of particulate form nutrients and favor the transport of P attached on particles (Green and Finlay, 2010). The trade-off between the dynamics in DIN:DIP ratio and the proportion of PN and PP in nutrient loading under changing hydrological conditions may determine the response of TN:TP loading ratio to climate variability. In the whole MRB where agricultural land is the most important source for total nutrient exports, the overall effect is TN:TP ratio showed a positive relationship with discharge (Leong et al., 2014). The annual discharge in the MRB, however, showed no significantly changing trend in recent decades (Figure 6-1). The discharge variability may not be the reason for the decreasing N:P ratio, but the increased extreme precipitation and intensified erosion still disproportionately favor the mobilization of legacy P and may amplify the declines in the N:P loading ratio (Goyette et al., 2019).

3.2.3. Wastewater discharge

Wastewater production, as the point N and P source delivered to stream and coastal ocean, is associated with urbanization and growing population. Nutrients in food are consumed by humans and then release into the environment as waste which is further managed by wastewater treatment plants (WWTPs). Metson et al. (2020) used the “nutrient footprint” method to estimate the average U.S. N:P molar ratio of food consumption, associated nutrient release, and treated wastewater as 19.0, 11.5, and 21.4, respectively. Thus, P is less efficiently used in human diet but more efficiently removed in WWTPs compared with N. Tong et al. (2020) found

that the rapid improvement in WWTPs in China has increased TN:TP ratio in wastewater discharge due to the higher removal efficiency of P over N. However, the SPARROW model estimated that N input from WWTPs decreased by 4.3% while P input increased 45% from 2002 to 2012 in the MRB (Robertson and Saad, 2021; Skinner and Maupin, 2019). Treatment technologies and nutrient retention capacities of WWTPs vary widely across the U.S. and the long-term dynamic wastewater discharge data across the MRB are not available, but it is possible that the N:P ratio of point-source input decreased in a certain period according to the available information. Considering the relatively small proportion of point-source in total nutrients loading (WWTPs contributed 5.4% N and 13.0% P in 2012) (Robertson and Saad, 2021), the impact of point-source on the decrease in TN:TP loading ratio may be shrunk.

3.2.4. Dam reservoirs, groundwater, land-use change

The contrasting behaviors of N and P along flow paths can reshape N:P ratio of nutrient export to coastal oceans. Streams tend to favor gaseous N loss, whereas lakes and reservoirs promote water column P loss through sediment setting (Alexander et al., 2008; Goyette et al., 2019; Mulholland et al., 2008). Dam construction within basins facilitated the retention of particulate forms of nutrients, and preferential removal of P over N in reservoirs increases N:P ratios delivered to the coastal ocean (Maavara et al., 2020). In groundwater, DIN converted to gas form is the predominant removal pathway, and DIP is generally removed through sorption or co-precipitation with Al, Ca, or Fe into mineral phases. Removal of P is often more efficient than N in groundwater, resulting in a strong increase of the N:P ratio along flow path (Slomp and Van Cappellen, 2004). Water retention capacities are influenced by changes in flow rate and landscape. The decrease in flow rate favors in-stream sediment deposition or precipitation of mineral phase in groundwater, which plays a more important role for P removal. Changes in land cover, for example, wetland converting to agricultural land, may cause the loss of water retention capacity, which would change the N:P ratio in downstream waters (Goyette et al., 2019). In the MRB, dam reservoir numbers increased from 549 in 1970 to 700 in 2000, which may favor P retention over N (Maavara et al., 2015), meanwhile, there is insufficient evidence of the long-term average water retention capacities were significantly altered by flow rate and land cover change after the 1990s. Therefore, water retention capacity change is not likely to be the reason for the declining N:P ratio of nutrient export.

3.3. Implications

The increasing use of fertilizer N over P across the MRB has led to the N:P loading ratio much higher than the "Redfield ratio", and the ratio starts to decrease since the latter 1980s as the riverine P loading kept increasing while N loading slightly decreased. Water column N:P ratio in coastal regions can be altered by changes in the N:P loading ratio, but also impacted by nutrients derived from deep ocean and sediment (Adhikari et al., 2015; Howarth et al., 2021; Smith, 2006). The N:P ratio of water column varies across the Gulf area and shift in different seasons (Turner and Rabalais, 2013). Nitrogen is generally identified as the ultimate limiting nutrient of the whole Gulf ecosystem, due to efficient recycling of P and loss of N to the atmosphere. However, the historical excessive N loading has led to P limitation of phytoplankton growth along the Louisiana shelf during spring and summer (Sylvan et al., 2006). If the N:P ratio of nutrient export from the MRB continues to decrease, the P limitation may be eliminated, and the primary production could further increase. Fennel & Laurent (2018) suggested that although P loading reductions have little effect on overall primary production in the Gulf, they can significantly reduce hypoxia because hypoxia development is facilitated by density stratification which also limits upwelling of P from sediment and makes primary production P limited. The Hypoxia Task Force (HTF, 2015) set a goal to reduce the 5-year average hypoxic zone area in the Gulf of Mexico to less than 5,000 km^2 by 2035 with an interim target of a 20% reduction of N and P loading from MRB by 2025 (relative to the 1980-1996 average). A dual nutrient reduction strategy as the most prudent management approach not only can reduce the requirement of single nutrient (N) reduction magnitude, but also ensure the stoichiometric balance (Dodds, 2006; Fennel and Laurent, 2018; Scavia et al., 2017). Nutrient control measures need to better address legacy nutrients, especially P, to meet nutrient reduction goals.

Legacy nutrients serve as a dominant and long-term nutrient source for receiving water, but also a potential important nutrient source for crop production. The nutrient management strategies require to efficient use of legacy nutrients to satisfy crop demand and reduce their loss to the surface water or atmosphere. Soil legacy N is mainly accumulated as soil organic N while P occurs as both organic matter and inorganic components (Meter et al., 2016; Rowe et al., 2016). Crop recovery of legacy soil N and P is impacted by soil organic nutrient mineralization rates and utilization of legacy P is also related to the P desorption rate. Understanding the

impacts of soil conditions (soil moisture, temperature, pH, texture, and soil mineral) and crop types on mineralization and desorption processes is critical to improving current beneficial management practices for mitigating legacy soil nutrient loss. Investigate Measures aimed at enhancing legacy soil nutrient utilization by crops include cultivation, tillage, intercropping, crop breeding, and moisture regulation (Chen et al., 2018). It is worth further investigating the differences of these measures in the effective utilization of P and N, as well as their influence on the stoichiometric ratio.

3.4. Uncertainty and limitation

Legacy nutrients are accumulated nutrients within the watershed (e.g., soil, vadose zone, groundwater, and sediments) due to the anthropogenic nutrient surplus from previous years. In the DLEM, the legacy nutrients are primarily represented by nutrient storage in soil organic and inorganic nutrient pools. However, the legacy nutrients stored in groundwater and river sediments have not been considered in the model. According to Meter et al. (2017), soil nutrient pools played a dominant role in the legacy nutrient effect in the MRB, thereby, the simulated results in this study still could capture the main variation characteristics of legacy nutrients.

In this study, we assumed all fertilizer and manure nutrients were applied to agricultural land, which may overestimate the total nutrient input in agricultural ecosystems. Additionally, aside from the nutrient inputs and outputs considered in this study, there existed other pathways of nutrient fluxes across the system, such as forest fire emission, human waste, and crop import. The overlook of these unconsidered fluxes and the uncertainties in anthropogenic nutrient input datasets may result in biases in estimated nutrient balance as well as legacy nutrients.

4. Conclusion

This study explored the processes and mechanisms of N and P inputs and remineralization in soils that lead to varying ratios of N to P loading to coastal Louisiana from the MRB. We found that relative differences in the long-term accumulation of N relative to P within the basin and their ultimate release following remineralization processes have led to changes in the N:P of loading to the coastal zone that differ from long-term trends in their inputs to the system from anthropogenic activities. According to the N and P budgets across the Mississippi River Basin, the accumulated N and P continued to increase but slowed down in

recent decades. Although both soil legacy N and P can serve as long-term sources for nutrient loading, P has a longer residence time and soil labile P declines more slowly than N. If the NUE of agricultural systems were 100% (no additional nutrient surplus), riverine N loading would decrease more dramatically due to the quick loss of soil labile N relative to P. Therefore, the N:P ratio of nutrient loading may decrease with time as the NUE of crops increases and legacy soil nutrients play a more important role in contributing to nutrient loading. The increased extreme precipitation and changes in the N:P ratio of point nutrient sources in the Mississippi River Basin may also decline N:P loading ratios. When addressing the impact of legacy nutrients on nutrient loading, combining the N and P under the same framework is conducive to controlling the stoichiometric balance in aquatic systems and improving ecosystem health.

References

Adhikari, P.L., White, J.R., Maiti, K., Nguyen, N., 2015. Phosphorus speciation and sedimentary phosphorus release from the Gulf of Mexico sediments: Implication for hypoxia. Estuar. Coast. Shelf Sci. 164, 77–85. https://doi.org/10.1016/j.ecss.2015.07.016

Alexander, R.B., Smith, R.A., Schwarz, G.E., Boyer, E.W., Nolan, J.V., Brakebill, J.W., 2008. Differences in Phosphorus and Nitrogen Delivery to The Gulf of Mexico from the Mississippi River Basin. Environ. Sci. Technol. 42, 822–830. https://doi.org/10.1021/es0716103

Bian, Z., Tian, H., Yang, Q., Xu, R., Pan, S., Zhang, B., 2021. Production and application of manure nitrogen and phosphorus in the United States since 1860. Earth Syst. Sci. Data 13, 515–527. https://doi.org/10.5194/essd-13-515-2021

Bouwman, A.F., Beusen, A.H., Billen, G., 2009. Human alteration of the global nitrogen and phosphorus soil balances for the period 1970–2050. Glob. Biogeochem. Cycles 23.

Cai, W.-J., Hu, X., Huang, W.-J., Murrell, M.C., Lehrter, J.C., Lohrenz, S.E., Chou, W.-C., Zhai, W., Hollibaugh, J.T., Wang, Y., Zhao, P., Guo, X., Gundersen, K., Dai, M., Gong, G.-C., 2011. Acidification of subsurface coastal waters enhanced by eutrophication. Nat. Geosci. 4, 766–770. https://doi.org/10.1038/ngeo1297

Chen, D., Shen, H., Hu, M., Wang, J., Zhang, Y., Dahlgren, R.A., 2018. Chapter Five - Legacy Nutrient Dynamics at the Watershed Scale: Principles, Modeling, and Implications, in: Sparks, D.L. (Ed.), Advances in Agronomy. Academic Press, pp. 237–313. https://doi.org/10.1016/bs.agron.2018.01.005

Conley, D.J., Paerl, H.W., Howarth, R.W., Boesch, D.F., Seitzinger, S.P., Havens, K.E., Lancelot, C., Likens, G.E., 2009. Controlling Eutrophication: Nitrogen and Phosphorus. Science 323, 1014–1015. https://doi.org/10.1126/science.1167755

Dodds, W.K., 2006. Nutrients and the "dead zone": the link between nutrient ratios and dissolved oxygen in the northern Gulf of Mexico. Front. Ecol. Environ. 4, 211–217. https://doi.org/10.1890/1540-9295(2006)004[0211:NATDZT]2.0.CO;2

Elser, J., Bennett, E., 2011. A broken biogeochemical cycle. Nature 478, 29–31. https://doi.org/10.1038/478029a

Elser, J.J., Bracken, M.E.S., Cleland, E.E., Gruner, D.S., Harpole, W.S., Hillebrand, H., Ngai, J.T., Seabloom, E.W., Shurin, J.B., Smith, J.E., 2007. Global analysis of nitrogen and phosphorus limitation of primary producers in freshwater, marine and terrestrial ecosystems. Ecol. Lett. 10, 1135–1142. https://doi.org/10.1111/j.1461-0248.2007.01113.x

Fennel, K., Laurent, A., 2018. N and P as ultimate and proximate limiting nutrients in the northern Gulf of Mexico: implications for hypoxia reduction strategies. Biogeosciences 15, 3121–3131. https://doi.org/10.5194/bg-15-3121-2018

Glibert, P.M., 2017. Eutrophication, harmful algae and biodiversity — Challenging paradigms in a world of complex nutrient changes. Mar. Pollut. Bull., Special Issue: Hong Kong Conference 2016 124, 591–606. https://doi.org/10.1016/j.marpolbul.2017.04.027

Glibert, P.M., Burkholder, J.M., 2011. Harmful algal blooms and eutrophication: "strategies" for nutrient uptake and growth outside the Redfield comfort zone. Chin. J. Oceanol. Limnol. 29, 724–738. https://doi.org/10.1007/s00343-011-0502-z

Goyette, J.-O., Bennett, E.M., Maranger, R., 2019. Differential influence of landscape features and climate on nitrogen and phosphorus transport throughout the watershed. Biogeochemistry 142, 155–174. https://doi.org/10.1007/s10533-018-0526-y

Green, M.B., Finlay, J.C., 2010. Patterns of hydrologic control over stream water total nitrogen to total phosphorus ratios. Biogeochemistry 99, 15–30. https://doi.org/10.1007/s10533-009-9394-9

Guildford, S.J., Hecky, R.E., 2000. Total nitrogen, total phosphorus, and nutrient limitation in lakes and oceans: Is there a common relationship? Limnol. Oceanogr. 45, 1213–1223. https://doi.org/10.4319/lo.2000.45.6.1213

Heil, C.A., Revilla, M., Glibert, P.M., Murasko, S., 2007. Nutrient quality drives differential phytoplankton community composition on the southwest Florida shelf. Limnol. Oceanogr. 52, 1067–1078. https://doi.org/10.4319/lo.2007.52.3.1067

Howarth, R.W., 2008. Coastal nitrogen pollution: A review of sources and trends globally and regionally. Harmful Algae, HABs and Eutrophication 8, 14–20. https://doi.org/10.1016/j.hal.2008.08.015

Howarth, R.W., Chan, F., Swaney, D.P., Marino, R.M., Hayn, M., 2021. Role of external inputs of nutrients to aquatic ecosystems in determining prevalence of nitrogen vs. phosphorus limitation of net primary productivity. Biogeochemistry. https://doi.org/10.1007/s10533-021-00765-z

Jones, J., Bruulsema, T., 2021. Nitrogen and Phosphorus Budgets for US Cropland: Agronomic and Environmental Metrics, in: AGU Fall Meeting 2021. AGU.

Justić, D., Rabalais, N.N., Turner, R.E., 1995. Stoichiometric nutrient balance and origin of coastal eutrophication. Mar. Pollut. Bull. 30, 41–46. https://doi.org/10.1016/0025-326X(94)00105-I

Lehman, E.M., 2007. Seasonal occurrence and toxicity of Microcystis in impoundments of the Huron River, Michigan, USA. Water Res. 41, 795–802. https://doi.org/10.1016/j.watres.2006.09.030

Leong, D.N.S., Donner, S.D., Hassan, M.A., Gabor, R., Drummond, J.D., 2014. Sensitivity of stoichiometric ratios in the Mississippi River to hydrologic variability. J. Geophys. Res. Biogeosciences 119, 1049–1062. https://doi.org/10.1002/2013JG002585

Li, J., Glibert, P.M., Gao, Y., 2015. Temporal and spatial changes in Chesapeake Bay water quality and relationships to Prorocentrum minimum, Karlodinium veneficum, and CyanoHAB events, 1991–2008. Harmful Algae 42, 1–14. https://doi.org/10.1016/j.hal.2014.11.003

Lohrenz, S.E., Redalje, D.G., Cai, W.-J., Acker, J., Dagg, M., 2008. A retrospective analysis of nutrients and phytoplankton productivity in the Mississippi River plume. Cont. Shelf Res., Coastal Ecosystem Responses to Changing Nutrient Inputs from Large Temperate and Subtropical Rivers 28, 1466–1475. https://doi.org/10.1016/j.csr.2007.06.019

Lu, C., Cao, P., Yi, B., Zhang, J., 2021. Spatial variations and temporal dynamics of agricultural nutrient budget: A high-resolution national database for the contiguous United States during 1970-2019. Presented at the AGU Fall Meeting 2021, AGU.

Maavara, T., Akbarzadeh, Z., Cappellen, P.V., 2020. Global Dam-Driven Changes to Riverine N:P:Si Ratios Delivered to the Coastal Ocean. Geophys. Res. Lett. 47, e2020GL088288. https://doi.org/10.1029/2020GL088288

Maavara, T., Parsons, C.T., Ridenour, C., Stojanovic, S., Dürr, H.H., Powley, H.R., Van Cappellen, P., 2015. Global phosphorus retention by river damming. Proc. Natl. Acad. Sci. 112, 15603–15608. https://doi.org/10.1073/pnas.1511797112

McDowell, R.W., Biggs, B.J.F., Sharpley, A.N., Nguyen, L., 2004. Connecting phosphorus loss from agricultural landscapes to surface water quality. Chem. Ecol. 20, 1–40. https://doi.org/10.1080/02757540310001626092

Meter, K.J.V., Basu, N.B., Cappellen, P.V., 2017. Two centuries of nitrogen dynamics: Legacy sources and sinks in the Mississippi and Susquehanna River Basins. Glob. Biogeochem. Cycles 31, 2–23. https://doi.org/10.1002/2016GB005498

Meter, K.J.V., Basu, N.B., Veenstra, J.J., Burras, C.L., 2016. The nitrogen legacy: emerging evidence of nitrogen accumulation in anthropogenic landscapes. Environ. Res. Lett. 11, 035014. https://doi.org/10.1088/1748-9326/11/3/035014

Meter, K.J.V., Cappellen, P.V., Basu, N.B., 2018. Legacy nitrogen may prevent achievement of water quality goals in the Gulf of Mexico. Science 360, 427–430. https://doi.org/10.1126/science.aar4462

Metson, G.S., MacDonald, G.K., Leach, A.M., Compton, J.E., Harrison, J.A., Galloway, J.N., 2020. The U.S. consumer phosphorus footprint: where do nitrogen and phosphorus diverge? Environ. Res. Lett. 15, 105022. https://doi.org/10.1088/1748-9326/aba781

Mulholland, P.J., Helton, A.M., Poole, G.C., Hall, R.O., Hamilton, S.K., Peterson, B.J., Tank, J.L., Ashkenas, L.R., Cooper, L.W., Dahm, C.N., Dodds, W.K., Findlay, S.E.G., Gregory, S.V., Grimm, N.B., Johnson, S.L., McDowell, W.H., Meyer, J.L., Valett, H.M., Webster, J.R., Arango, C.P., Beaulieu, J.J., Bernot, M.J., Burgin, A.J., Crenshaw, C.L., Johnson, L.T., Niederlehner, B.R., O'Brien, J.M., Potter, J.D., Sheibley, R.W., Sobota, D.J., Thomas, S.M., 2008. Stream denitrification across biomes and its response to anthropogenic nitrate loading. Nature 452, 202–205. https://doi.org/10.1038/nature06686

Paerl, H.W., Gardner, W.S., Havens, K.E., Joyner, A.R., McCarthy, M.J., Newell, S.E., Qin, B., Scott, J.T., 2016. Mitigating cyanobacterial harmful algal blooms in aquatic ecosystems impacted by climate change and anthropogenic nutrients. Harmful Algae, Global Expansion of Harmful Cyanobacterial Blooms: Diversity, ecology, causes, and controls 54, 213–222. https://doi.org/10.1016/j.hal.2015.09.009

Peñuelas, J., Poulter, B., Sardans, J., Ciais, P., van der Velde, M., Bopp, L., Boucher, O., Godderis, Y., Hinsinger, P., Llusia, J., Nardin, E., Vicca, S., Obersteiner, M., Janssens, I.A., 2013. Human-induced nitrogen–phosphorus imbalances alter natural and managed ecosystems across the globe. Nat. Commun. 4, 2934. https://doi.org/10.1038/ncomms3934

Peñuelas, J., Sardans, J., 2022. The global nitrogen-phosphorus imbalance. Science. https://doi.org/10.1126/science.abl4827

Peñuelas, J., Sardans, J., Rivas-ubach, A., Janssens, I.A., 2012. The human-induced imbalance between C, N and P in Earth's life system. Glob. Change Biol. 18, 3–6. https://doi.org/10.1111/j.1365-2486.2011.02568.x

Ptacnik, R., Jenerette, G.D., Verschoor, A.M., Huberty, A.F., Solimini, A.G., Brookes, J.D., 2005. Applications of ecological stoichiometry for sustainable acquisition of ecosystem services. Oikos 109, 52–62. https://doi.org/10.1111/j.0030-1299.2005.14051.x

Qin, B., Zhang, Y., Zhu, G., Gong, Z., Deng, J., Hamilton, D.P., Gao, G., Shi, K., Zhou, J., Shao, K., Zhu, M., Zhou, Y., Tang, X., Li, L., 2020. Are nitrogen-to-phosphorus ratios of

Chinese lakes actually increasing? Proc. Natl. Acad. Sci. U. S. A. 117, 21000–21002. https://doi.org/10.1073/pnas.2013445117
Robertson, D.M., Saad, D.A., 2021. Nitrogen and Phosphorus Sources and Delivery from the Mississippi/Atchafalaya River Basin: An Update Using 2012 SPARROW Models. JAWRA J. Am. Water Resour. Assoc. 57, 406–429. https://doi.org/10.1111/1752-1688.12905
Rowe, H., Withers, P.J.A., Baas, P., Chan, N.I., Doody, D., Holiman, J., Jacobs, B., Li, H., MacDonald, G.K., McDowell, R., Sharpley, A.N., Shen, J., Taheri, W., Wallenstein, M., Weintraub, M.N., 2016. Integrating legacy soil phosphorus into sustainable nutrient management strategies for future food, bioenergy and water security. Nutr. Cycl. Agroecosystems 104, 393–412. https://doi.org/10.1007/s10705-015-9726-1
Scavia, D., Bertani, I., Obenour, D.R., Turner, R.E., Forrest, D.R., Katin, A., 2017. Ensemble modeling informs hypoxia management in the northern Gulf of Mexico. Proc. Natl. Acad. Sci. 114, 8823–8828. https://doi.org/10.1073/pnas.1705293114
Skinner, K.D., Maupin, M.A., 2019. Point-source nutrient loads to streams of the conterminous United States, 2012 (USGS Numbered Series No. 1101), Point-source nutrient loads to streams of the conterminous United States, 2012, Data Series. U.S. Geological Survey, Reston, VA. https://doi.org/10.3133/ds1101
Slomp, C.P., Van Cappellen, P., 2004. Nutrient inputs to the coastal ocean through submarine groundwater discharge: controls and potential impact. J. Hydrol. 295, 64–86. https://doi.org/10.1016/j.jhydrol.2004.02.018
Smil, V., 2000. Phosphorus in the environment: natural flows and human interferences. Annu. Rev. Energy Environ. 25, 53–88.
Smith, V.H., 2006. Responses of estuarine and coastal marine phytoplankton to nitrogen and phosphorus enrichment. Limnol. Oceanogr. 51, 377–384. https://doi.org/10.4319/lo.2006.51.1_part_2.0377
Stackpoole, S.M., Stets, E.G., Sprague, L.A., 2019. Variable impacts of contemporary versus legacy agricultural phosphorus on US river water quality. Proc. Natl. Acad. Sci. 116, 20562–20567. https://doi.org/10.1073/pnas.1903226116
Steffen, W., Richardson, K., Rockstrom, J., Cornell, S.E., Fetzer, I., Bennett, E.M., Biggs, R., Carpenter, S.R., de Vries, W., de Wit, C.A., Folke, C., Gerten, D., Heinke, J., Mace, G.M., Persson, L.M., Ramanathan, V., Reyers, B., Sorlin, S., 2015. Planetary boundaries: Guiding human development on a changing planet. Science 347, 1259855–1259855. https://doi.org/10.1126/science.1259855
Sterner, R.W., Elser, J.J., 2017. Ecological stoichiometry. Princeton university press.
Swaney, D.P., Howarth, R.W., 2019. Phosphorus use efficiency and crop production: Patterns of regional variation in the United States, 1987–2012. Sci. Total Environ. 685, 174–188. https://doi.org/10.1016/j.scitotenv.2019.05.228
Sylvan, J.B., Dortch, Q., Nelson, D.M., Maier Brown, A.F., Morrison, W., Ammerman, J.W., 2006. Phosphorus Limits Phytoplankton Growth on the Louisiana Shelf During the Period of Hypoxia Formation. Environ. Sci. Technol. 40, 7548–7553. https://doi.org/10.1021/es061417t
Tan, Z., Leung, L.R., Li, H.-Y., Tesfa, T., Zhu, Q., Yang, X., Liu, Y., Huang, M., 2021. Increased extreme rains intensify erosional nitrogen and phosphorus fluxes to the northern Gulf of Mexico in recent decades. Environ. Res. Lett. 16, 054080. https://doi.org/10.1088/1748-9326/abf006

Tong, Y., Wang, M., Peñuelas, J., Liu, X., Paerl, H.W., Elser, J.J., Sardans, J., Couture, R.-M., Larssen, T., Hu, H., Dong, X., He, W., Zhang, W., Wang, X., Zhang, Y., Liu, Y., Zeng, S., Kong, X., Janssen, A.B.G., Lin, Y., 2020. Improvement in municipal wastewater treatment alters lake nitrogen to phosphorus ratios in populated regions. Proc. Natl. Acad. Sci. U. S. A. 117, 11566–11572. https://doi.org/10.1073/pnas.1920759117

Turner, R.E., Rabalais, N.N., 2013. Nitrogen and phosphorus phytoplankton growth limitation in the northern Gulf of Mexico. Aquat. Microb. Ecol. 68, 159–169. https://doi.org/10.3354/ame01607

Turner, R.E., Rabalais, N.N., Justic, D., 2006. Predicting summer hypoxia in the northern Gulf of Mexico: Riverine N, P, and Si loading. Mar. Pollut. Bull. 52, 139–148. https://doi.org/10.1016/j.marpolbul.2005.08.012

US EPA, O., 2021. Northern Gulf of Mexico Hypoxic Zone [WWW Document]. URL https://www.epa.gov/ms-htf/northern-gulf-mexico-hypoxic-zone (accessed 8.26.21).

Van de Waal, D.B., Verspagen, J.M.H., Lürling, M., Donk, E.V., Visser, P.M., Huisman, J., 2009. The ecological stoichiometry of toxins produced by harmful cyanobacteria: an experimental test of the carbon-nutrient balance hypothesis. Ecol. Lett. 12, 1326–1335. https://doi.org/10.1111/j.1461-0248.2009.01383.x

Vitousek, P.M., Naylor, R., Crews, T., David, M.B., Drinkwater, L.E., Holland, E., Johnes, P.J., Katzenberger, J., Martinelli, L.A., Matson, P.A., Nziguheba, G., Ojima, D., Palm, C.A., Robertson, G.P., Sanchez, P.A., Townsend, A.R., Zhang, F.S., 2009. Nutrient Imbalances in Agricultural Development. Science 324, 1519–1520. https://doi.org/10.1126/science.1170261

Wang, Y.P., Law, R.M., Pak, B., 2010. A global model of carbon, nitrogen and phosphorus cycles for the terrestrial biosphere. Biogeosciences 7, 2261–2282. https://doi.org/10.5194/bg-7-2261-2010

Zhang, Q., Fisher, T.R., Trentacoste, E.M., Buchanan, C., Gustafson, A.B., Karrh, R., Murphy, R.R., Keisman, J., Wu, C., Tian, R., 2021. Nutrient limitation of phytoplankton in Chesapeake Bay: Development of an empirical approach for water-quality management. Water Res. 188, 116407.

Chapter 7. Conclusions and future works

This study focuses on the dynamics of N and P along the land-ocean continuum and their response to climate and anthropogenic activities. A riverine P module was integrated into the Dynamic Land Ecosystem Model (DLEM) Terrestrial-Aquatic modeling framework, making the model able to connect N and P cycling across terrestrial and aquatic ecosystems. Meanwhile, long time-series gridded datasets of manure N and P production and application were developed to evaluate spatial and temporal variations of anthropogenic nutrient inputs to terrestrial ecosystems. The model combined with the datasets was applied to hindcast N and P loading from land to coastal ocean over a century-long time scale. This study investigated the impact of multiple environmental factors (e.g., climate, atmospheric CO_2 concentration, synthetic fertilizer and livestock manure application, atmospheric deposition, land-use change, and wastewater discharge) on nutrient loading based on simulation experiments. The legacy soil nutrient was estimated based on long-term nutrient sources and sinks established in the simulation. Then the impacts of legacy soil nutrients on nutrient loading and N:P stoichiometry were assessed by comparing nutrient loading results under different scenarios.

The major conclusions are as follows:

(1) High-resolution grid-level datasets of animal manure N and P production and their application in cropland were generated in this study. Both manure N and P production and application in the U.S. significantly increased over 1860-2017. The dominant livestock contributing to total manure nutrient production changed from milk cows to beef cows and to poultry over the study period. The increase in livestock numbers is the major reason for increased manure nutrient production before the 1980s. Thereafter, when livestock numbers became stable, manure nutrient production still increased due to the enhanced livestock body weight. Manure nutrient production and application intensified inside the Midwest and expanded toward the Southeastern coastline. Moreover, manure nutrient production became more concentrated in many hot spots resulting from the construction of CAFOs. The substantial enrichment of manure nutrients in the South Atlantic-Gulf after the 1970s could bring high risks to water quality in the Gulf of Mexico and the Atlantic Ocean.

(2) Riverine P loading from a typical agricultural basin, the Mississippi River Basin, during 1901-2018 was simulated by integrating a riverine P module into the DLEM. The decadal average of TP export increased significantly since the 1960s and reached 163.1 Gg P yr^{-1} in the 1990s, then declined in the 2000s, but increased again to 174.8 Gg P yr^{-1} in the 2010s. The PIP flux dominated the P export, accounting for 48-54% of TP export, followed by DIP (30-35% of TP export), POP (9-10%), and DOP (6-8%) fluxes. From the 1960s to the post-2010s, DIP, DOP, POP, PIP, and TP increased by 42%, 53%, 60%, 53%, and 50%, respectively. Riverine DIP loading change is dominated by the increasing application of P fertilizer and manure as well as land-use change. Climate variability and P fertilizer are two key contributors to PIP export since the 1970s. The changes in riverine DOP and POP exports were primarily impacted by climate and land-use change. In recent decades, more frequent extreme precipitation events have exacerbated soil erosion accompanied by particulate form P loss. Land conversion to cropland contributed to the increase of DIP load, but reduced DOP, POP, and PIP loads. Rising atmospheric CO_2 concentrations played an increasingly important role in increasing organic P export and decreasing inorganic P exports.

(3) The decadal average total N sources and sinks in the MRB increased from 5.05 and 3.09 Tg N yr^{-1} in the 1900s to 20.57 and 16.68 Tg N yr^{-1} in the 2010s, respectively. Meanwhile, total P sources and sinks increased from 0.42 and 0.56 Tg P yr^{-1} to 2.57 and 1.90 Tg P yr^{-1}, respectively. Both N and P balances substantially increased from the 1930s to the 1970s, then N balance experienced a decreasing trend since the 1980s, while P balance dramatically decreased in the 1980s due to the reduction in P fertilizer usage and leveled off thereafter. The accumulation of soil legacy N and P continued to increase but slowed down after 1980. If anthropogenic nutrient surpluses were reduced or suspended, soil legacy N would decline more quickly than legacy P, leading to the decreasing N:P stoichiometric ratio of nutrient loading. As nutrient use efficiency of crops increased in the MRB in recent decades, the legacy soil nutrient became a more important loading source. Simultaneously, enhanced extreme precipitation facilitated soil erosion which disproportionately favors the mobilization of legacy P may also contribute to the decline in the N:P loading ratio.

Uncertainties in this study are mainly derived from input datasets, model structures, and parameters applied in simulations. Several input datasets were only available in recent decades,

thus assumptions and methods were adopted to extend datasets back to the year 1900. For example, fertilizer nutrient input data provided by USDA were available after 1960, and we assumed that the change in fertilizer nutrient usage in the U.S. during 1900-1960 was consistent with global fertilizer nutrient consumption data. The climate data before and after 1980 were derived from two data sources (CRUNCEP and GRIDMET) with different spatial resolutions. Information was lost and biases were generated when spatial data were downscaled or upscaled to match the resolution required by the model. Variations in fertilizer and manure nutrient application within a year could affect the nutrient loading at a seasonal scale, but the timing of fertilizer and manure application was not explicitly considered. Concerning model structures, numerous mechanisms that impact nutrient loading, such as dam constructions, resuspension of river sediment, channel straightening, bank stabilization, loss of wetlands, and occlusion of floodplain swamps, were not accounted for or over-simplified in the model. Dam reservoirs disturbed the transport of water and nutrients along river networks and can act as nutrient sinks by stimulating the deposition of particles in waters. Bottom sediment in river channels can act as a nutrient source for water through resuspension processes. DLEM considers lateral fluxes of nutrient through surface runoff and subsurface runoff as the key mechanism for nutrient entering rivers, but the model simplifies the transport of groundwater and the soil nutrient exchange with groundwater, which is an important source of nutrient for streams. Overlook of these processes could affect the estimation of nutrient loading, especially before the 1970s when observation data were not available.

In our future work, first, we will try to reduce uncertainties and improve the accuracy of simulated results. The nutrient input datasets could be refined according to the nutrient management strategies of farmers. A process-based dam module will be added to the model to address the impact of dam reservoirs on nutrient loading. Second, we will build the linkages between riverine exports and water quality in coastal oceans. The sensitivity and response of hypoxia area to riverine exports of different nutrient species from land can be investigated. Additionally, we plan to evaluate the temporal pattern of C:N:P ratios of riverine inputs reaching coastal oceans based on the fully coupled C-N-P model. The changes in C:N:P ratios of riverine export may drive the variations of stoichiometry, nutrient limitation, ecosystem structure, and function inside coastal oceans. Third, we will project the nutrient loading from land to ocean under different climate and social-economic scenarios. Future simulations could help seek

efficient nutrient management strategies for stakeholders, which is critical for sustainable agriculture and pollution control.